AD-A053 262 TEXAS UNIV AT DALLAS RICHARDSON F/G 4/1
AURORAL DATA ANALYSIS.(U)
JAN 78 J D WINNINGHAM, W J HEIKKILA F19628-76-C-0005
UNCLASSIFIED AFGL-TR-78-0008 NL

| OF |
AD
A053262

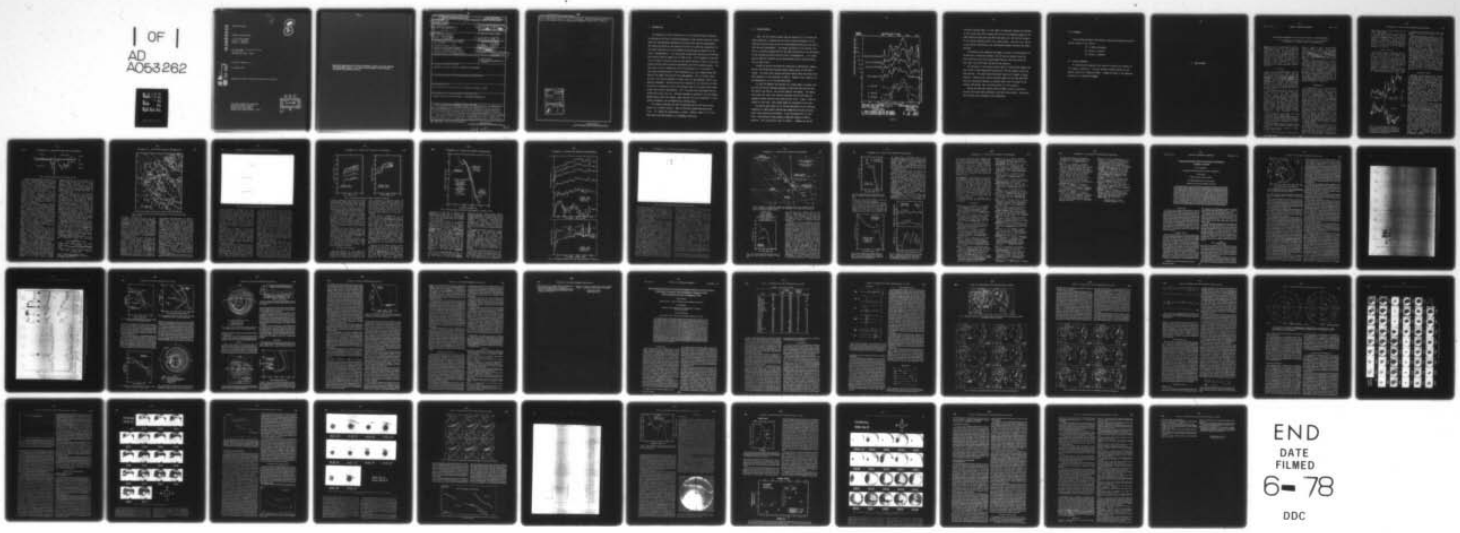

END
DATE
FILMED
6-78
DDC

AFGL-TR-78-0008

AURORAL DATA ANALYSIS

J. David Winningham
Walter J. Heikkila
Gordon G. Shepherd

The University of Texas at Dallas
P.O. Box 688
Richardson, Texas 75080

Scientific Report No. 2

4 January 1978

Approved for public release; distribution unlimited

AIR FORCE GEOPHYSICS LABORATORY
AIR FORCE SYSTEMS COMMAND
UNITED STATES AIR FORCE
HANSCOM AFB, MASSACHUSETTS 01731

Qualified requestors may obtain additional copies from the Defense Documentation Center. All others should apply to the National Technical Information Service.

SECURITY CLASSIFICATION OF THIS PAGE (When Data Entered)

REPORT DOCUMENTATION PAGE	READ INSTRUCTIONS BEFORE COMPLETING FORM
1. REPORT NUMBER: AFGL-TR-78-0008	2. GOVT ACCESSION NO. / 3. RECIPIENT'S CATALOG NUMBER
4. TITLE (and Subtitle): AURORAL DATA ANALYSIS.	5. TYPE OF REPORT & PERIOD COVERED: Scientific Report No. 2, 1 Aug 76 - 31 Jul 77
	6. PERFORMING ORG. REPORT NUMBER
7. AUTHOR(s): J. David Winningham, Walter J. Heikkila, Gordon G. Shepherd*	8. CONTRACT OR GRANT NUMBER(s): F19628-76-C-0005
9. PERFORMING ORGANIZATION NAME AND ADDRESS: The University of Texas at Dallas, P.O. Box 688, Richardson, Texas 75080	10. PROGRAM ELEMENT, PROJECT, TASK AREA & WORK UNIT NUMBERS: 62101F, 7663 08AC, 17 08
11. CONTROLLING OFFICE NAME AND ADDRESS: Air Force Geophysics Laboratory, Hanscom AFB, Massachusetts 01731, Captain Edward J. Weber/PHI/Monitor	12. REPORT DATE: 4 Jan 78; 13. NUMBER OF PAGES: 50 (12 51p)
14. MONITORING AGENCY NAME & ADDRESS (if different from Controlling Office)	15. SECURITY CLASS. (of this report): UNCLASSIFIED; 15a. DECLASSIFICATION/DOWNGRADING SCHEDULE

16. DISTRIBUTION STATEMENT (of this Report)

APPROVED FOR PUBLIC RELEASE; DISTRIBUTION UNLIMITED

17. DISTRIBUTION STATEMENT (of the abstract entered in Block 20, if different from Report)

18. SUPPLEMENTARY NOTES

*York University, 4700 Keele St., Downsview, Ontario, Canada

19. KEY WORDS (Continue on reverse side if necessary and identify by block number)

AURORAL PARTICLES, MAGNETOSPHERE - IONOSPHERE INTERACTIONS

20. ABSTRACT (Continue on reverse side if necessary and identify by block number)

During the previous year three papers have been published in refereed journals. In addition, two more were accepted for publication and one is in the reviewing process. Each deals with the effects produced by auroral particles on the ionosphere and atmosphere and in turn with how the dynamics of auroral particles is influenced by terrestrial and interplanetary magnetic activity.

Significant progress has been made in defining the electron energy sub-range most responsible for 6300 A emissions. Surprisingly the task is simpler than originally envisioned. All electrons of energies greater than a few hundred eV

DD FORM 1 JAN 73 1473 EDITION OF 1 NOV 65 IS OBSOLETE

UNCLASSIFIED

SECURITY CLASSIFICATION OF THIS PAGE (When Data Entered)

391 647

have no appreciable effect on red-line emissions. Thus the empirical relationship will be derived from one energy band extending from 60 eV to ~ 300 eV.

I. INTRODUCTION

The objectives of this contract are: (1) to relate the 6300 A emissions as observed by the ISIS-2 scanning photometer to the causative electron fluxes which are simultaneously observed by the ISIS-2 Soft Particle Spectrometer. The energy sub-region of the electron flux which is primarily responsible for the 6300 A emissions will be delineated to the accuracy available with the ISIS-2 instrumentation. It is hoped that an empirical relation can be derived that relates electron energy flux to 6300 A flux. (2) To compare the particle fluxes and 6300 A emissions (and the conclusions derived in Item 1) with simultaneous electron density profiles obtained by the ISIS-2 topside sounder. The basic goal of such a comparison will be to ascertain if it is possible to infer gross characteristics of the ionosphere (e.g. f_0F_2, plasma trough boundaries) from 6300 A and particle flux measurements. (3) To relate, where possible, the results obtained in items 1 and 2 to the dynamical effects produced by substorms. Specifically we will evaluate if it is possible to infer the motion of boundaries such as the poleward edge of the low-altitude plasma trough from indirect measurements. (4) To analyze the simultaneous data obtained with ISIS-2, the AFGL Airborne Ionospheric Laboratory, and the Defense Meteorological Satellite System. Again the goal will be to ascertain if ionospheric parameters can be determined by indirect means.

This report represents the work accomplished during the second twelve months of a 39 month contract. Most of the work accomplished during the first 24 months was preparatory in nature. However, items 1 & 3 of the objectives have been brought to a reasonable conclusion.

II. ACCOMPLISHMENTS

Item 1 of the contract states that one objective is "to relate the 6300 A emissions as observed by the ISIS-2 scanning photometer to the causative electron fluxes which are simultaneously observed by the ISIS-2 Soft Particle Spectrometer. The energy sub-region of the electron flux which is primarily responsible for the 6300 A emissions will be delineated to the accuracy available with the ISIS-2 instrumentation. It is hoped that an empirical relation can be derived that relates electron energy flux to 6300 A flux."

Originally we had envisioned the necessity of determining, independently, the relationship between several energy bands and the 6300 A fluxes. This would have required defining regions where one energy band would dominate in the production of 6300 A. However, this turned out to be unneccessary, as will be described below.

In order to expedite the analysis of a large number of passes, UTD and York University developed programs to merge the data from the SPS, ASP (5577 A and 3914 A), and the RLP (6300 A) instruments. The energy flux within the local loss cone was evaluated from the SPS data and computer plotted along with the three optical lines. Figure 1 shows an example of this plot. Four energy bands are selectable at one time.

Ten passes were chosen for an initial evaluation of the technique. Inspection of these passes revealed the comparison problem to be much easier than originally envisioned. It was discovered that to first order > 300 electron fluxes produce a negligible amount of 6300 A emission. This can be easily seen in Figure 1. Between 63° and 68°

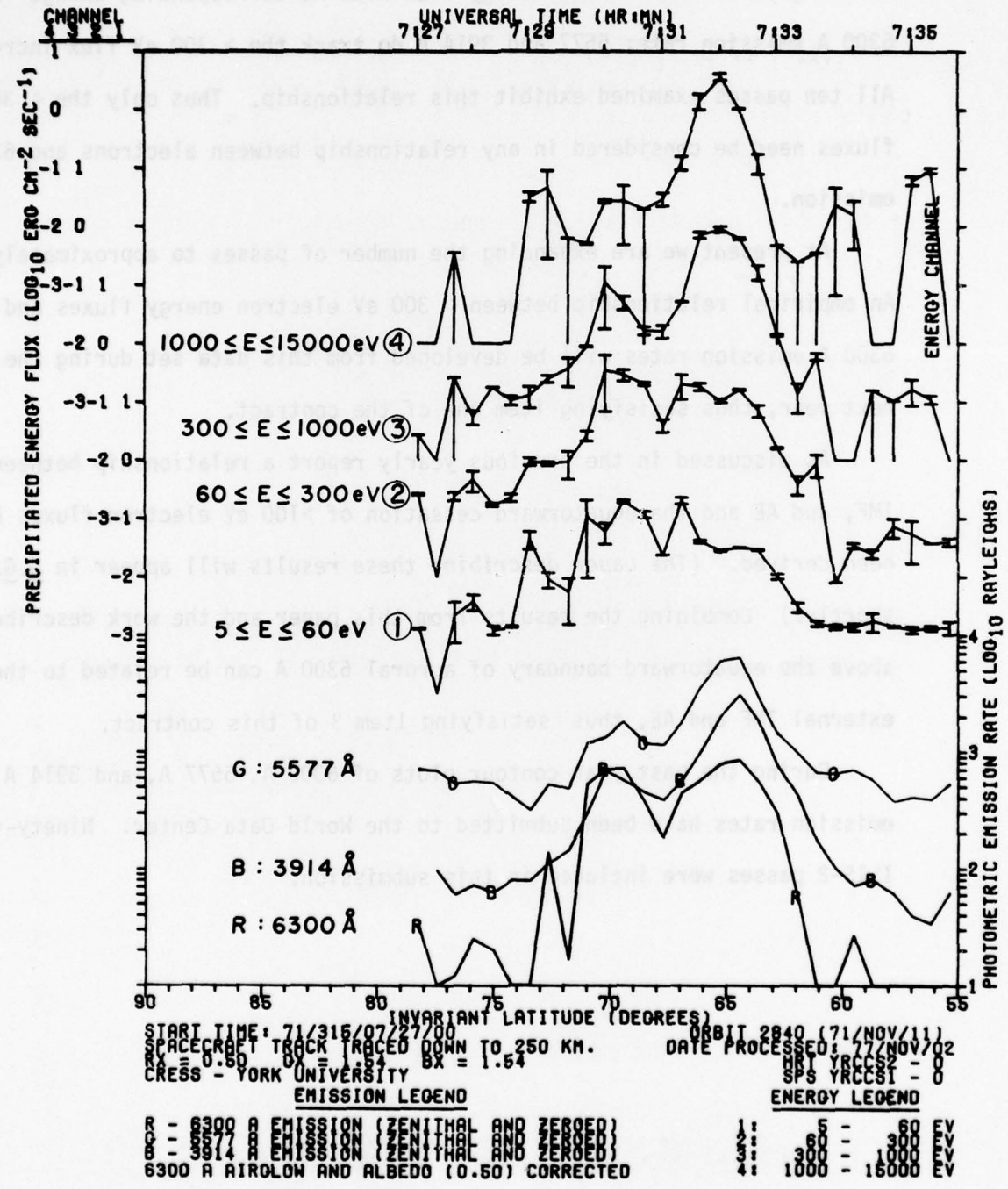
CHANNEL
4 3 2 1
UNIVERSAL TIME (HR:MN)
7:27
7:29
7:31
7:33
7:35
PRECIPITATED ENERGY FLUX (LOG10 ERG CM-2 SEC-1)
1000≤E≤15000eV ④
300≤E≤1000eV ③
60≤E≤300eV ②
5≤E≤60eV ①
ENERGY CHANNEL
G : 5577 Å
B : 3914 Å
R : 6300 Å
PHOTOMETRIC EMISSION RATE (LOG10 RAYLEIGHS)
INVARIANT LATITUDE (DEGREES)
90
85
80
75
70
65
60
55
SIARI TIME: 71/315/07/27/00
SPACECRAFT TRACK TRACED DOWN TO 250 KM.
RX = 0.50 DX = 1.54 BX = 1.54
CRESS - YORK UNIVERSITY
ORBIT 2840 (71/NOV/11)
DATE PROCESSED: 77/NOV/02
HRT YRCCS2 = 0
SPS YRCCS1 = 0
EMISSION LEGEND
R - 6300 A EMISSION (ZENITHAL AND ZEROED)
G - 5577 A EMISSION (ZENITHAL AND ZEROED)
B - 3914 A EMISSION (ZENITHAL AND ZEROED)
6300 A AIRGLOW AND ALBEDO (0.50) CORRECTED
ENERGY LEGEND
1: 5 - 60 EV
2: 60 - 300 EV
3: 300 - 1000 EV
4: 1000 - 15000 EV

Figure 1.

invariant latitude there is a two orders of magnitude increase and decrease in the greater than 300 eV energy flux with no corresponding change in the 6300 A emission rate; 5577 and 3914 A do track the > 300 eV flux increase. All ten passes examined exhibit this relationship. Thus only the < 300 eV fluxes need be considered in any relationship between electrons and 6300 A emission.

At present we are expanding the number of passes to approximately 50. An empirical relationship between < 300 eV electron energy fluxes and 6300 A emission rates will be developed from this data set during the next year, thus satisfying item one of the contract.

As discussed in the previous yearly report a relationship between the IMF, and AE and the equatorward cessation of >100 eV electron fluxes has been derived. (The paper describing these results will appear in J.G.R. shortly.) Combining the results from this paper and the work described above the equatorward boundary of auroral 6300 A can be related to the external IMF and AE, thus satisfying Item 3 of this contract.

During the past year contour plots of 6300 A, 5577 A, and 3914 A emission rates have been submitted to the World Data Center. Ninety-five ISIS-2 passes were included in this submission.

III. PERSONNEL

The following personnel contributed to the work performed during the period covered by this report:

Dr. J. David Winningham

Dr. Walter J. Heikkila

Dr. Gordon G. Shepherd

IV. RELATED CONTRACTS

All publications covered by this specific contract are attached to this report as section V. The most relevant related contract to the present contract is F19628-75-C-0032. F19628-75-C-0032 is the immediate predecessor to F19628-76-C-0005

V. PUBLICATIONS

VOL. 82, NO. 13 JOURNAL OF GEOPHYSICAL RESEARCH MAY 1, 1977

ROCKET-BORNE MEASUREMENTS OF THE DAYSIDE CLEFT PLASMA: THE TORDO EXPERIMENTS

J. D. Winningham,[1] T. W. Speiser,[2] E. W. Hones, Jr.,[3] R. A. Jeffries,[3] W. H. Roach,[3] D. S. Evans,[4] and H. C. Stenbaek-Nielsen[5]

Abstract. Results are presented from low-energy plasma analyzers (12 eV to 12 keV) carried on two rockets launched into the dayside cleft during January 1975. We conclude that (1) atmospheric interaction becomes important for <1-keV electrons at approximately 250 km, (2) characteristics of particles in 'inverted V's' observed in the afternoon cleft are consistent with their interpretation as being due to parallel electric field acceleration from a constant source population, and (3) magnetospheric 'energetic' (>2 keV) electrons intermingle with 'magnetosheathlike' plasma in the cleft.

Introduction

The past two years have marked a dramatic upsurge in sounding rocket launches into the low-altitude cleft region. Prior to 1974 only four instrumented rocket payloads [Maynard and Johnstone, 1974; Ledley and Farthing, 1974] and one thermite barium release [Mikkelsen and Jorgensen, 1974] had been launched into or in the vicinity of the cleft. The instrumented payloads were launched from Hall Beach, Northwest Territories (Λ= 79.7°), on March 15, 18, 19, and 22, 1971, and the barium release from Sondre Stromfjord, Greenland (Λ= 74.5°), on December 10, 1972.

In contrast, from June 1974 to November 1975, 15 rockets were fired in the cleft region from launch sites at Cape Parry, Northwest Territories, Canada, and Sondre Stromfjord, Greenland. Ungstrup et al. [1975a] reported results from two rockets launched from Greenland in July 1974; these payloads were more comprehensive than their predecessors as they included particle spectrometers, dc electric and magnetic probes, and thermal plasma sensors. During December 1974 through January 1975, two major campaigns, totaling 11 rockets, were executed in Canada (Cape Parry, Northwest Territories, Λ = 74.5°) and Greenland (Sondre Stromfjord). These launchings included extensive plasma and field instrumentation, optical sensors, shaped charge barium injections, and lithium releases [Haerendel, 1975; Torbet et al., 1975; Ungstrup et al., 1975b; Temerin et al., 1975; Shepherd et al., 1975, 1976; Winningham et al., 1975a; Wescott et al., 1975; Stenbaek-Nielsen et al., 1975; Jeffries et al., 1975; Torbet and Carlson, 1975].

Another series consisting of two rocket launches was completed during November 1975 at Cape Parry. These vehicles included particle detectors, barium lined shaped charges, plasma drift detectors, and energetic particle sensors.

In this paper we will present results from the soft particle spectrometer (SPS) [Heikkila et al., 1970] instruments carried as an environmental monitor on Tordo Uno and Dos. The Tordo Uno and Dos programs were designed by the Los Alamos Scientific Laboratory and the University of Alaska Geophysical Institute, and the rockets were launched from Cape Parry by the Sandia Laboratories on January 6 and 11, 1975, 2349:02 and 0025:02 UT, respectively.

Instrumentation

The primary objective of the Tordo campaign was the injection of barium ions into the low-altitude cleft (initial results from the shaped charge barium releases are described in the paper by Jeffries et al. [1975]). In addition to the shaped charge, a low- energy (12 eV to 12 keV) plasma analyzer (SPS) similar to the one on the Isis 1 and 2 satellites [Heikkila et al., 1970] was carried as a monitor to locate the detonation point relative to the cleft. For proper barium injection payloads were actively stabilized in relation to the local magnetic field, the result being a unique SPS pitch angle of 45°. The SPS concurrently measured the differential energy spectrum of both electrons and positive ions in 15 logarithmically spaced steps from 12 eV to 12 keV every 3.2 s. In addition, there was a sixteenth step at zero energy to monitor the background count rate. Each energy level was held for 0.2 s, and the count rate was sampled eight times during this period. Multiple sampling was employed in order to evaluate possible temporal/spatial aliasing occurring during the 3.2 s required to complete a stepping sequence.

The energy band pass of the SPS was set at 32% (being a divergent electrostatic lens, the SPS resolution is determined by a field stop), and the geometric factor (not including the energy band pass) was 8.6×10^{-4} cm^2 sr. In order to match the energy band passes at full width at half maximum (FWHM), 22 logarthmically

[1]Center for Space Sciences, University of Texas at Dallas, Richardson, Texas 75080.
[2]Department of Astro-Geophysics and Cooperative Institute for Research in Environmental Sciences, University of Colorado, Boulder, Colorado 80302.
[3]Los Alamos Scientific Laboratory, Los Alamos, New Mexico 87545.
[4]Space Environment Laboratory, National Oceanic and Atmospheric Administration, Boulder, Colorado 80302.
[5]Geophysical Institute, University of Alaska, Fairbanks, Alaska 99701.

Paper number 6A0955.

spaced steps would be required instead of the 15 used on these flights.

The energy-analyzed particles were detected by 14-stage RCA discrete dynode electron multipliers [Bunting, et al., 1972], and the subsequent pulses were amplified by high gain bandwidth amplifiers [Smith, 1972]. Postacceleration was employed to increase the detection efficiency of the multipliers at low energies. The pulse train from each amplifier was $\log_2$ compressed and stored for subsequent telemetry to the ground.

Magnetic Conditions

Tordo Uno was launched on January 6, 1975, at 2349:02 UT (approximately 1330 magnetic local time). The Kp value for the 3-hour period including the flight was 6+ and for the following period was 8-. Figure 1a gives AU and AL for the 6-hour period bracketing the Tordo Uno flight. It should be noted that the AE index shown is based on the standard 11 auroral zone stations plus data from an additional 8 stations in Greenland (courtesy of T. S. Jorgensen) and Scandanavia (courtesy of R. S. Pellinen). Inspection of Figure 1a indicates that the magnetosphere was in an extreme state of agitation during this 6-hour period. During the flight, AE was as large as 750γ. Solar wind magnetic field data were not available for this period.

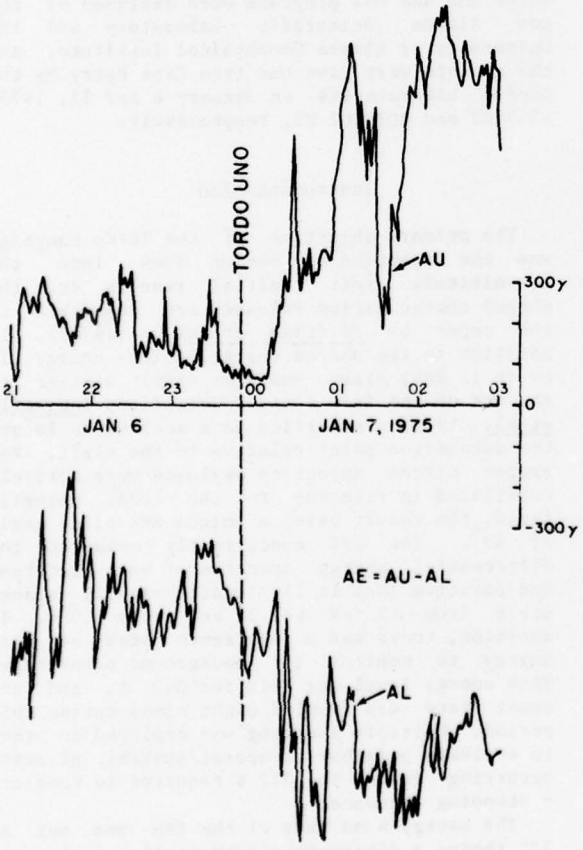

Fig. 1a. AU and AL indices for January 6, 1975. The auroral index is constructed of the standard 11 auroral zone stations plus an additional 8 stations on the nightside in Greenland and Scandanavia.

Tordo Dos was launched on January 11, 1975, at 0025:02 UT (approximately 1400 magnetic local time). The two days encompassing the Tordo Dos flight were relatively quiet; January 10 was a Q day and January 11 was a QQ day. The Kp value for the last 3-hours of January 10 was 1+, and for the first 3-hours of January 11 the Kp value was 2. Examination of Figure 1b shows that magnetic activity was weaker and more representative of classical substorm morphology during the 6-hour period bracketing Tordo Dos than during Tordo Uno. The flight of Tordo Dos occurred during the recovery phase of a small high-latitude substorm (maximum AE = 250γ).

Interplanetary magnetic field data from Imp 8 were available during the Tordo Dos flight and are presented in Figure 2. The IMF went southward at 2216 UT on January 10 and remained southward or close to zero until 0102 on January 11, when it became positive again. A more detailed description of the motion of the cleft and its relation to the IMF during January 10 and 11 can be found in the work of Stiles et al. [1977].

Experimental Results

Tordo Uno. As was mentioned in the previous section, Tordo Uno was launched during a period of prolonged magnetic activity. Examination of the bottomside sounder records from Cape Parry and Sachs Harbour (see Jeffries et al. [1975] and Stiles et al. [1977] for a more complete description) indicated that the equatorward edge of the cleft was south of Cape Parry. The general characteristics of the ionograms indicated precipitation of particles at both Parry and Sachs. As a result of the above considerations a decision was made to launch westward in order to avoid possible exiting the precipitation region northward into the polar cap. Figure 3 shows the projection of the rocket trajectory to 100 km along the earth's magnetic field. From Figure 3 it can be seen that the rocket traveled from approximately 75° to 76.4° invariant latitude.

A synoptic view of the electron data from Tordo Uno is presented in the energy-time spectrogram format in Figure 4. This format is essentially the same as that used for Isis 1 and 2 spectrograms [see Winningham et al., 1975b], with the addition of the altitude profile (solid line) to the energy flux panel and the launch universal date and time at top left. The Z axis (grey scale) of the spectrogram (top panel) has been scaled to give the count per 11.11 ms instead of the actual acumulation period. This was done in order to have the same relationship, between count/accumulation period and grey scale, as that in the Isis 1 and 2 spectrograms.

One of the most striking features observed in the electron spectrogram is the absence of major spatial/temporal structure. This was not the case for Tordo Dos, as will be seen in the following section. Throughout the Tordo Uno flight the count/accumulation period (differential energy flux) maximized at approximately 100-200 eV.

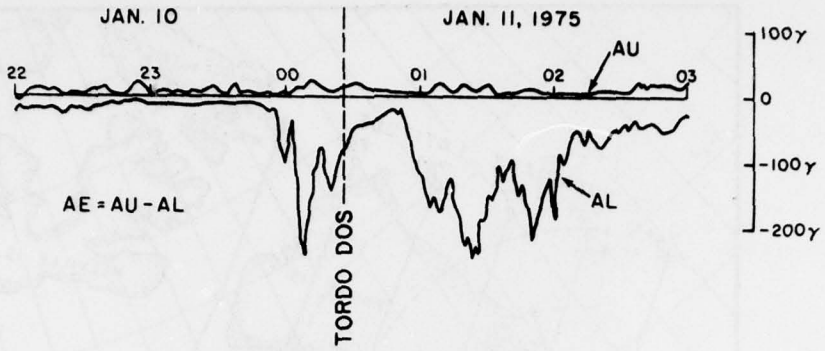

Fig. 1b. Same as Figure 1a but for January 11, 1975.

A 6300-Å scanning photometer belonging to G. G. Shepherd, York University, and an all-sky camera were operated at Sachs Harbour during the Tordo campaign. The photometer indicated a uniform glow of about 300 R, increasing to 1 k R toward the south of Cape Parry during the flight of Tordo Uno. Also the all-sky camera data showed a lack of any discrete aurora.

A more quantitative presentation of the data is given in Figures 5, 6, and 7. Figure 5 presents electron differential flux versus altitude, Figure 6 a representative electron spectrum near apogee, and Figure 7 differential flux versus time. Inspection of Figure 5 and 7 reveals, as did inspection of Figure 4, the absence of dramatic acceleration events (see Figure 8 for comparison).

Throughout the flight the electron spectrum can be divided into two relatively distinct regions, above and below approximately 2 keV. Below 2 keV the spectrum appears to be comprised of a low-energy 'primary' plus 'secondary' population, the primary portion of the spectrum being broader than a Maxwellian curve. For reference, a Maxwellian curve has been included in Figure 6 and has been normalized to the 87-eV experimental point (most of the spectra around apogee exhibit a relative maximum at 87 eV). Also included in Figure 6 are representative near-concurrent plasma mantle and magnetosheath spectra measured by Hawkeye (courtesy of L. A. Frank). The Hawkeye data will be considered again in the discussion section.

The electron spectrum above 2 keV was statistically poor but well above the noise level. Typical counting rates were less than 100/s. The spectrum presented in Figure 6 is an average of 26 spectra (83.2 s) beginning at 2350:36.8 and ending at 2352:00 UT. The deviation of each individual spectrum from the average was minor. This high-energy portion of the electron spectra increased and decreased throughout the flight (see Figure 7a) independently of the lower energy population.

Examination of Figures 5a and 5b reveals a sharp increase of flux with altitude between 180 and 250 km. This altitude related variation was energy dependent, lower energies displaying the largest increase with increasing altitude. Above 250 km (2350:56 UT) the dependence was mainly spatial and/or temporal, not altitudinal. From 2350:56 to 2353:26.4 UT there was a steady increase in the electron flux at energies between 87 and 1021 eV that was energy independent (Figure 7). At 2353:26.4 UT an abrupt increase in magnitude was observed in all energy channels below 1021 eV. The only spectral change occurring was a slight enhancement in the lowest energy channel (12 eV). At 2354:30.4 UT an abrupt decrease was observed, after which time the flux remained at values close to the preincrease level except for three narrow bursts.

At energies below 87 eV an initial flux increase with altitude was also observed. However, at later times the flux profiles were not identical to those at higher energies discussed earlier. The initial slow increase was observed in the 52.8-eV channel but not in the 30.8-, 18.9-, and 11.7-eV channels. The 30.8-eV sample exhibited a relatively flat profile with altitude prior to the increase. At 18.9 and 11.7 eV a relative maximum was observed, the 18.9-eV sample leading the 11.7-eV sample in either space or time (2351:30 and 2352:00 UT, respectively). As in the higher energy channels, an abrupt increase and decrease in flux was observed after 2353:26.4 UT.

Throughout the flight positive ion fluxes were weak. At apogee the peak ion flux occurred in the few hundred electron volt range with flux levels of approximately 10^3 cm^{-2} sr^{-1} s^{-1}.

Tordo Dos. Ionosonde returns obtained prior to launch indicated that the cleft was poleward of Cape Parry and close to, but poleward of, Sachs Harbour. (The ionosonde returns for this day are described in detail by Stiles et al. [1977].) The decision had been reached that Tordo Dos would be launched across the equatorward boundary of the cleft. In order to accomplish this goal the launch azimuth was set as close to magnetic north as range safety requirements would allow (Figure 3).

From high voltage turnon at 0026:27.6 UT (180 km) to 0028:13.2 UT (390 km), downcoming

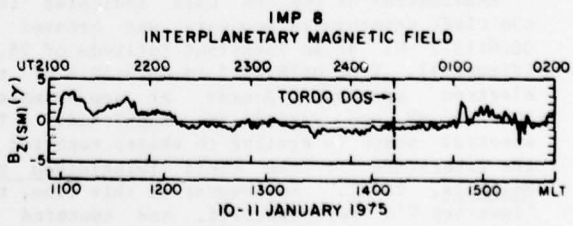

Fig. 2. Interplanetary magnetic field Z component (solar magnetospheric) from Imp 8 for January 10-11, 1975.

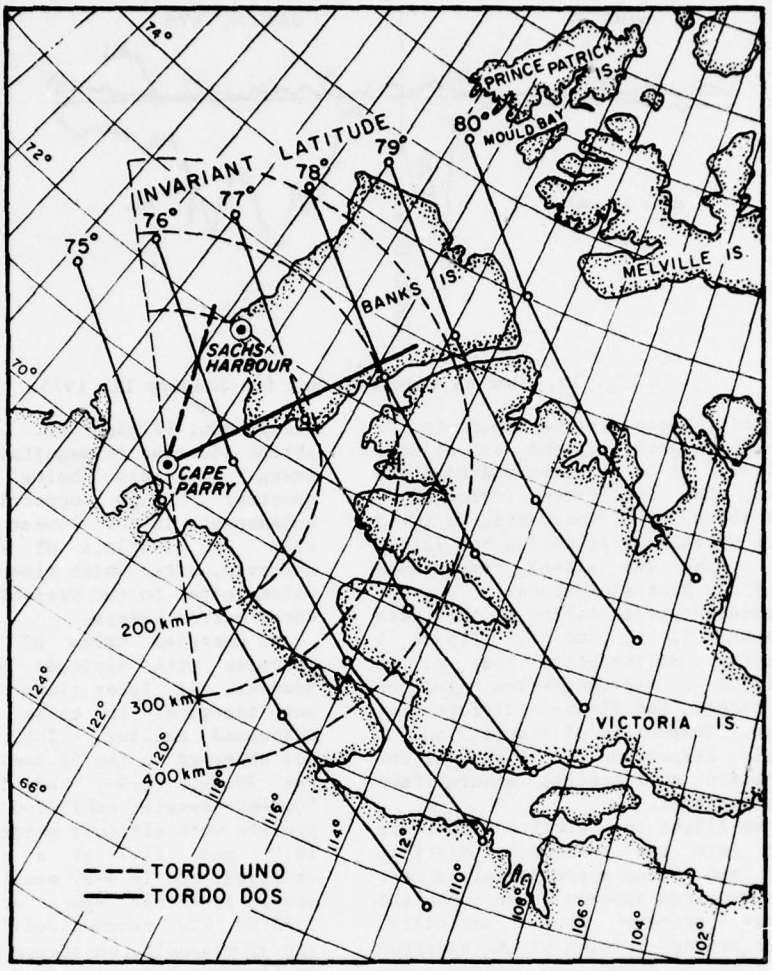

Fig. 3. Tordo Uno and Dos trajectories projected to 100 km along the earth's magnetic field.

atmospheric photoelectrons and very weak high-energy electrons were observed (Figure 8). A maximum in the photoelectron flux was observed between approximately 300 and 340 km. Mantas and Bowhill [1975] predict a maximum in the downcoming photoelectron flux at approximately 290 km for a 90° solar zenith angle. Our peak was above this altitude, but the zenith angle (100°) was also larger. In addition, electron density fluctuations, causing the observed spread F, would result in fluctuations in the atmospheric photoelectron flux and a smearing of the altitudinal profile (G. P. Mantas, private communication, 1976).

Examination of the SPS data indicates that the cleft equatorward boundary was crossed at 0028:13.2 UT at an invariant latitude of 76.4° (Figure 9). From 0028:13.2 to 0029:10.8 UT the electron spectrum peaked at approximately 100-200 eV and varied in magnitude. The spectral shape is similar to shapes reported in the literature for the cleft [Winningham and Heikkila, 1974]. Subsequent to this time, two 'inverted V's' were observed, one centered at 0029:26.8 and the other at 00:31 UT. Morphologically, inverted V's are regions in energy-time spectrograms where the maximum count rate (region of maximum darkness or lightness, depending of film polarity) moves first to higher energy then to lower energy with advancing time, producing an inverted V shape. Between the two inverted V's the electron spectra were either peaked in the 100- to 200-eV range or were due to atmospheric photoelectrons.

Inspection of each electron spectrum during passage through the inverted V's indicated that on a gross scale the peak in the electron distribution function (particles cm^{-2} sr^{-1} eV^{-1} s^{-1}) was increasing and then decreasing in both energy and magnitude. In addition, several relative maxima were observed (see Figure 12). The spectrum in Figure 10a was obtained just prior to the first 'energized' spectrum in the second inverted V. It is well fitted by a Maxwellian distribution (dashed curved) with a 'temperature' of 1.7×10^6 °K and a density of 0.5 cm^{-3} (assuming isotropy). The solid circles represent a correction for atmospheric photoelectrons utilizing the spectrum measured at 0030:11.6 UT. Spectra in Figure 10b are representative of the peaked distributions in the second inverted V.

All-sky camera data were obtained from Sachs Harbour, which at the time of Tordo Dos had just

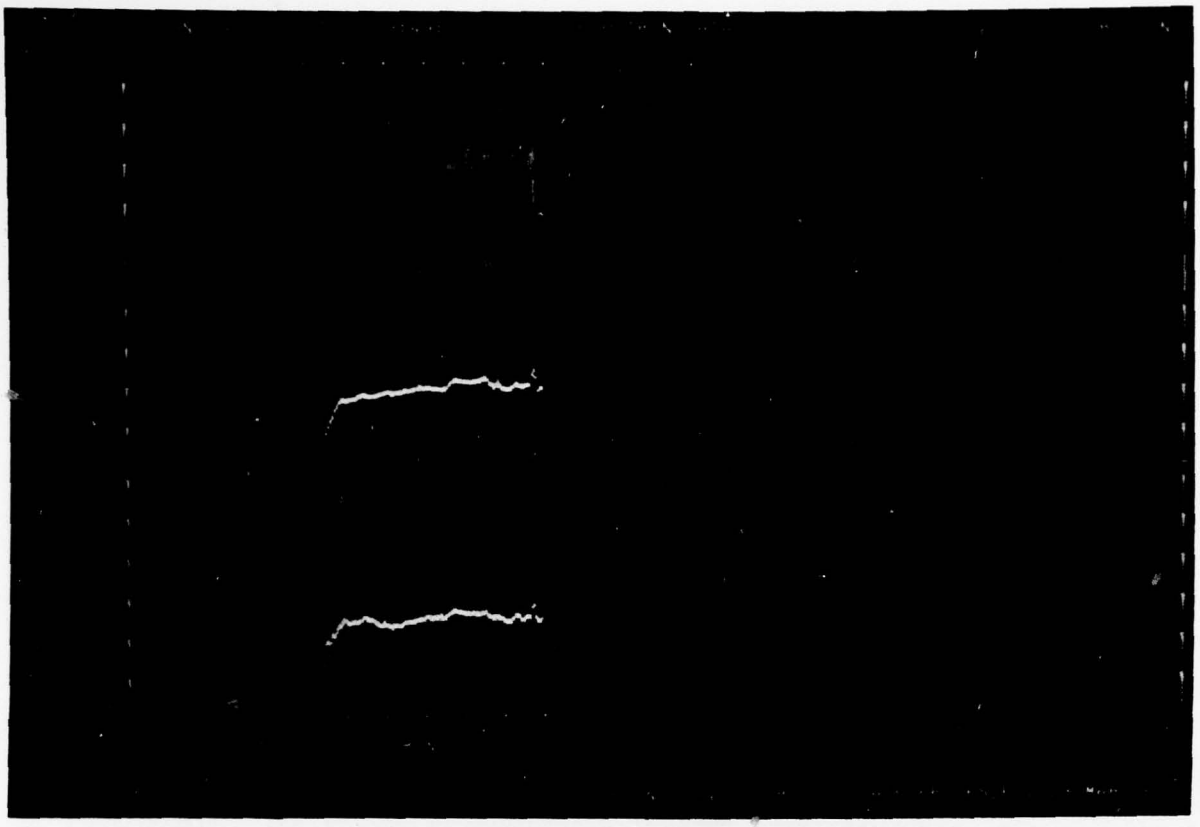

Fig. 4. Electron energy-time spectrogram for Tordo Uno.

entered astronomical twilight (12° solar depression angle). In the all-sky camera data, faint auroras are visible toward the north, and their positions are plotted in Figure 9 together with those of the two inverted V events observed by the rocket particle detectors and cleft returns deduced from the ionosonde data. All the data shown have been mapped to an altitude of 160 km. The height of 160 km used for calculating the position of the auroras was selected on the basis of the energy spectra (Figure 8) and luminosity profiles derived by Rees [1963].

As can be seen in Figure 9, auroras were observed only in the vicinity of the second inverted V event. No auroral form associated with the first event could be discerned in the data. This at first appeared strange considering the very similar energies and energy fluxes in the two events. As will be discussed below, the explanation is to be found in a combination of viewing angles from Sachs Harbour and the latitudinal width of the two precipitation events.

From Figure 8 we find a characteristic energy in the two events of 1 keV and an energy flux of about 1 erg/cm^2 s sr or 3 ergs/cm^2 s (assuming isotropy). For a 1-keV characteristic energy, Rees and Luckey [1974], calculate a column emission rate of 0.16 kR/erg/cm^2 s in 4278 Å and a corresponding emission rate ratio 5577/4278 Å of 6. Thus the estimated brightness of the form, if overhead, would be 3 x 0.16 x 6 = 3 kR in 5577Å. The forms are not overhead but are off to the northeast at an elevation angle of about 45° and 35°, respectively, and the SPS data (Figure 8) indicate the latitudinal width of the precipitation in the second event to be 3 times that of the first. Romick and Belon [1967] have calculated the brightness of an aurora for various values of width, position relative to the observer, and height luminosity profile. They find that the brightness of an arc 0.3° wide at an elevation angle of 35° (very similar to the values for the second inverted V event) would be 0.35 of the overhead value. Further, they find that auroras well away from the zenith have a brightness roughly proportional to their thickness, all other things being equal. With these corrections for aspect and width applied the auroras associated with the two inverted V events would appear with a brightness of 0.3 and 1 kR with respect to an observer at Sachs Harbour.

Under ideal conditions the 35-mm f 1.2 all-sky camera used at Sachs Harbour can resolve forms of slightly less than 1 kR in 5577 Å [Romick and Brown, 1971]. Thus the aurora associated with the first inverted V event (0.3 kR) should not be visible in the all-sky data even under ideal conditions, and given the twilight condition during the experiment, the aurora (1 kR) associated with the second inverted V should only be marginally detectable, which is in good agreement with the actual data.

It should be noted that the 6300-Å photometer

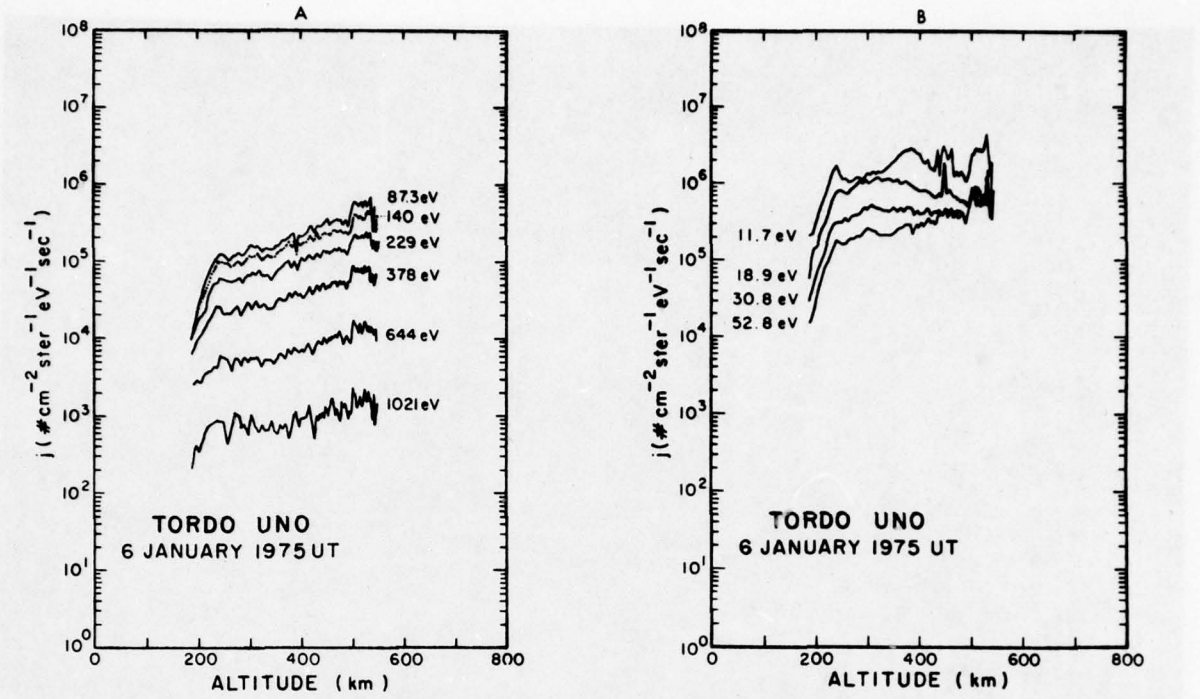

Fig. 5. Differential number flux versus altitude for Tordo Uno.

observed, in addition to the auroral form also detected by the all-sky camera, a faint arc just north of Sachs Harbour at an invariant latitude of 76.4°. The photometer was scanning geographic north-south and thus was pointing away from the rocket trajectory, and it is uncertain what relevance these measurements have to the observations along the rocket trajectory.

A strong oblique E layer return is seen in the Cape Parry ionograms, and several returns are also seen in the Sachs Harbour ionograms. By assuming that the returns come from ionospheric structures aligned along constant magnetic latitude a triangulation can be made to determine the location of the irregularity. By triangulating on the strongest oblique E layer return its position was found to lie within the region of the second inverted V event as shown in Figure 9.

From Figure 9 it can be seen that the cleft as measured by the SPS was indeed poleward of Sachs Harbour by a few tenths of a degree. The position of the cleft as determined by the SPS (76.4°) is coincident with the aforementioned weak red arc even though they are separated by approximately 4° of longitude.

As in Tordo Uno, the proton fluxes were very weak. It should be noted that the SPS as used in Tordo Uno and Dos was approximately 20 times more sensitive than were the Isis SPS's. (The main increase in sensitivity is due to the increased accumulation period.)

Discussion and Conclusions

The exact location of the Tordo Uno measurements relative to the cleft boundaries is difficult to establish. Only one detail can be stated with certainty, that is, Tordo Uno was poleward of the equatorward boundary of the cleft. Comparison of Tordo Uno positive ion fluxes with Isis results indicate a position in the poleward portion of the cleft. This conclusion is based on two characteristics of the positive ions, namely, their low intensity and low average energy. Typical results from Isis show the hardest and most intense fluxes at the equatorward edge of the cleft with a subsequent poleward softening and decrease in intensity.

Another possible interpretation of the results would be that the observed electrons are polar rain electrons [Winningham and Heikkila, 1974]. However, several facts argue against this interpretation. The observed density of the primary electrons is as high as approximately 5 cm^{-3}. Winningham and Heikkila's [1974] results show the polar rain fluxes to be only a few percent of the cleft fluxes. If these densities were measured in the polar cap, cleft densities would be >100 cm^{-3} and by inference, magnetosheath densities would be at least as large. Such cleft densities are rarely observed. An even more telling argument comes from concurrent measurements of solar wind densities by Imp 7 (courtesy of W. C. Feldman) and magnetosheath densities by Hawkeye (Figure 6) (courtesy of L_3 A. Frank). Both were approximately 10 cm^{-3} during the period of Tordo Uno.

Comparison with the Hawkeye results (Figure 6) indicates a factor of approximately 2 decrease in density between the magnetosheath and the poleward portion of the cleft. The results of Akasofu et al. [1973] demonstrate that the poleward portion of the cleft maps to the inner edge of the magnetospheric boundary layer (see their Figure 11). Additionally Akasofu et al. show the boundary layer

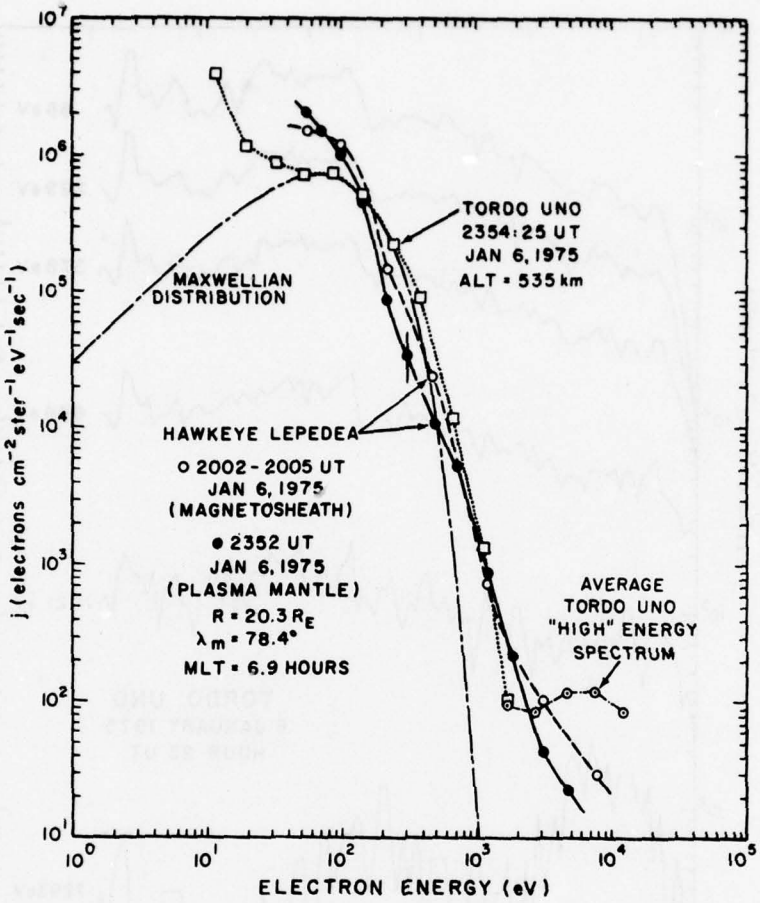

Fig. 6. Electron spectra from Tordo Uno and Hawkeye for January 6, 1975.

densities to be less than or equal to the magnetosheath density and to decrease with increasing inward penetration of the boundary layer. Thus the most consistent interpretation of the results places Tordo Uno in the poleward portion of the cleft.

The 'high-energy' portion of the electron spectrum observed by Tordo but not by Hawkeye in Figure 6 can be attributed to an internal magnetospheric source, i.e., drifting energetic electrons from the nightside. Recent papers by McDiarmid et al. [1976] and Haerendel and Paschmann [1975] have shown that trapped energetic electrons are observed concurrently with entry layer and cleft plasma. Eastman et al. [1976] find that electron spectra in the boundary layer develop high-energy (few keV) tails with increasing inward penetration of the boundary layer and have associated these to leakage of magnetospheric plasma into the boundary layer. In the present case, Tordo Uno sampled only inside the loss cone, and thus nothing can be said concerning the pitch angle distribution. Spectrally, the electrons are similar to low-altitude polar satellite measurements in the same region [Winningham, 1972].

The initial energy-dependent increase in electron flux with altitude (<250 km) is due to the interaction of the primary beam [Banks et al., 1974, Figure 16] with the atmosphere. Above this altitude, spatial and/or temporal changes predominate. In summary, Tordo Uno and the associated barium jet were launched into the poleward portion of the afternoon cleft which contained unenergized magnetosheathlike electrons. With reference to the work by Jeffries et al. [1975], Figure 3 shows the path of the barium plasma leaving the vicinity of Tordo Uno to be essentially directly antisolar across the polar cap into the nightside auroral zone.

By comparison, we know the position of Tordo Dos vis-à-vis the cleft equatorward boundary relatively well. Tordo Dos was launched equatorward of the cleft, crossed its equatorward boundary, and encountered two inverted V's in the cleft prior to barium injection. In assuming the cleft boundary to be zonal (i.e., parallel to magnetic latitude) over the short longitude span traversed and to be fixed for the duration of the Tordo Dos flight, barium injection occurred approximately 1.9° into the cleft. The latter assumption is supported by concurrent results from the sounders.

The electron precipitation observed in Tordo Dos was dramatically different from Tordo Uno. 'Monoenergetic' peaks were observed (Figure 10b) in the electron spectra, and the energy of these peaks varied systematically, i.e., the inverted V's. Such behavior has been attributed to

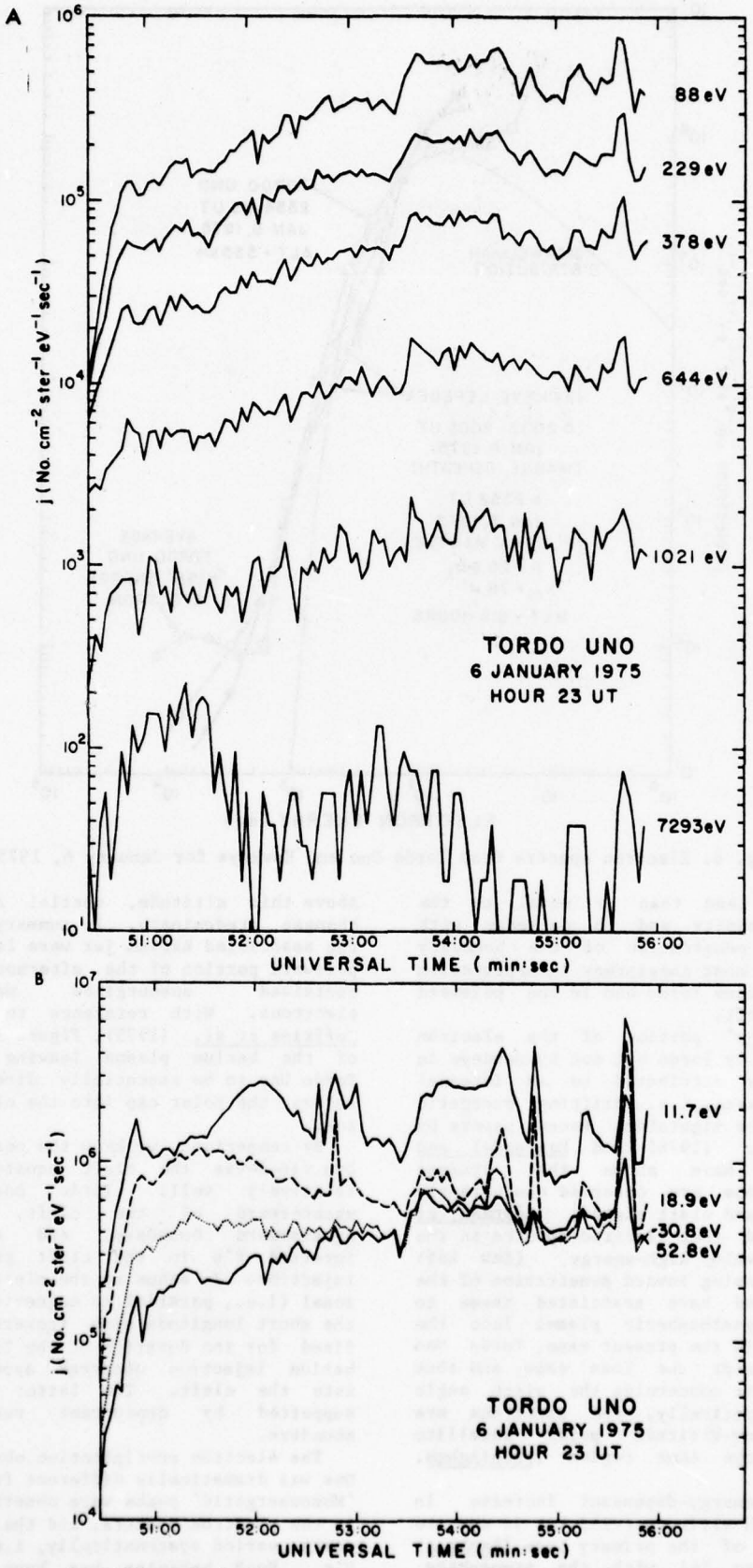

Fig. 7. Differential energy flux versus time (distance) for Tordo Uno.

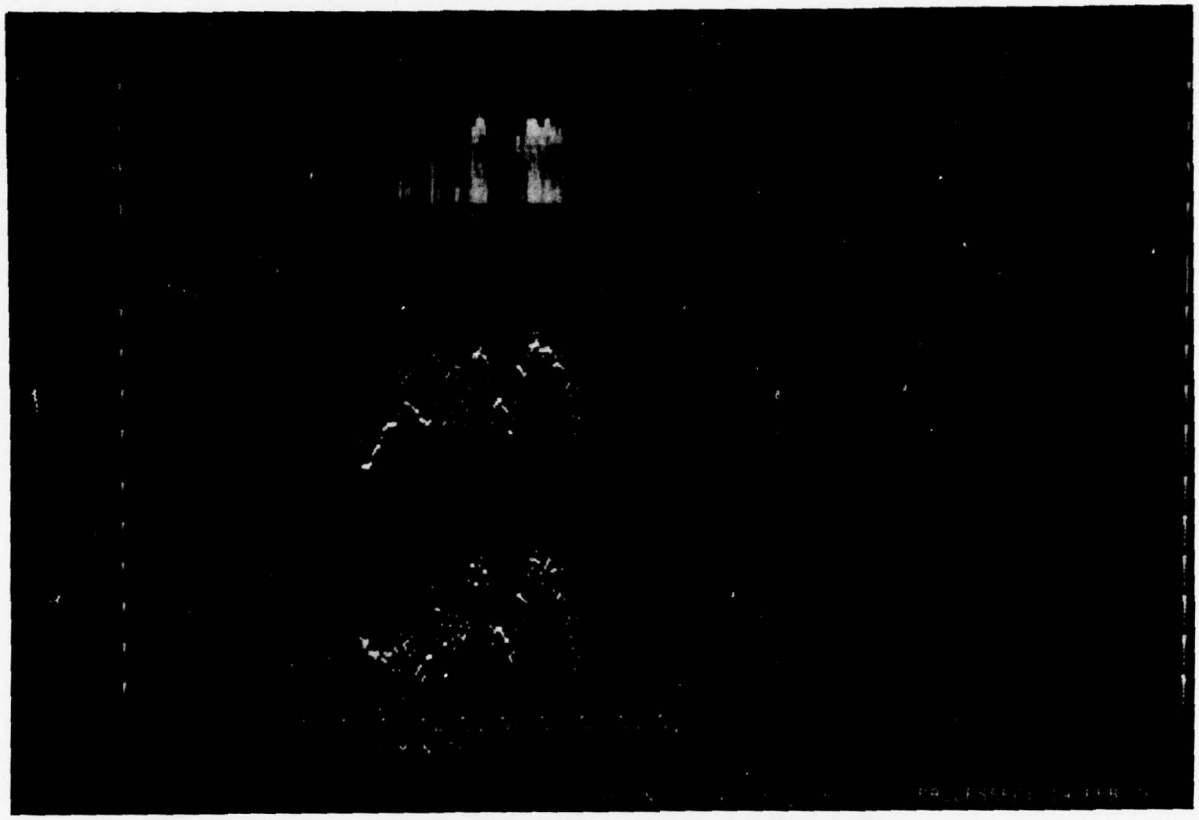

Fig. 8. Electron energy-time spectrogram for Tordo Dos.

acceleration by an electric field parallel to the earth's magnetic field [Burch et al., 1976, and references therein]. To investigate this possibility, the numerical model of Evans [1974] was applied to the data. It should be noted that the experimental data are inadequate in pitch angle and spectral resolution to prove or or disprove uniquely any theory; only consistency can be shown.

With the aforementioned reservations in mind the experimental spectra are easily derivable from Evans' model. An example of a spectrum from the second inverted V is given in Figure 11. A least squares Maxwellian fit is made to the high-energy tail of the observed fluxes, and the temperature of the assumed Maxwellian plasma at the top of the accelerator is determined as indicated on the figure. The probable error from the least squares fit is also indicated. The initial Maxwellian is allowed to fall through a potential drop V_o, producing a jetted beam at the bottom of the accelerator. The beam then produces backscattered and secondary electrons upon interaction with the atmosphere. those upgoing electrons with energies less than eV_o are reflected by the parallel electric field and would be observed by the instrument as low energy downgoing particles. The Maxwellian fit together with a choice of V_o fixes the density n of the assumed Maxwellian plasma. The accelerating potential is then varied, producing the solid curve at low energies in Figure 11, until a 'best fit' to the data is obtained. Thus for this model the only free parameters which we vary are V_o and the B Ratio, the ratio of magnetic field strengths at the accelerator exit and at the top of the atmosphere.

For the backscatter calculations we used the electron impact ionization cross section for atomic oxygen from Banks et al. [1974] (see also Opal et al. [1971]). Use of the cross section for N_2 would increase the low-energy fluxes by about 12% at about 100 eV.

Figure 12 presents the results of these calculations for the second inverted V. All points except the first and last are derived or 'fitted' quantities. This first point (denoted by a circle) corresponds to the 'nonaccelarated' spectrum (Figure 10a) encountered just prior to the second inverted V (see Figure 12). The last point (also denoted by a circle) is from a temperature fit only at that point. It can be seen that even though the potential varied dramatically, the density (assuming source isotropy) and the temperature were constant within one standard deviation. In addition, the 'nonaccelerated' density and temperature lie within the same bounds.

Note that the nonaccelerated values are local quantities and the derived quantities refer to the input of the 'linear accelerator,' as described above. Thus the inverted V has as its source population a Maxwellian with a density of 0.87 ± 0.25 cm^{-3} and a temperature of 117 ± 24 eV.

If all the assumptions in Evans' model are valid in this case, the approximate position of the exit of the accelerator can be determined

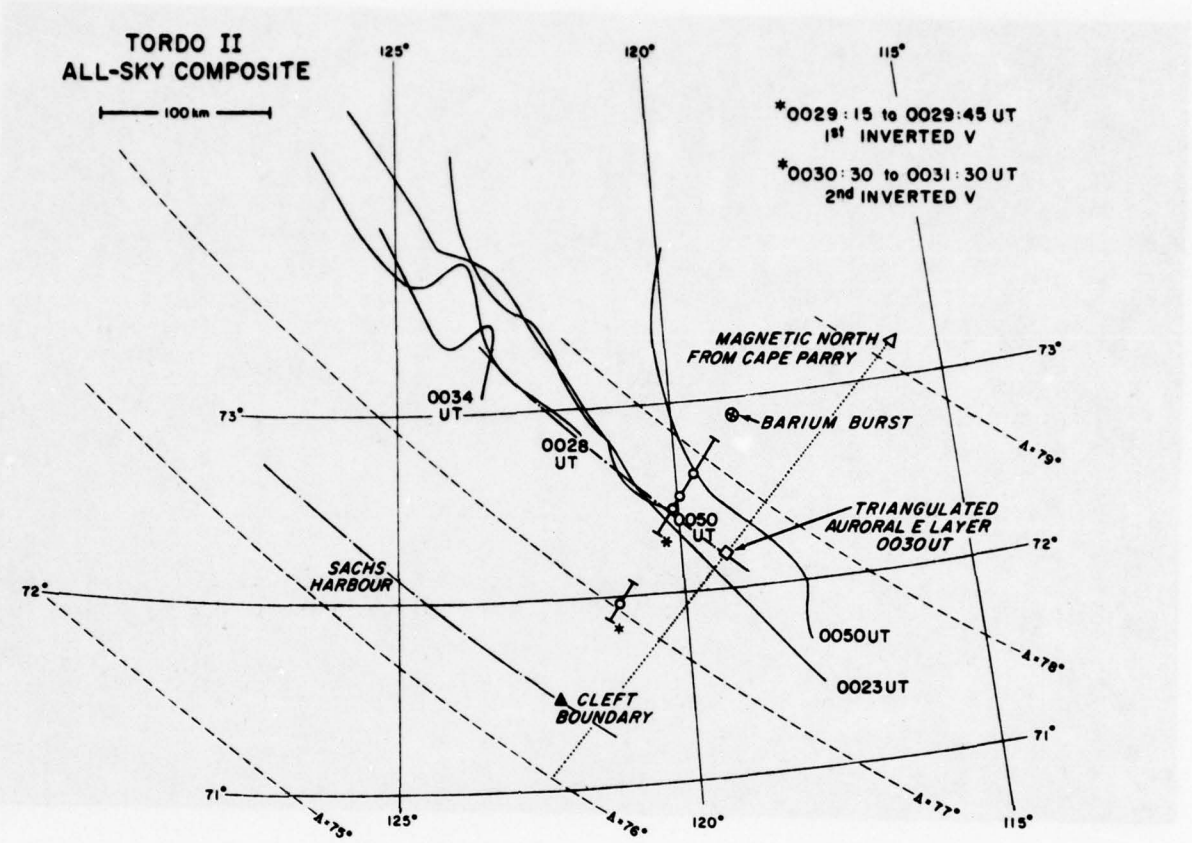

Fig. 9. Schematic of geographic location of observed auroral arcs, inverted V events, barium release, and returns observed by the ionosondes. All positions have been reduced to the 160-km altitude level.

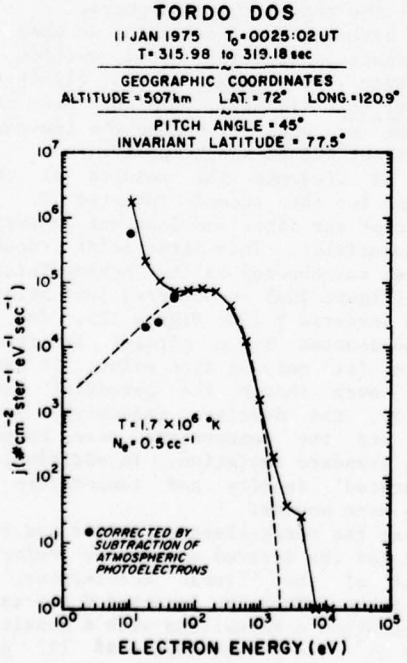

Fig. 10a. Electron spectrum obtained prior to entry into second inverted V observed by Tordo Dos.

from the B Ratio. The derived value of 12.5 gives an approximate lower limit of $1R_E$ above Tordo or 2 R_E geocentric. This value is consistent with the lower limit value obtained by assuming that the collimation cone had expanded just enough to include the measured pitch angle.

Our results are in basic agreement with those of Burch et al. [1976] except for one feature. Burch et al. pointed out that in all the cleft inverted V's they observed the characteristic energy (temperature) went up as the acceleration potential increased. They interpreted this as a heating as well as an acceleration of the source population. The results as shown in Figure 12 indicate that no statistically important heating occurred for this second inverted V event on Tordo Dos. However, some remarks on the nature of the high energy tail are in order. We found that with few exceptions the more high energy data points we included in the least squares routine, the hotter the temperature of the plasma. Thus the high energy tail in the inverted V event is non-Maxwellian. Since the potential is chosen primarily to find a fit to the lower energy portion of the spectrum and since this depends mostly on the fluxes near the peak of the beam, we used only two or three data points near the beam maximum to determine the temperature for the results shown in Figure 12 (for example, in Figure 11, fluxes at energies of 634.4, 1033, and 1655 eV). In addition, data

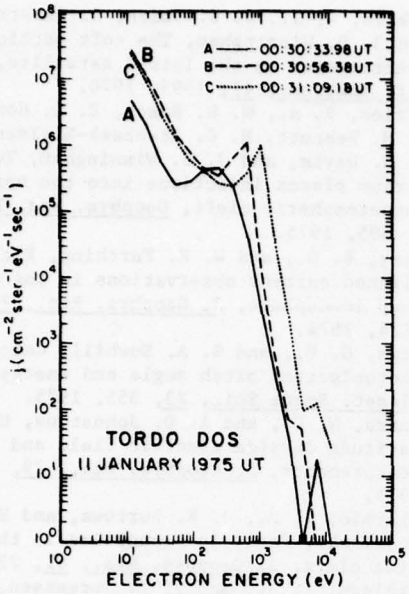

Fig. 10b. Representative electron spectra obtained in second inverted V observed by Tordo Dos.

points at the lower intensity levels are experimentally less well determined.

To test this apparent disagreement with Burch et al., we ran new 'fits' using the criterion that we would use all data in the tail with flux values greater than 10^3 cm^{-2} s^{-1} sr^{-1} eV^{-1}. By using this criterion, only 8 of the 23 cases are changed. (In one case, at t= 0030:30, the temperature went from 54 to 127 eV, but we could no longer find a reasonable 'fit' to the spectrum.) The temperatures of these eight cases did come out higher than before, necessitating reduced values for V_o in some cases, with a general trend of temperature and V_o proportionality. Linear regression analysis in this case yields a temperature of 0.06 V_o + 102 eV, but the correlation is not high (correlation coefficient is 0.35).

It therefore appears that our analysis is consistent with no apparent heating of the plasma at energies near the beam maximum, but some heating at higher energies proportional to V_o cannot be ruled out. It is equally possible that the non-Maxwellian nature of the tail is a feature of the original plasma (see Figure 10a).

Burch et al. [1976] reported the cleft inverted V's to be in a region of antisunward convection. No convection measurements were available at the position of the Tordo Dos inverted V's. However, the barium streak was released approximately 7 km poleward of the second inverted V and drifted antisunward at approximately constant magnetic latitude [Jeffries et al., 1975, Figure 3].

In conclusion, Tordo Dos crossed the equatorward boundary of the cleft, traversed approximately 1.9° of its extent, and encountered two inverted V's. The inverted V's

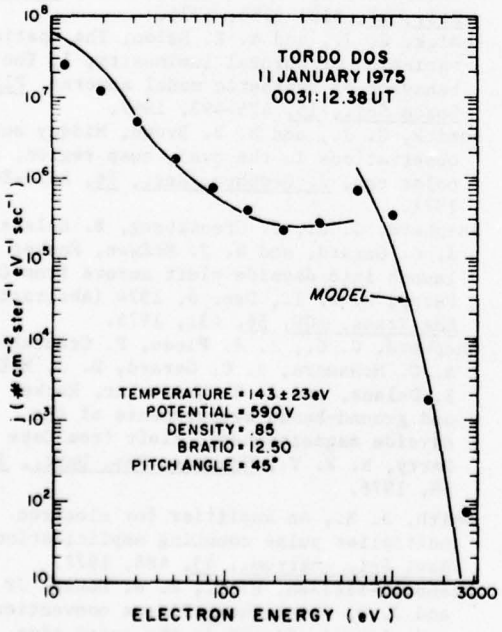

Fig. 11. Experimental and modeled electron spectrum for second inverted V in Tordo Dos data. Model spectrum generated by using the numerical model of Evans [1974].

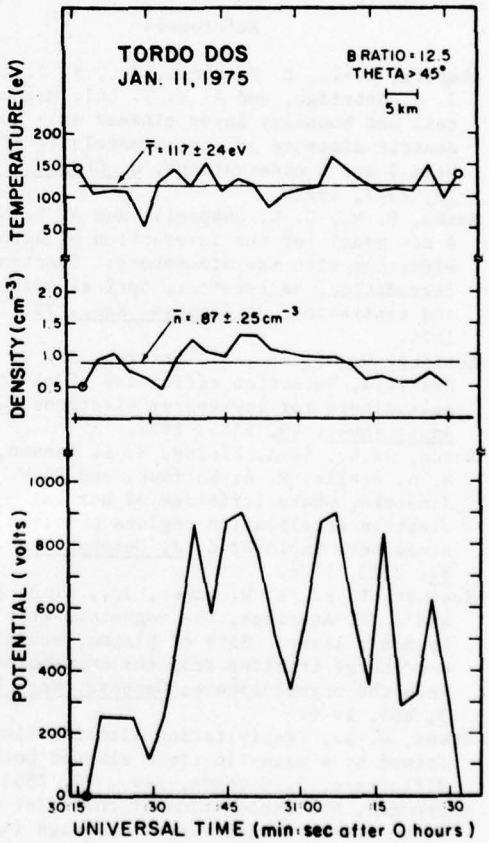

Fig. 12. Density and temperature derived from Evans' [1974] model for source spectrum of second inverted V observed by Tordo Dos and the necessary potential drop. See text.

can be well modeled by the model of Evans [1974] by utilizing a constant source temperature and density and a varying potential. A 'best guess' places the accelerator at a minimum geocentric distance of 2 R_E. The barium injected just subsequent to the second inverted V drifted essentially parallel to the cleft (i.e., at approximately constant magnetic latitude) and antisunward as opposed to the perpendicular and antisunward motion of Tordo Uno. The cloud motion and its dynamics will be detailed in a subsequent paper.

Acknowledgments. The UTD portion of this work was supported by ERDA contracts P/O KH-69046-1 and LC5-83449-1, Air Force Geophysics Laboratory contract F19628-76-C-005, and the National Aeronautics and Space Administration grant NGR 44-004-124. The support of the Geophysical Institute was supported by NASA contract NGR 02-001-087. One of us (T.W.S.) would like to thank the Space Environment Laboratory, NOAA, Boulder, Colorado, for support, computer time, and technical assistance. Thanks go to Harold Fishbine, C. R. Thompson, Jack Frazier, and Lou Wadel, whose technical efforts made the present paper possible.

The Editor thanks I. B. McDiarmid and I. S. Mikkelsen for their assistance in evaluating this paper.

References

Akasofu, S.-I., E. W. Hones, Jr., S. J. Bame, J. R. Asbridge, and A. T. Y. Lui, Magnetotail and boundary layer plasmas at a geocentric distance of approximately 18 RE: Vela 5 and 6 observations, J. Geophys. Res., 78, 7527, 1973.

Banks, P. M., C. R. Chappell, and A. F. Nagy, A new model for the interaction of auroral electrons with the atmosphere: Spectral degradation, backscatter, optical emission, and ionization, J. Geophys. Res., 79, 1459, 1974.

Bunting, W. D., Jr., J. Tarstrup, and W. J. Heikkila, Detection efficiency of electron multipliers for low-energy electrons, J. Appl. Phys., 43, 1585, 1972.

Burch, J. L., S. A. Fields, W. B. Hanson, R. A. Heelis, R. A. Hoffman, and R. W. Janetzke, Characteristics of auroral electron acceleration regions observed by Atmosphere Explorer C, J. Geophys. Res., 81, 2223, 1976.

Eastman, T. E., E. W. Hones, Jr., S. J. Bame, and J. R. Asbridge, The magnetospheric boundary layer: Site of plasma, momentum and energy transfer from the magnetosheath into the magnetosphere, Geophys. Res. Lett., 3, 685, 1976.

Evans, D. S., Precipitating electron fluxes formed by a magnetic field aligned potential difference, J. Geophys. Res., 79, 2853, 1974.

Haerendel, G., Exploration of the polar cusp by an international rocket campaign (abstract), Eos Trans. AGU, 56, 430, 1975.

Haerendel, G., and G. Paschmann, Entry of solar wind plasma into the magnetosphere, in Physics of the Hot Plasma in the Magnetosphere, edited by B. Hultqvist and L. Stenflo, pp. 23-43, Plenum, New York, 1975.

Heikkila, W. J., J. B. Smith, J. Tarstrup, and J. D. Winningham, The soft particle spectrometer in the Isis-1 satellite, Rev. Sci. Instrum., 41, 1393, 1970.

Jeffries, R. A., W. H. Roach, E. W. Hones, Jr., E. M. Wescott, H. C. Stenbaek-Nielsen, T. N. Davis, and J. D. Winningham, Two barium plasma injections into the northern magnetospheric cleft, Geophys. Res. Lett., 2, 185, 1975.

Ledley, B. G., and W. H. Farthing, Field-aligned current observations in the polar cusp ionosphere, J. Geophys. Res., 79, 3124, 1974.

Mantas, G. P., and S. A. Bowhill, Calculated photoelectron pitch angle and energy spectra, Planet. Space Sci., 23, 355, 1975.

Maynard, N. C., and A. D. Johnstone, High-latitude dayside electric field and particle measurements, J. Geophys. Res., 79, 3111, 1974.

McDiarmid, I. B., J. R. Burrows, and E. E. Budzinski, Particle properties in the day-side cleft, J. Geophys. Res., 81, 221, 1976.

Mikkelsen, I. S., and T. S. Jorgensen, Electric fields in the cleft region observed by Ba^+ clouds (abstract), Eos Trans. AGU, 55, 70, 1974.

Opal, C. B., W. K. Peterson, and E. C. Beatty, Measurement of secondary electron spectra produced by electron impact ionization of a number of simple gases, J. Chem. Phys., 55, 4100, 1971.

Rees, M. H., Auroral ionization and excitation by incident energetic electrons, Planet. Space Sci., 11, 1209-1218, 1963.

Rees, M. H., and D. Luckey, Auroral electron energy derived from ratio of spectroscopic emissions, 1, Model computations, J. Geophys. Res., 79, 5181-5185, 1974.

Romick, G. J., and A. E. Belon, The spatial variation of auroral luminosity, 1, The behavior of synthetic model auroras, Planet. Space Sci., 15, 475-493, 1967.

Romick, G. J., and N. B. Brown, Midday auroral observations in the oval, cusp region, and polar cap, J. Geophys. Res., 76, 8420-8424, 1971.

Shepherd, G. G., F. Creutzberg, B. Delana, J. C. Gerard, and D. J. McEwen, Rocket launch into dayside cleft aurora from Cape Parry, N. W. T., Dec. 6, 1974 (Abstract), Eos Trans. AGU, 56, 431, 1975.

Shepherd, G. G., J. F. Pieau, F. Creutzberg, A. G. McNamara, J. C. Gerard, D. J. McEwen, B. Delana, and J. H. Whitteker, Rocket and ground-based measurements of the dayside magnetospheric cleft from Cape Parry, N. W. T., Geophys. Res. Lett., 3, 69, 1976.

Smith, J. B., An amplifier for electron multiplier pulse counting amplicications, Rev. Sci. Instrum., 43, 488, 1972.

Stenbaek-Nielsen, H. C., E. W. Hones, Jr., and J. D. Winningham, Plasma convection and electric fields in the quiet time magnetospheric cleft from the Tordo Dos experiment (abstract), Eos Trans. AGU, 56, 432, 1975.

Stiles, G. S., E. W. Hones, Jr., J. D. Winningham, R. P. Lepping, and B. J. Delana,

Ionosonde observations of the northern magnetospheric cleft during December 1974 and January 1975, J. Geophys. Res., 82, 67, 1977.

Temerin, M., C. W. Carlson, F. S. Mozer, and M. C. Kelly, Rocket measurements of polar cusp electric fields and plasma density (abstract), Eos Trans. AGU, 56, 430, 1975.

Torbet, R. B., and C. W. Carlson, Impulsive ion injection into the polar cap, paper presented at Summer Advanced Study School, Magnetospheric Particles and Fields, Def. Nucl. Agency, Lockheed Palo Alto Res. Lab., and Off. of Nav. Res., Graz, Austria, 1975.

Torbet, R. B., K. A. Anderson, and C. W. Carlson, Observations of low and medium energy particles in the polar cusp (abstract), Eos Trans. AGU, 56, 430, 1975.

Ungstrup, E., A. Bahnsen, J. K. Olesen, F. Primdahl, F. Spangslev, W. J. Weikkila, D. M. Klumpar, J. D. Winningham, U. Fahelson, C.-G. Falthammar, and A. Pedersen, Geophys. Res. Lett., 2, 345, 1975.

Ungstrup, E., A. Bahnsen, J. K. Olesen, F. Primdahl, F. Spangslev, W. J. Heikkila, D. M. Klumpar, J. D. Winningham, U. Fahleson, C.-G. Falthammar, and A. Pedersen, Particle, field, and plasma observations in the low altitude prenoon cleft (abstract), Eos Trans. AGU, 56, 430, 1975b.

Wescott, E. M., H. C. Stenbaek-Nielsen, T. N. Davis, R. A. Jeffries, W. H. Roach, and E. W. Hones, Jr., Anti-solar polar cap convection and magnetic field configuration observations from the disturbed time Tordo Uno magnetospheric cleft injection experiment (abstract), Eos Trans. AGU, 56, 432, 1975.

Winningham, J. D., Characteristics of magnetosheath plasma observed at low-altitudes in the dayside magnetospheric cusps, in Earth's Magnetospheric Processes, edited by B. M. McCormac, pp. 68-80, D. Reidel, Dordrecht, Netherlands, 1972.

Winningham, J. D., and W. J. Heikkila, Polar cap auroral electron fluxes observed with Isis 1, J. Geophys. Res., 79, 949, 1974.

Winningham, J. D., R. A. Jeffries, E. W. Hones, Jr., and T. N. Davis, Cleft particle observations in conjunction with barium shaped charge releases (abstract), Eos Trans. AGU, 56, 432, 1975a.

Winningham, J. D., F. Yashuhara, S.-I. Akasofu, and W. J. Heikkila, The latitudinal morphology of 10-eV to 10-keV electron fluxes during magnetically quiet and disturbed times in the 2100-0300 MLT sector, J. Geophys. Res., 80, 3148, 1975b.

(Received October 4, 1976;
accepted December 13, 1976.)

VOL. 82, NO. 29 JOURNAL OF GEOPHYSICAL RESEARCH OCTOBER 1, 1977

Numerical Model of the Convecting F_2 Ionosphere at High Latitudes

W. C. KNUDSEN

Lockheed Palo Alto Research Laboratory, Palo Alto, California 94304

P. M. BANKS

Utah State University, Logan, Utah 84322

J. D. WINNINGHAM AND D. M. KLUMPAR

University of Texas at Dallas, Richardson, Texas 75080

Time-dependent behavior of tubes of *F* layer plasma is computed for tubes carried around several flow paths in the polar region. The flow paths are those proposed previously by Knudsen (1974). Ionization sources include direct and scattered solar photons and measured fluxes of precipitating energetic electrons. Computed electron concentrations are compared with measured concentrations from topside sounder data obtained in the same satellite pass as the energetic electron flux data. The following conclusions are drawn: The proposed convection pattern produces a tongue of *F* layer plasma over the polar cap with electron concentrations consistent with the measured concentrations. Had the *F* layer been assumed to be nonconvecting over the polar cap, the computed concentrations would have been a factor of 10 too small. Rapid convection of plasma across the cleft prevents significant increase in N_mF_2 at the cleft. Rapid convection must exist through the intense nightside auroral energetic particle precipitation zones, or a compensating electron loss mechanism must develop to prevent the buildup of an ionization ridge. A mid-latitude trough is formed by the proposed convection pattern with only normal *F* layer recombination processes operating. The low concentration in the trough is maintained by scattered solar EUV photons. The trough predicted by the numerical model is not observed in the topside sounder data.

INTRODUCTION

In a previous paper, *Knudsen* [1974] presented a model for the convection field of the high-latitude *F* layer and evaluated semiquantitatively the expected time-dependent behavior of a tube of *F* layer plasma carried around the polar regions by the field. The proposed field appeared to explain many of the high-latitude *F* layer anomalies. The purpose of the present paper is to present the initial results of a more detailed numerical study of the behavior of the high-latitude *F* layer. Tubes of ionization are subjected to time-dependent ionization rates from both solar photons and precipitating energetic electrons as the tubes follow the convection field proposed in the previous paper, and the time-dependent response of the plasma within the tube is computed.

NUMERICAL MODEL

The time-dependent behavior of the plasma within a magnetic flux tube was computed with a numerical code developed by *Schunk and Walker* [1973]. The code solves the coupled momentum and continuity equations for NO^+, O_2^+, and O^+ ions in the *E* and *F* regions. Minor changes were made in the code to permit the addition of ionization rates resulting from energetic electron fluxes and also from solar EUV scattered into the nightside of the ionosphere. The code was also modified to permit the base of the flux tube to change in latitude and longitude with elapsed time in a prescribed manner.

The code does not solve the energy balance equation, and consequently, it is necessary to specify T_e and T_i. For this study we have set both T_e and T_i equal to the neutral gas temperature T_n. Heating of the thermal electron gas by fluxes of soft electrons with energies of a few tens of electron volts is thus neglected, and the enhancement of electron concentrations at altitudes above approximately 400 km in response to electron heating will not be reproduced in the model.

The variations of the neutral constituents N_2, O_2, and O with latitude and local time were derived from the model atmosphere of *Jacchia* [1971] for winter (solar declination, $-23°$) and medium solar activity ($\bar{F}_{10.7} = 130 \times 10^{-22}$ W m^{-2} Hz^{-1}). The NO density was the same as that used by *Schunk and Walker* [1973].

The numerical solution was obtained over the altitude range 120–500 km. The upper altitude limit was set at 500 km to ensure proper convergence of the solution for reasonably sized time steps. The fluxes of NO^+ and O_2^+ were set equal to zero at the upper boundary. To simulate the loss of O^+ through operation of the polar wind, the upward velocity of O^+ ions at the 500-km boundary was assumed to be constant at 10 m s^{-1}. At the lower boundary the O_2^+ and NO^+ concentrations were arbitrarily set to 10^9 cm^{-3}. Also at this boundary the O^+ density was assumed to be in chemical equilibrium and was set equal to

$$[O^+] = \frac{P(O^+)}{k_1[N_2] + k_2[O_2]}$$

where $[O^+]$, $[N_2]$, and $[O_2]$ are the appropriate densities and $P(O^+)$ the ion production rate of O^+; k_1 and k_2 are reaction rates defined by *Schunk and Walker* [1973]. The concentrations of NO^+ and O_2^+ near the lower boundary are governed primarily by chemical reaction rates, so that their concentrations a short distance above the lower boundary are insensitive to the arbitrarily assigned values.

The gyrofrequency of the ions is comparable to or less than their collision frequency at and below an altitude of approximately 180 km. The ions do not 'follow' the flux tubes below this altitude. We may expect therefore that the model results

Paper number 7A0474.

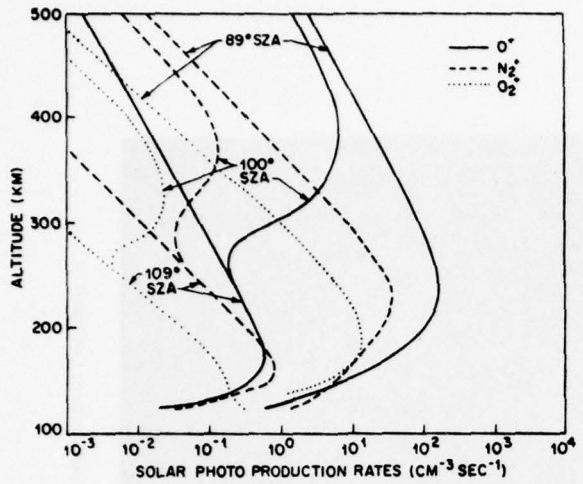

Fig. 1. Production rates of O^+, N_2^+, and O_2^+ by solar photons at three SZA's computed by the numerical model. Those at 109° SZA represent background rates from scattered photons.

below 180 km will be in error at the E and F_1 altitudes near boundaries separating regions of different ion production rates.

The vertical drift which may be imparted to the plasma by the electric field causing the convection of the plasma and also by neutral winds has been neglected in this first model. Vertical drift was felt to be a second-order effect which could be studied after first-order effects were clarified. Some discussion of the expected drift is given by *Knudsen* [1974].

The displacement of the magnetic pole from the geographic pole imparts a universal time dependence into the high-latitude F layer concentration, which is to be the subject of a future study. For the present study we assume that the magnetic and geographic axes are collinear.

The ionization sources included in the model are solar EUV photons, both direct and scattered, and precipitating electrons. The method of calculating the direct photo-ionization rates for N_2, O_2, and O is described by *Schunk and Walker* [1973]. We are interested in the high-latitude F layer during winter in the present study and have calculated the Chapman grazing incidence function using −23° for the solar declination angle. To simulate the ionization rates from scattered EUV, the ionization rates from direct photons were added to background ionization rates produced by scattered photons. The background ionization rates were computed with the same code that was used for the direct ionization rates with the following changes. The solar zenith angle was set to zero, and the photon fluxes in the 11 spectrum intervals suggested by *Hinteregger et al.* [1965] were set to zero except for the wavelength intervals 1027–911 Å, 630–460 Å, and 370–280 Å. The fluxes in these intervals were set at 1×10^7, 1×10^7, and 1×10^8 photons cm^{-2} s^{-1}, respectively, and correspond to H Lyman β, He I 485 Å, and He Lyman α [*Chen and Harris*, 1971]. The total photo-ionization rates from both the direct and the scattered photons for three solar zenith angles (SZA's) are given in Figure 1. Those for a SZA of 109° are effectively the background rates with no contribution from the direct rates.

Ionization rates from precipitating electrons were computed by using energy distribution functions measured by the soft particle spectrometer (SPS) on the Isis 2 satellite. The energy-time spectrograms over the northern polar cap on December 15 (day 349, orbit 3278), 1971, are shown in Figures 2 and 3. The satellite crossed the northern polar cap from approximately 1200 MLT (magnetic local time) to 2300 MLT (Figures 2 and 3). Spectra at times labeled 1–11 were selected as being representative and were used in computing the ionization rates produced by the electrons. The locations of the satellite at the times at which the spectra were recorded are shown in Figure 7. The electron precipitation was assumed to be uniform in local time for approximately 3 hours on either side of the satellite track in both the dayside cleft region and the nightside auroral region. Auroral oval emission data in 5577 Å and 3914 Å recorded on the Isis 2 satellite [*Lui and Anger*, 1973] indicate that on the nightside of the oval the precipitation was, in fact, more intense in the premidnight sector than in the postmidnight sector.

The data from the satellite pass shown represent a quiet period. The AE index was below 100 γ for 28 hours prior to the pass except for two short excursions. Sixteen hours prior to the pass the AE index went as high as 300 γ during a 2-hour period, and approximately 3 hours before the pass it rose to approximately 150 γ for a 2-hour period.

The proton number and energy fluxes over the polar region for the pass shown were 2 orders of magnitude lower than the corresponding electron fluxes and have been neglected as an important source of ionization.

Electron spectra for several pitch angles in the downgoing hemisphere at each of the 11 regions enumerated in Figures 2 and 3 have been analyzed and used to derive the spectra illustrated in Figures 4 and 5. The precipitating flux was reasonably uniform with pitch angle, and the spectra shown are considered representative of the spectra observed at each region. The SPS on Isis 2 measures electron flux down to 5 eV. For the purpose of computing ionization rates from these fluxes we have arbitrarily extended the measured 10-eV fluxes to 1 eV at a constant level. Since the numerical code used for computing thermal plasma behavior does not balance energy and since electrons with less than 10-eV energy produce no significant ionization, this extrapolation has no significant effect on the numerical results.

The ion production rates from the electron spectra presented above were computed with an early version of a computer code for the interaction of energetic electrons with the atmosphere developed by *Banks et al.* [1974]. Production rates for regions 2 and 9, representative of the cleft and nightside auroral regions, are shown in Figure 6.

The flow paths around which the plasma tubes were carried in the numerical simulation are those presented in an earlier paper by *Knudsen* [1974] and are reproduced as Figure 7. Results were obtained only for paths labeled II–VI. The flow paths define the motion of plasma tubes as seen by an observer in a nonrotating frame of reference looking down on the north polar cap. That is, the motion includes corotation so that the exposure of the plasma tubes to solar EUV photons is properly simulated. The tubes of plasma were convected across the dayside cleft at a velocity of 1 km/s and on across the cap at a velocity of 0.5 km/s. They were again convected across precipitation region 7 (Figure 3) at 1 km/s. Equatorward of the limit of closed field lines the tubes were convected between successive dots in 1 hour. Analysis of energetic electrons measured on Isis 2 at greater than 20 keV, greater than 40 keV, and greater than 200 keV indicates that the field lines were closed equatorward of 69°Λ (16 min, 40 s, Figure 3) and that no trapped distributions existed poleward of 70°Λ in the night

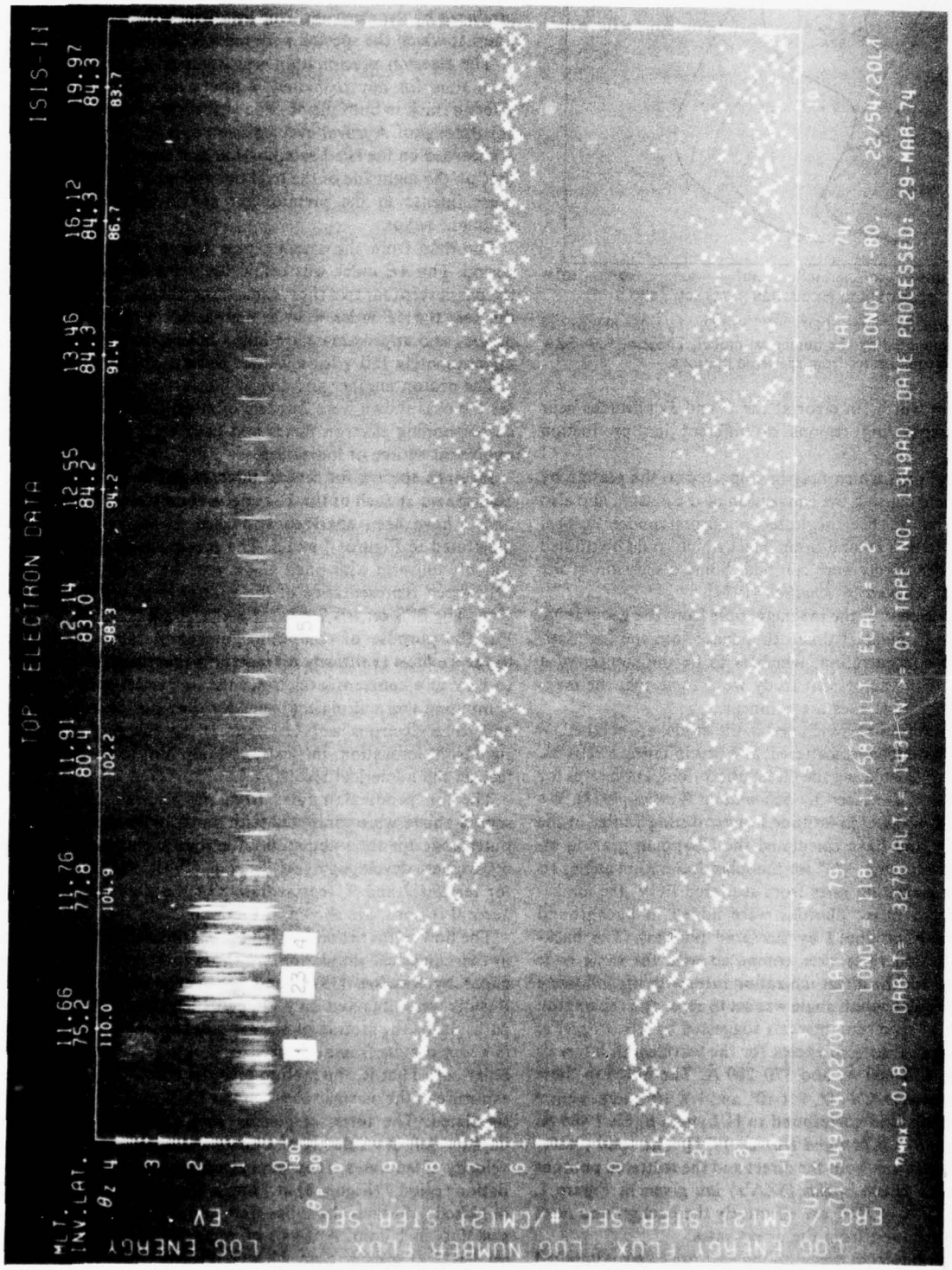

Fig. 2. Energy-time spectrogram for electrons from the Isis 2 soft particle spectrometer, December 15, 1971, local noon portion. Locations at which electron spectra were analyzed for use in the model are labeled.

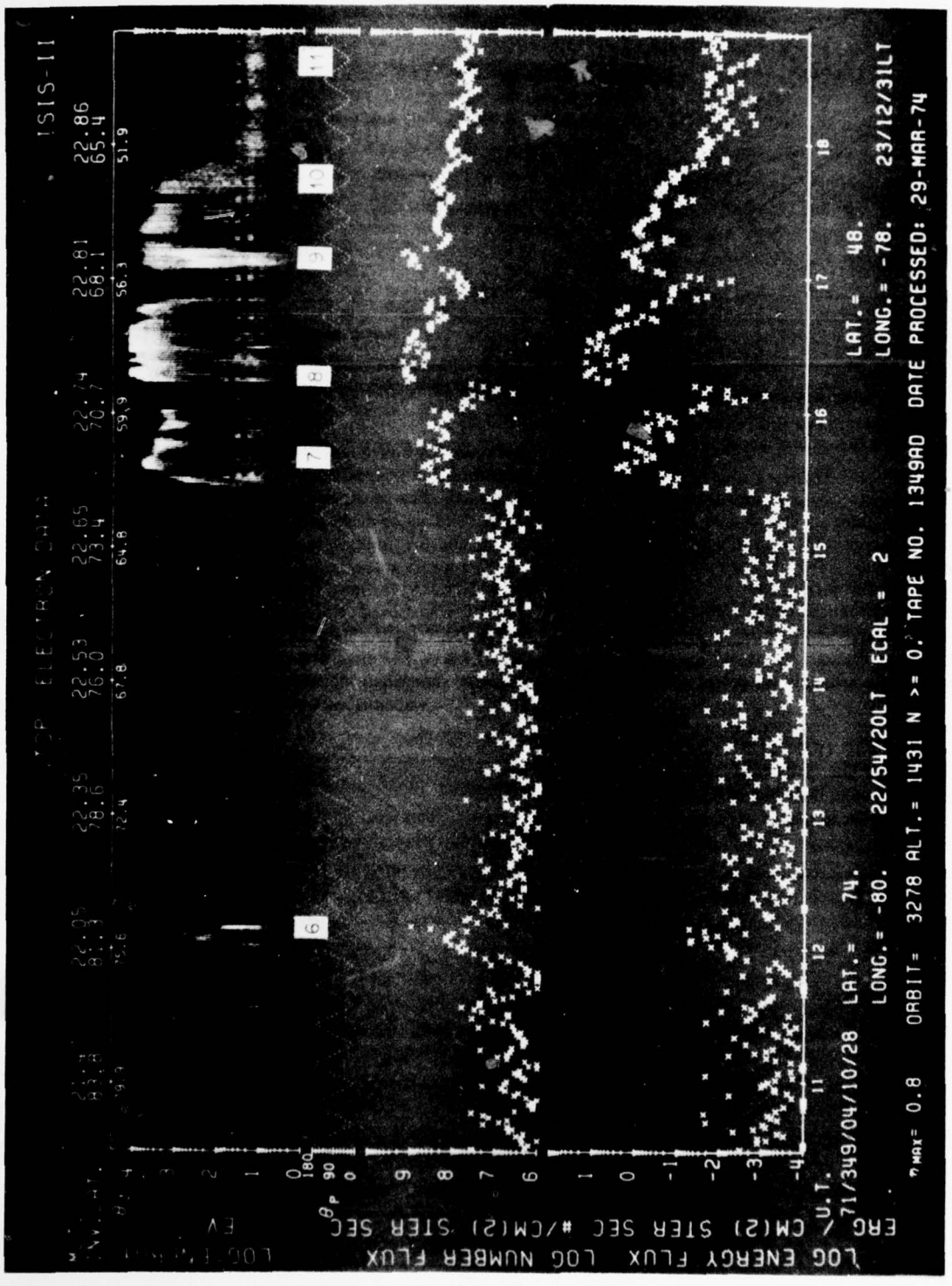

Fig. 3. Energy-time spectrogram for electrons from the Isis 2 soft particle spectrometer, December 15, 1971, local midnight portion. Locations at which electron spectra were analyzed for use in the model are labeled.

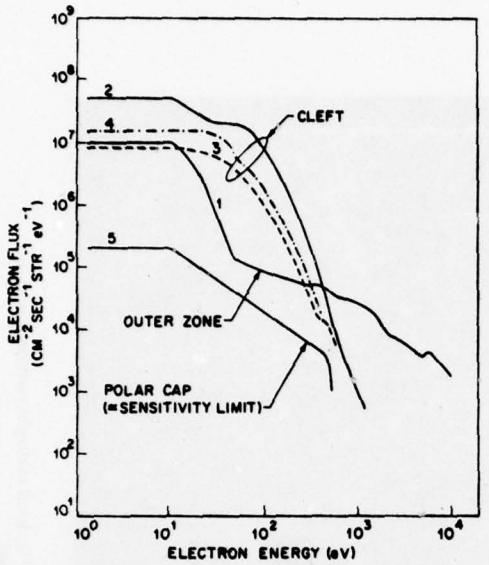

Fig. 4. Representative electron particle flux as a function of energy. Numbers refer to locations labeled in Figure 2.

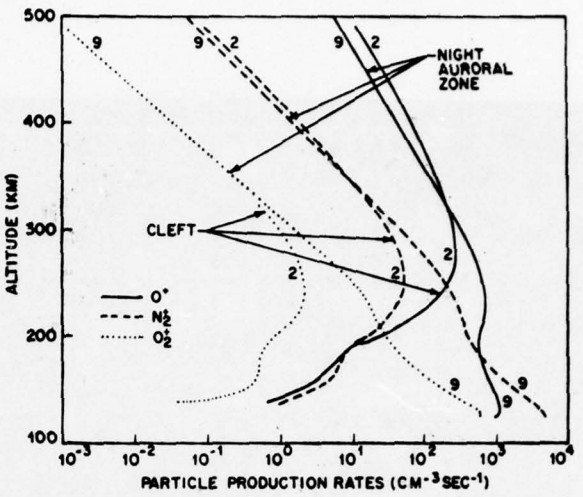

Fig. 6. Production rates of O^+, N_2^+, and O_2^+ ions by the electron particle fluxes at locations 2 and 9 of Figures 2 and 3.

sector (16 min, 20 s, Figure 3) (J. R. Burrows, private communication, 1976). The limit of closed field lines in the night sector of Figure 7 is consistent with this observed boundary. The tubes were convected slowly through precipitation regions 8–10 as required by the model, and as we shall see, these precipitation regions produced considerable ionization in the slowly convecting tubes.

The flow pattern of Figure 7 in the dayside cleft region and over the polar cap is reasonably consistent with that derived from vector ion velocity data by *Heelis et al.* [1976]. Flow across the cleft and into the polar cap is observed between approximately 0900 and 1500 MLT as has been assumed herein, and the general flow pattern of Heelis et al. presented with corotation removed in their Figure 8 would, with corotation restored, look similar to that of our Figure 7. The Harang discontinuity and stagnation points must exist in any reasonable model at approximately the locations indicated in Figure 7, and the flow must approach corotation in the vicinity of 55°Λ. The major discrepancy between experimental measurements and the 'time average' representation presented in Figure 7 appears to be in the magnitude of the velocity equatorward but in the near vicinity of the limit of the closed field lines. The measured velocity is of the order of 1 km/s, whereas the model velocities with corotation removed are of the order of 0.1 km/s. The measured velocity does approach corotation velocity somewhere between 70°Λ and 50°Λ [*Heelis et al.*, 1976]. The velocities with which the plasma tubes were trans-

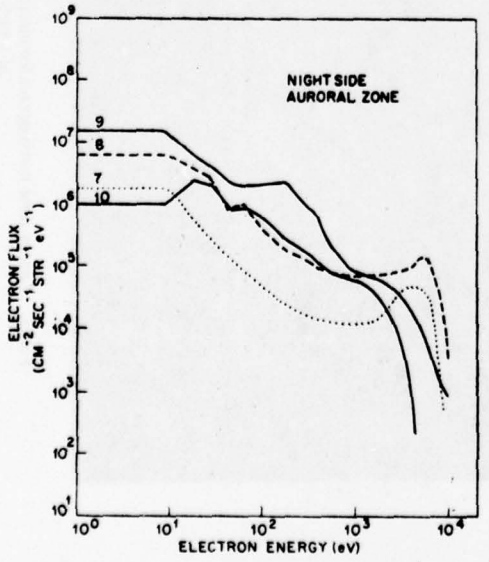

Fig. 5. Representative electron particle flux as a function of energy. Numbers refer to locations labeled in Figure 3.

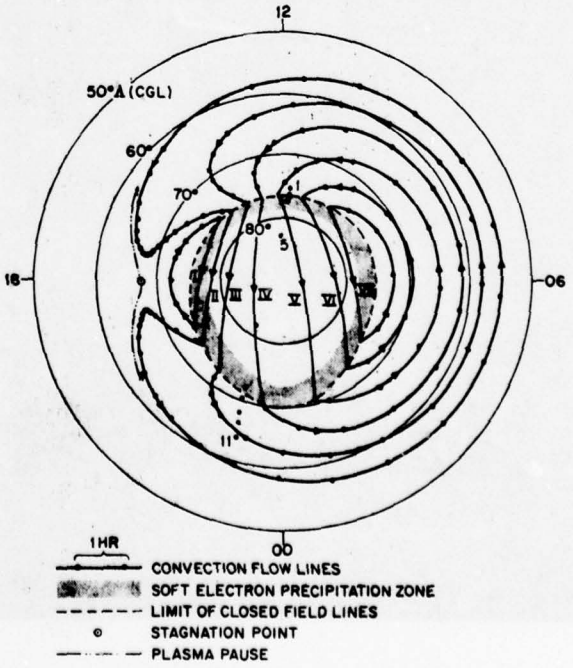

Fig. 7. Flow paths around which time-dependent plasma response was computed. Locations of electron spectra are indicated by the numbered dots. Numbers correspond to those in Figures 2 and 3.

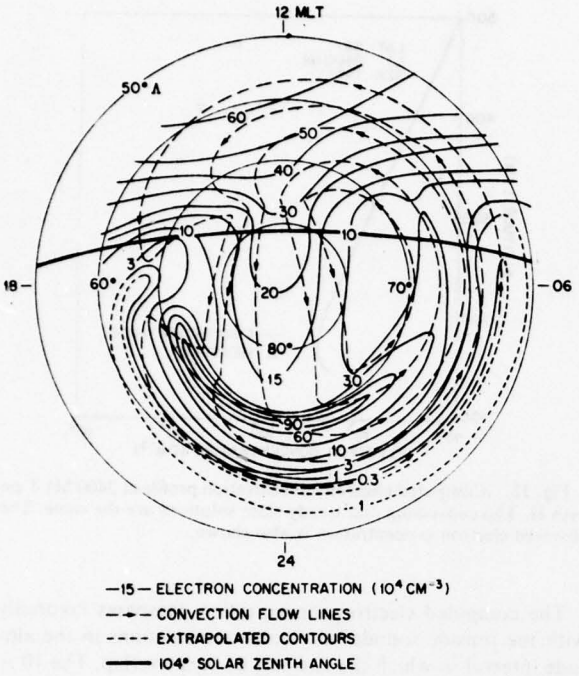

Fig. 8. Contours of N_mF_2 derived from the numerical analysis. The short-dashed portions of contours are extrapolated contours.

ported across the cleft and polar cap are reasonably consistent with observation.

The finite time steps in the numerical analysis were less than or equal to 5 min. In regions where the ion production rate was changing rapidly, the time step was decreased appropriately.

RESULTS

Contours N_mF_2 derived from the numerical results are shown in map view in Figure 8. The maximum electron concentration in each vertical profile around the several flow paths was plotted and subsequently contoured. The short-dashed portions of the contours equatorward of the lowest latitude path on the nightside of the earth are extrapolated. Numerical

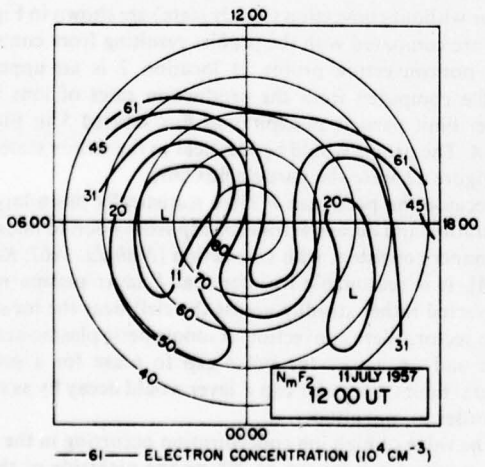

Fig. 9. Synoptic N_mF_2 contours for the Antarctic polar region (after *Sato and Rourke* [1963] and reproduced by *Thomas and Andrews* [1969]). Coordinates are geographic coordinates.

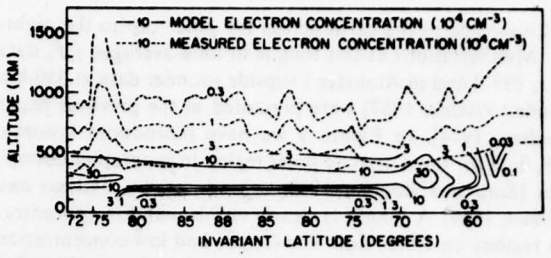

Fig. 10. Comparison of numerically computed electron concentration with that measured by the topside sounder experiment on Isis 2 in vertical profile.

computations for flow paths equatorward of the plasmapause were not performed for this study. Figure 9 shows experimental data included for later comparison.

A local noon–midnight vertical profile comparison of the numerically computed electron concentration with the observed electron concentration is shown in Figure 10. The observed data are from the topside sounder experiment on Isis 2 for the same pass as that from which the energetic electron flux data were derived. Comparison of the model results with the topside sounder data is meaningful in the altitude interval 350–500 km.

In Figure 11 we show a comparison of the computed electron concentration in vertical profile with the plasma tube convecting and with it stationary (steady state) at two locations along path IV. The observed electron concentration is also indicated. Figure 12 shows the computed electron concentration at midnight on path II. The plasma within the convecting tube in this region of path II is in a steady state condition.

DISCUSSION

The computed electron concentration shown in map view in Figure 8 shows several of the features characteristic of the polar ionosphere. First, a 'tongue' of plasma extends from the

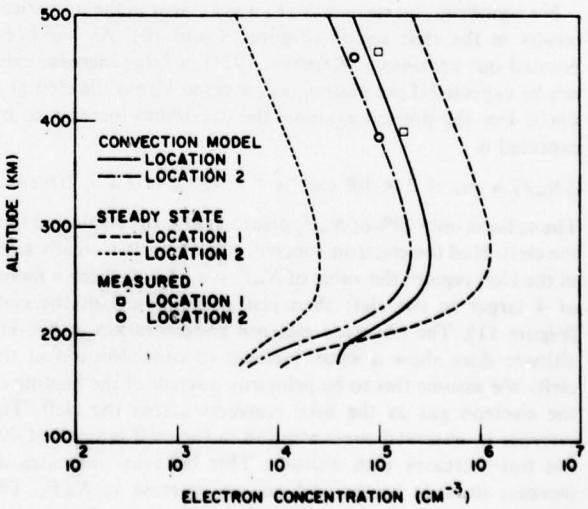

Fig. 11. Comparison of numerically computed electron concentration profiles, convecting and steady state, in the cleft (location 1) and within the polar cap (location 2) with measured concentration. Location 1 corresponds to 77° Λ, 1154 MLT, 100° SZA, and particle spectrum 2. Location 2 corresponds to 84° Λ, 2100 MLT, 117° SZA, and particle spectrum 5.

local noonside of the earth across the polar cap to the nightside. Manifestations of this tongue in time-averaged $\int_o F_2$ data [*Pike*, 1971] and in Alouette I topside sounder data at 350-km altitude [*Nishida*, 1967] were presented in the previous paper [*Knudsen*, 1974]. In Figure 9 we have reproduced synoptic $N_m F_2$ data for the Antarctic polar region in geographic coordinates [*Sato and Rourke*, 1963; reproduced by *Thomas and Andrews*, 1969]. A tongue is clearly visible with low concentration regions on either side. The tongue and low concentration regions on either side are reproduced in the numerical results. Not present in Figure 9 are the ridge of ionization produced by auroral electron precipitation and the deep trough present in the numerical results. These discrepancies will be addressed hereafter. The region of low concentration on the local evening side of the tongue in the numerical model results from the presence of a stagnation point outside the region of particle precipitation (Figure 7) and direct solar photon production. Near the stagnation point in local winter the tubes of plasma move sufficiently slowly for the concentration to decay to low values. The region of low concentration on the morning side of the tongue in the numerical model results from lack of significant exposure of the plasma tubes to the sun and to the more intense nightside auroral electron precipitation at latitudes below 70°Λ in the present model.

The direct solar photons are able to produce a significant F layer for solar zenith angles from 0° up to approximately 104° (compare Figure 1). On the midnight side of the 104° SZA of Figure 8, only the scattered photons make a contribution to the ion production.

In the time-averaged data presented by *Nishida* [1967] a maximum existed in the evening sector at about 60°Λ. The cause of the maximum is uncertain, although *Nishida* [1967] assumed that it was a manifestation of the mid-latitude evening increase [*Evans*, 1965]. The data used for the averaging included data from August 29 to November 10, so that the stagnation point would have been illuminated by direct solar photons at nearly all universal times. The maximum is not evident in the data presented by *Pike* [1971] or by *Sato and Rourke* [1964].

No significant increase in $N_m F_2$ was evident in the numerical results in the cleft region (Figures 8 and 10). As has been pointed out previously [*Knudsen*, 1974], a large increase cannot be expected if the plasma is convected across the cleft at 1 km/s. For the present example the maximum increase to be expected is

$$\Delta N_m F_2 \simeq \dot{p}\tau_c \simeq 2 \times 10^2 \text{ cm}^{-3}\text{ s}^{-1} \times 120 \text{ s} \simeq 2.4 \times 10^4 \text{ cm}^{-3}$$

The value is only 10% of $N_m F_2$ prior to entry of the plasma into the cleft. Had the electron concentration been in a steady state in the cleft region, the value of $N_m F_2$ would have been a factor of 4 larger in the cleft than just equatorward of the cleft (Figure 11). The observed electron concentration at 400-km altitude does show a small increase in concentration at the cleft. We assume this to be primarily a result of the heating of the electron gas as the tube convects across the cleft. The increase in observed concentration in the cleft is small at 400 km but increases with altitude. This behavior indicates an increase in scale height and not an increase in $N_m F_2$. The increase would be independent of altitude if the electron and ion temperature were held constant, as is evidenced in the numerical results of Figure 11. As has been pointed out previously, the numerical model did not include energy balance, and the electron and ion temperatures were arbitrarily set equal to the neutral temperature.

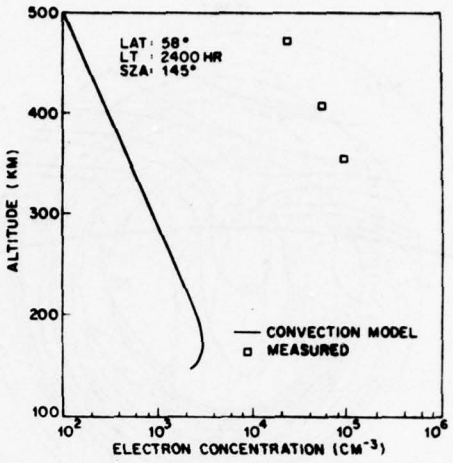

Fig. 12. Computed electron concentration profile at 2400 MLT on path 11. The convecting and steady state solutions are the same. The observed electron concentration is also shown.

The computed electron concentration compares favorably with the topside sounder electron concentrations in the altitude interval in which the two sets of data overlap. The 10×10^4 cm^{-3} contours of both sets of data coincide rather well from 75°Λ on the dayside to 75°Λ on the nightside of the model. The prominent variations in concentration exhibited by the topside sounder data, especially at higher altitude, are produced by increases in the electron and ion temperatures. This is evidenced, as was previously mentioned, by the decrease in electron concentration variation as the altitude decreases. The model results are not expected to reproduce these variations because the electron and ion temperatures were held constant. The increase in concentration of the model results at 67°Λ in the night sector resulted from the increase in ion production rate produced by energetic electrons (regions 8–10). The concentration trough at ~57°Λ results from a lack of production and a long decay time. These latter features do not occur in the experimental data.

The nearly constant value of $N_m F_2$ over the polar cap evidently results from rapid convection of plasma from the dayside of the cleft. The concentration profiles that would occur without convection (steady state) are shown in Figure 11 and are compared with the profiles resulting from convection. The nonconvecting profile at location 2 is an upper limit profile computed from the production rates of ions for the upper limit particle precipitation flux labeled 5 in Figures 2 and 4. The profile would be identical to the steady state profile in Figure 12 were the particle flux zero.

Because the polar cap F layer statistically has a large concentration and decays across the cap from noon to midnight in a manner consistent with convection [*Nishida*, 1967; *Knudsen*, 1974], it is reasonable to infer that F layer plasma must be convected rather steadily across the cleft near the local noontime sector. Were convection of ionospheric plasma across the cleft and on across the polar cap to cease for a period of several hours, the polar cap F layer would decay by as much as an order of magnitude.

The ridge of high ion concentration occurring in the numerical results equatorward of 70° on the nightside of the earth (Figure 8) is produced by assumed slow convection of plasma through the intense particle precipitation zones represented by spectra 8 and 9 of Figure 3. This ridge of ionization is not

present in the observed electron concentration (Figure 10). Statistical studies also show little or no enhancement in the nightside auroral zone [see *Knudsen*, 1974]. Suppression of such a ridge could be accomplished by moving the plasma through these zones rapidly. Rapid convection would not permit buildup of ionization in a tube as it crossed the zone(s) of high particle precipitation. The buildup may also be suppressed through an increased loss rate within the auroral zone [*Schunk et al.*, 1976].

A trough region of low ion concentration was produced in the numerical results equatorward of the ridge of high ion concentration from approximately 1800 MLT to 0600 MLT. The trough resulted from the slow convection of plasma near the evening stagnation point at which location the solar zenith angle was too large for direct solar photons to maintain the F_2 layer ion concentration at a high value against the normal ion loss processes and polar wind escape. A 'steady state' level of ion concentration of flow line II around the nightside of the polar region was maintained by the scattered solar photon flux level assumed to be present in the model. The trough disappears on the morning side as the plasma tube emerges into the direct solar photon flux. The ionization level in the trough would be least near midnight and greater toward the evening and morning sectors in a more realistic model in which the scattered solar photon flux decreased with increasing solar zenith angle.

The deep trough evident in the numerical results (Figures 8 and 10) did not appear in the topside sounder data. The probable explanation is that variation of the convection electric field and hence flow paths with time prevents the development of the deep trough. The flow paths must be steady for periods of the order of 24 hours for a deep trough to develop in the manner suggested by *Knudsen* [1974] and demonstrated in the present numerical results. As was pointed out earlier, the magnetic AE index was small and steady except for two short excursions for 28 hours prior to the orbit selected for analysis. Hence the conditions for development of a trough by slow convection would seem to have been fulfilled as well as one could expect. Resolution of this discrepancy must await future studies.

SUMMARY AND CONCLUSIONS

The time-dependent behavior of the F layer plasma within a magnetic flux tube is computed for the tube carried around several flow paths in the polar regions. The flow paths are those proposed in a previous paper by *Knudsen* [1974]. As the tube traverses each path, it is subjected to time-dependent ionization rates from direct and scattered solar photons and precipitating energetic electrons. Ionization rates for the energetic electrons are computed from energy spectra observed by the Isis 2 soft particle spectrometer. The numerical results are presented in the form of a map view of N_mF_2 contours, electron concentration in vertical section over the magnetic pole from noon to midnight, and several vertical profiles of electron concentration at several locations for both convecting and nonconvecting flux tubes. The computed electron concentrations are compared with observed electron concentrations from topside sounder data obtained in the same satellite pass as the energetic electron flux data.

The proposed convection field produced a tongue of F layer plasma extending from the dayside of the cleft over the polar cap with concentrations consistent with the observed concentrations. Had the F layer been assumed to be stationary (nonconvecting) within the polar cap, the computed concentrations would have been a factor of 10 too small. Concentration 'lows' on either side of the tongue are consistent with some previously observed synoptic data. No significant increase in N_mF_2 occurred at the cleft in the model results. This behavior is consistent with the observed behavior. In diffusive equilibrium an increase of approximately 4 in concentration would have existed.

The presence of the polar cap F layer with peak electron concentrations typically in excess of 10^5 cm^{-3} implies, when it is interpreted in the light of the present study and a previous study [*Knudsen*, 1974], that F layer plasma is rather steadily convected across the cleft in the local noontime sector and on across the polar cap.

A ridge of ionization not present in the observed ionosphere was predicted by the numerical simulation in the nightside auroral zone. Several zones of particle precipitation were measured by the Isis 2 satellite, and the plasma tubes were transported at high velocity (1 km/s) only through the highest latitude zone. Evidently, the plasma tubes are transported rapidly across zones of high precipitation, and/or some additional loss mechanism is operative in the precipitation zones.

A trough of low electron concentration was predicted by the numerical model which extended from approximately 1800–2400 MLT to approximately 0600 MLT. The electron concentration in the trough was constant with local time and maintained by the assumed constant flux of solar EUV photons scattered into the night ionosphere. No trough was present in the Isis 2 topside sounder data. A satisfactory explanation for the latter discrepancy must await future studies.

Acknowledgments. The authors wish to thank J. H. Whitteker, C. D. Anger, and J. R. Burrows for supplying electron concentration, airglow, and energetic electron flux data, respectively. R. W. Schunk kindly made his computer program available and helped greatly with discussions of the program behavior. This research was supported by Lockheed independent research funds, NASA contract NASw 2550, NSF grant DES75-03985, and AFGL contract F19628-76-C-0005.

The Editor thanks J. A. Fedder and H. Rishbeth for their assistance in evaluating this paper.

REFERENCES

Banks, P. M., C. R. Chappell, and A. F. Nagy, A new model for the interaction of auroral electrons with the atmosphere: Spectral degradation, backscatter, optical emission, and ionization, *J. Geophys. Res.*, *79*, 1459, 1974.

Chen, W. M., and R. D. Harris, An ionospheric E region nighttime model, *J. Atmos. Terr. Phys.*, *33*, 1193, 1971.

Evans, J. V., Cause of the mid-latitude evening increase, *J. Geophys. Res.*, *70*, 1175, 1965.

Heelis, R. A., W. B. Hanson, and J. L. Burch, Ion convection velocity reversals in the dayside cusp, *J. Geophys. Res.*, *81*, 3803, 1976.

Hinteregger, H. E., L. A. Hall, and G. Schmidtke, Solar XUV radiation and neutral particle distribution in the July 1963 thermosphere, *Space Res.*, *5*, 1175, 1965.

Jacchia, L. G., Revised static models of the thermosphere and exosphere with empirical temperature profiles, *Spec. Rep. 332*, Smithson. Astrophys. Observ., Cambridge, Mass., 1971.

Knudsen, W. C., Magnetospheric convection and the high-latitude F_2 ionosphere, *J. Geophys. Res.*, *79*, 1046, 1974.

Lui, A. T. Y., and C. D. Anger, A uniform belt of diffuse auroral emission seen by the Isis-2 scanning photometer, *Planet. Space. Sci.*, *21*, 799, 1973.

Nishida, A., Average structure and storm time change of the polar topside ionosphere at sunspot minimum, *J. Geophys. Res.*, *72*, 6051, 1967.

Pike, C. P., A comparison of the north and south polar F layers, *J. Geophys. Res.*, *76*, 6875, 1971.

Sato, T., and G. F. Rourke, Antarctic Research and Data Analysis, *Sci. Rep. 8*, AVCO Corp., Wilmington, Mass., 1963.

Sato, T., and G. F. Rourke, F region enhancements in the Antarctic, *J. Geophys. Res.*, *69*, 4591, 1964.

Schunk, R. W., and J. C. G. Walker, Theoretical ion densities in the lower ionosphere, *Planet. Space Sci.*, *21*, 1875, 1973.

Schunk, R. W., P. M. Banks, and W. J. Raitt, Effects of electric fields and other processes upon the nighttime high-latitude *F* layer, *J. Geophys. Res.*, *81*, 3271, 1976.

Thomas, J. O., and M. K. Andrews, The trans-polar exospheric plasma, 3, A unified picture, *Planet. Space Sci.*, *17*, 433, 1969.

(Received July 26, 1976;
accepted May 23, 1977.)

VOL. 82, NO. 32 JOURNAL OF GEOPHYSICAL RESEARCH NOVEMBER 1, 1977

The Development of Auroral and Geomagnetic Substorm Activity After a Southward Turning of the Interplanetary Magnetic Field Following Several Hours of Magnetic Calm

KNUD LASSEN

Geophysics Section II, Danish Meteorological Institute, Copenhagen, Denmark 2100

J. R. SHARBER

Department of Physics and Space Sciences, Florida Institute of Technology Melbourne, Florida 32901

J. D. WINNINGHAM

Center for Space Sciences, University of Texas at Dallas, Richardson, Texas 75080

A comprehensive study of growth phase and substorm activity following a period of magnetic calm has been conducted through a network of all-sky camera stations, auroral zone magnetic observatories, and particle detectors aboard the Isis 1 satellite. We have carefully documented the observations with the following results. The preexpansive phase arc which extended at least from 17 to 05 MLT was responsible for an energy input rate of $\simeq 3 \times 10^{10}$ ergs/s before breakup. An equatorward drift of this arc of 6 km/min, observed only in the evening sector, remained until after the expansive phase, when its motion stopped abruptly at the time of the maximum poleward displacement of the arcs. Electrons responsible for the prebreakup arc had energies of $\simeq$1–5 keV. Protons of $\simeq$4-keV energy were measured equatorward of the electron arc. During the expansive phase, symmetrically traveling disturbances were observed propagating eastward in the evening sector and westward in the morning sector. The propagation stopped for 1–2 min at the time of maximum expansion and then continued, thus suggesting a momentary variation in the rate of convection. Equivalent currents consistent with observed magnetic perturbations represented approximately the same *DPZ* (twin vortex) pattern before the expansive phase as during it; however, although the magnitude of the currents was greater during the expansive phase, the dominant feature during this phase was an intense westward auroral electrojet. The camera observations of diffuse cloudlike aurora showed an injection of $\simeq$40-keV electrons during the expansive phase along the auroral oval between midnight and 0400 corrected geomagnetic time. Movement of the cloud indicated an eastward gradient drift of the electron population.

INTRODUCTION

On the basis of data from an extensive body of all-sky camera documentation and polar magnetograms, *Akasofu* [1964] outlined the substorm sequence. Although his initial description has been modified slightly [*Akasofu*, 1968; *Montbriand*, 1971], it remains essentially correct in ordering the observed geophysical phenomena into a consistent picture. Since that time an enormous effort has gone into further documenting substorm-related phenomena and into establishing the cause of the onset of the substorm expansive phase (see review by *Rostoker* [1972]). Whereas in Akasofu's description the substorm sequence is initiated by the sudden breakup of an auroral arc accompanied by a steep decrease of the horizontal component of the magnetic field, it was claimed by *McPherron* [1970] that the complete substorm sequence includes a disturbance period which he denoted the substorm growth phase. According to his statement, intervals of magnetic calm may be followed by significant deviations of the horizontal component of the magnetic field prior to the start of the expansion phase of a magnetospheric substorm.

Since McPherron's suggestion that a growth phase exists, several authors [*Iijima and Nagata*, 1972; *McPherron et al.*, 1973; *Kokubun and Iijima*, 1975] (and others) have contributed to the study of the phenomenon by giving more detailed descriptions of the signatures which are observed to be characteristic of that situation. The authors appear to agree in the opinion that the onset of an isolated substorm is preceded by a growth phase, which is closely related to the north-to-south change of the interplanetary magnetic field (IMF), following it with a delay of 10–20 min. The signatures of this growth phase observed on the ground are the following: a gradual decrease in H, the horizontal magnetogram, at auroral zone stations before its sharp drop; a gradual decrease in H at low latitudes (especially in the evening–midnight sector); the growth of a polar equivalent current of the twin vortex mode (especially in the polar cap); and the equatorward motion of auroras [*Kokubun and Iijima*, 1975].

In opposition to the above mentioned view, *Akasofu et al.* [1973] have suggested that the changes in the magnetic field characteristic of the growth phase have limited significance, since these changes do not themselves result in the onset of the expansive phase. They suggested instead that the mechanism which triggers the expansive phase is an internal one, largely independent of external factors related to convection such as the southward turning of the interplanetary magnetic field. In continuation of this suggestion, *Akasofu* [1975] has demonstrated that the southward turning of the B_z component and the subsequent chain of processes, proposed by *McPherron et al.* [1973], do not have any significance in causing the expansive phase. Substorms are frequently being triggered in direct relation to such a chain of processes, in which the 'growth phase' of the substorm may then appear as part of the

Paper number 7A0679.

TABLE 1. Stations Used in This Study

Station	Symbol	Geographic Latitude, deg	Geographic Longitude, deg	Corrected Geomagnetic Latitude, °N	Observation
Alert	AT	82.5	295.5	86	M
Thule	TH	77.5	290.8	86	A, M
Resolute Bay	RB	74.7	265.2	84	M
Godhavn	GO	69.2	306.5	77.5	A, M
Ny Aalesund		78.9	11.9	75.5	A
Søndre Strømfjord	SS	67.0	309.2	75.5	A
Baker Lake	BL	64.3	264.0	75	M
Heiss Island	BT	80.6	58.5	74.5	M
Fort Churchill	FC	58.8	265.9	71	A
Narssarssuaq	NAR	61.2	314.6	68	A, M
Great Whale River	GW	55.3	282.2	68	A, M
Dixon Island	DI	73.5	80.4	67.5	M
Tromsø	TR	69.7	18.9	66.5	A, M
Reykjavik	RY	64.2	338.3	66	M
Tixi Bay	TI	71.6	129.0	65	M
Murmansk	MM	69.0	33.1	64.5	S, M
Kiruna	KI	67.8	20.4	64.5	M
College	CO	64.9	212.2	64.5	M
Meanook	ME	54.6	246.6	64	M
Wellen	WE	66.2	190.2	60	M
Lerwick	LE	60.1	358.8	59	M
Bangui	BA	4.4	18.6	5	M
M'Bour	MB	14.6	343.0	21	M
San Juan	SJ	18.1	293.8	30	M
Fredericksburg	FR	38.2	282.6	50	M
Tucson	TU	32.2	249.2	40	M
Honolulu	HO	21.3	202.0	21	M

complete substorm picture. However, they may as well be released at a later stage, after the end of the B_z negative interval, as long as the area of the polar cap is greater than a certain minimum value, namely, the area after a prolonged period of large positive B_z. Once the polar cap has achieved this minimum value, no substorm can be released until a new southward turning of the IMF has initiated erosion of field lines on the dayside of the magnetosphere with the accompanying features of increasing convection, observable from ground-based observatories.

No matter whether the growth phase is an integral part of the substorm phenomenon, as proposed by McPherron, or more likely an independent B_z negative, increased convection phenomenon in accordance with the statements of Akasofu, there is still a need for further detailed study of the development of the geomagnetic and auroral activity observed after the southward turning of the IMF.

On February 25, 1969, the Isis 1 satellite happened to pass over the premidnight sector of the auroral oval during a geophysical situation which appears to have been identical with the substorm growth phase defined by McPherron. The event followed a period of low substorm activity, characterized by values of AE less than 200 γ during the 34 hours before the substorm and less than 60 γ during the last 6 hours. By combining the satellite particle measurements with ground-based observations we have been able to report in the following a careful documentation of the development of the auroral and magnetic activity through the growth phase and the subsequent substorm onset and expansion phase as well as of the particle precipitation preceding the substorm onset. Our observations give a detailed picture of the gradual development of auroral and geomagnetic activity which follows the southward turning of the interplanetary magnetic field and which, in this particular event, is completed by the onset of a substorm with remarkable poleward expansion.

DATA SOURCES

In our study we made use of ground-based observations made during the event at the stations listed in Table 1, together with particle measurements from the Isis 1 satellite and magnetic field measurements from the satellites Explorer 35 and Heos 1. The ground-based observations are auroral all-sky photographs (A in column 6 of Table 1), spectrograms (S in column 6), and geomagnetic records (M in column 6).

The interplanetary magnetic field was measured by the satellites Explorer 35 in the evening quadrant ($(X, Y, Z)_{SE} = (-8, +63, -61)\ R_E$) and Heos 1 in the forenoon quadrant ($(X, Y, Z)_{GSM} = (11, -31, 14)\ R_E$). Both satellites appear to have been outside the shock front. None of the records was complete; thus detailed results from Heos 1 are missing during 0000–0300 UT, but hourly averages do exist for this interval [*King*, 1975]. Similarities of gross features of the B_z variation at the two satellites indicate a time lag between them of about 30 min. From the position of the satellites it is estimated then that the B_z variations at the front of the magnetopause occur 15–17 min earlier than those at Heos 1. Hence the B_z variations observed at Heos 1 have been referenced to the front of the magnetosphere by a shift of 15 min toward earlier hours. In Figure 1 they have been shown together with magnetic records from the stations Tromsø, Reykjavik, Narssarssuaq, Great Whale River, and Fort Churchill, which were all situated in the 18–04 magnetic time sector of the auroral zone. In the figure the stations are ordered from east to west. Each arrow represents 200 γ. The magnetic H records from a number of mid- and low-latitude stations are shown in Figure 2. The stations are ordered from east to west, with the most easterly

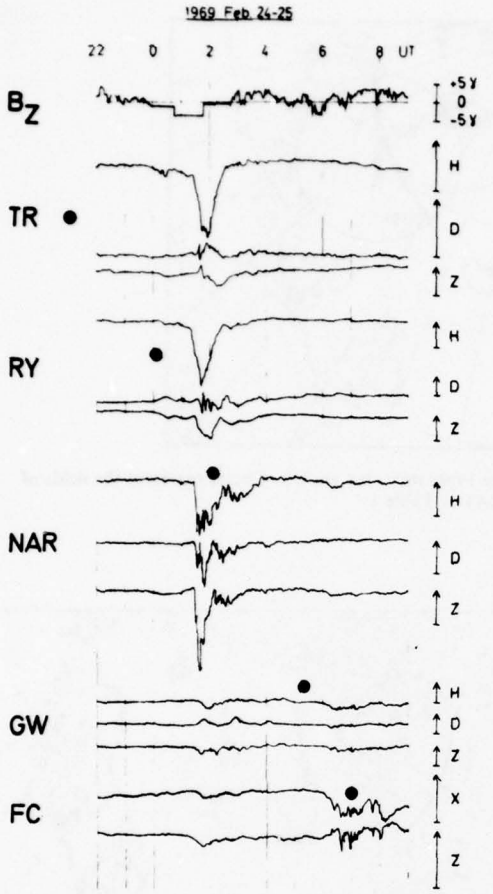

Fig. 1. Normal magnetograms from the auroral zone stations Tromsø, Reykjavik, Narssarssuaq, Great Whale River, and Fort Churchill, February 24–25, 1969. Each arrow represents a variation of 200 γ. The dots indicate station geomagnetic midnight. Top curve: B_z (vertical GSM coordinate) as measured at Heos 1, referenced to the front of the magnetosphere by a shift of 15 min toward earlier hours.

one (Bangui) at the top of the figure. Each arrow in the figure represents 20 γ.

At the time of the substorm the nightside of the auroral zone was situated between western Siberia in the east and Northwest Territories in the west, with the magnetic midnight meridian crossing the Iceland-Greenland area. Conditions were not ideal for auroral observations. The moon was in its third quarter; the Soviet cameras, Reykjavik, Kiruna, and several stations in Greenland were not in operation because of bad weather, and most of the remaining stations had some cloud cover early in the evening. Nevertheless, eight well-distributed cameras were available for a study of the development of the auroral display in the course of the night (Table 1 and Figure 3). At each of the stations the sky was photographed with one exposure per minute except at Tromsø, where three exposures per minute were taken. The photographs have been used as a basis for the description of the distribution of the aurora; a selected series has been transformed to synoptic maps in geographical coordinates, shown here as Figures 4*a* and 4*b*. In projecting the auroral forms on the maps a mean height of 110–120 km has been assumed for the lower border of the arcs and bands.

MAGNETIC OBSERVATIONS

The IMF had been directed northward for several hours when the decrease of B_z began between 2200 and 2300 UT. Because of the oscillatory character of the change it is difficult to determine the exact hour when B_z went negative; after 2345–2350, B_z was definitely negative. The first departure from several hours of magnetic quiet was observed at approximately the same time, i.e., at 2345–0015 at the auroral zone stations situated near and shortly after magnetic midnight (Figures 1 and 5). The departure is seen as a gradual decrease of H, but D and Z are also affected. In the evening sector, Great Whale and Fort Churchill were little influenced by the disturbance before 0100 UT (Figures 1 and 6). At the low-latitude stations situated in the evening sector a gradual decrease of H set in between 0000 and 0030 UT and continued until the expansive phase onset at 0130. The onset is recognized as a sudden decrease of H in Figure 1. In Figure 2 it appears as the onset of a positive bay in the midnight sector and of a negative bay of comparable magnitude in the evening–afternoon sector. The transition takes place near the longitude of San Juan. At San Juan a flat depression is observed from shortly after midnight to 0300 UT, with only a small negative perturbation to be seen in connection with the expansion phase of the substorm. The gradual decrease of H at mid- and low-latitude stations as well as the flat depression observed at San Juan may be caused by an increase of a cross-tail or ring current system, which becomes detectable in the records about ½ hour after the change of sign of B_z.

The magnetic signatures of this event are in agreement with the description given by *McPherron* [1970]. Following a decrease of B_z to negative values a growth phase of about 1½-hour duration is observed, characterized by a gradual decrease of H at low latitudes and by a contemporary change of the magnetic elements at auroral latitudes in the direction in which they are subsequently changed by the substorm. The growth phase is superseded by the expansion phase initiated by the sharp onset at about 0130.

Before the end of the recovery phase of this substorm a new onset is noticed at 0210–0215 at the low-latitude stations, especially at Bangui and M'Bour. In the auroral zone the magnetic bay is most clearly recorded at Narssarssuaq; at Tromsø the onset is recognized as an abrupt change of the slope in H. The magnetic activity from this double substorm dies away by about 0400 UT. After 2 hours calm a new moderate substorm is observed in the midnight sector (Fort

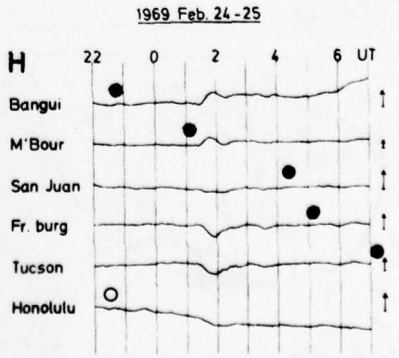

Fig. 2. Horizontal variation at low- and mid-latitude stations, February 24–25, 1969. Length of arrows is 20 γ. The dots indicate station midnight; the open circle at Honolulu indicates noon.

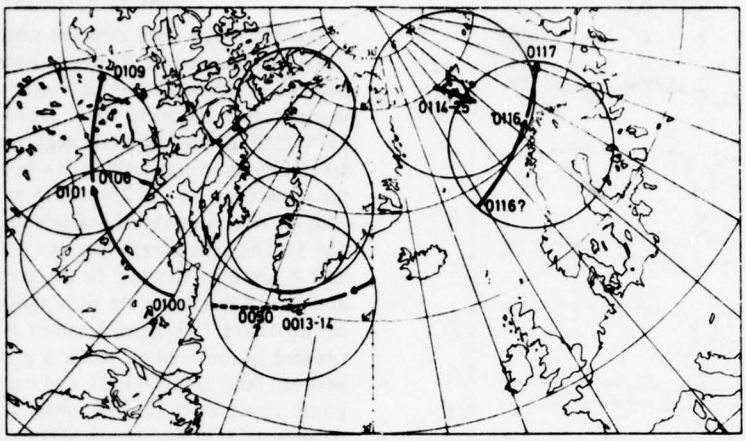

Fig. 3. Development of presubstorm arc, February 25, 1969. The times indicated are UT. Circles represent the fields of view of camera stations (A) of Table 1.

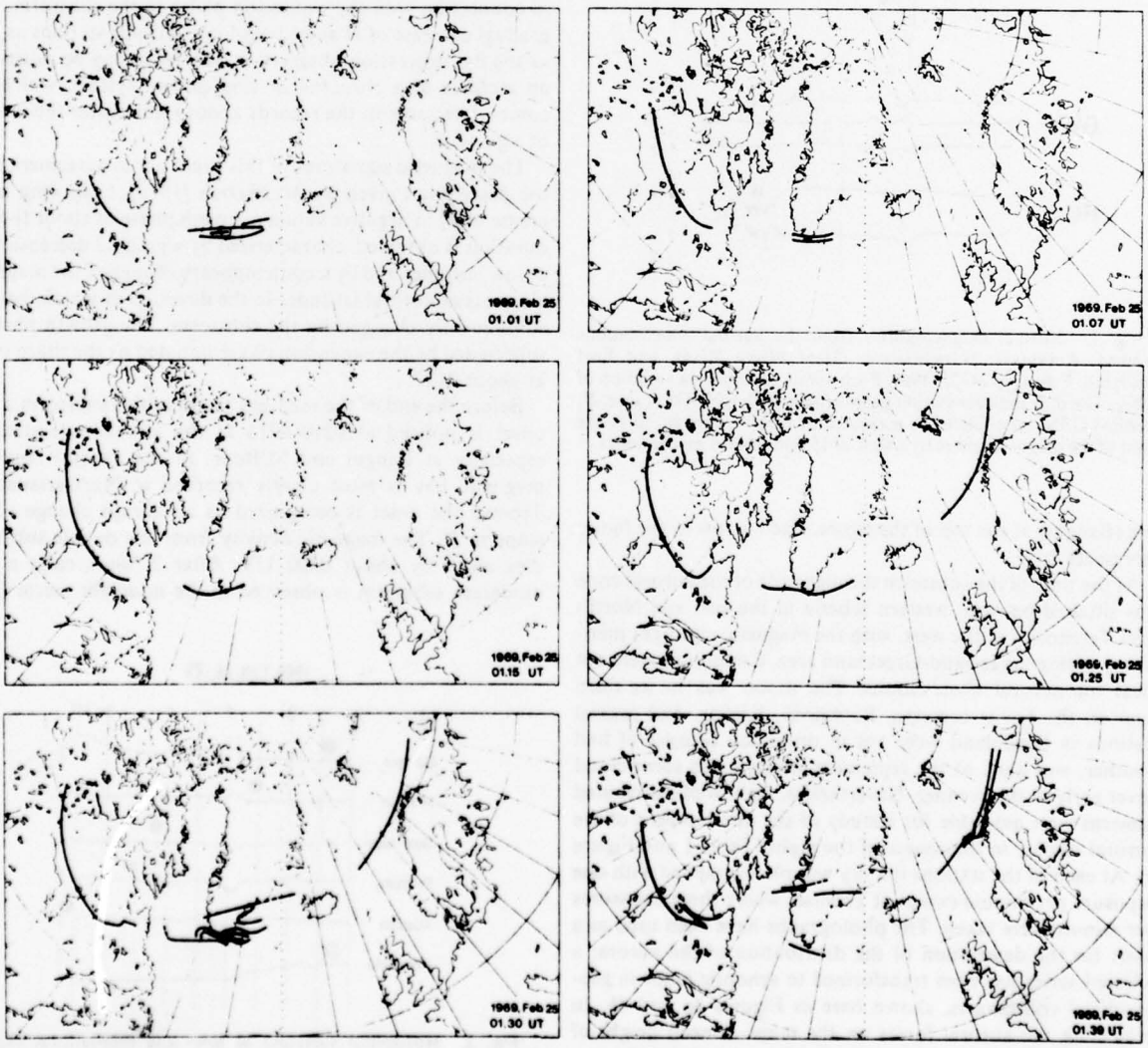

Fig. 4*a*. Development of auroral display, February 25, 1969. Growth phase and poleward expansion.

Churchill, Figure 1). We shall comment further on the onset of this substorm in a later section.

We have used the ground magnetometer data in the construction of equivalent current vectors to represent the current distribution before and after breakup at 0130 UT. This enables a comparison of the current system during the growth phase with that during the time of maximum expansion. We have taken the time of the satellite crossing of the arc (0115 UT) as a time during which we would consider the growth phase to be well in progress. The equivalent current vectors which could produce the magnetic perturbations at a number of polar cap and auroral zone stations at the time of the crossing have been drawn in a corrected geomagnetic latitude/time diagram in Figure 7. Also shown are the equivalent current vectors derived from the same stations during the time of maximum disturbance of the event. The maximum magnetic disturbance was measured during the 20 min immediately following the poleward expansion; the situation at 0150 UT has been chosen for construction of the current vectors. The quiet level for both graphs has been defined as the level which immediately preceded the onset of the event, i.e., during 2200–2400 UT. The equivalent current system during the growth phase is similar to the system corresponding to $B_z < -1\ \gamma$ in the winter months (*DPZ* system) as constructed by *Friis-Christensen and Wilhjelm* [1975]. In this system, which is believed to depict the magnetic field produced by field-aligned current sheets in the auroral oval and by a Hall current maintained by the electric field between the sheets, the disturbance vectors over the polar cap are of the same order of magnitude as those in the post-midnight auroral oval. In Friis-Christensen and Wilhjelm's paper (their Figure 5) the equivalent vectors are approximately 2 times the magnitude of those found here, in accordance with the fact that their parameter $\bar{B}_z$ (the 2-hour average of the actual and preceding hour) is numerically greater in their data than in ours.

Following a further decrease of B_z the equivalent currents during the maximum disturbance at 0150 UT are more intense than those at 0115 by a factor of 2, thus being comparable to the average currents of Figure 5 of *Friis-Christensen and Wilhjelm* [1975]. Superimposed on the *DPZ* system we find at

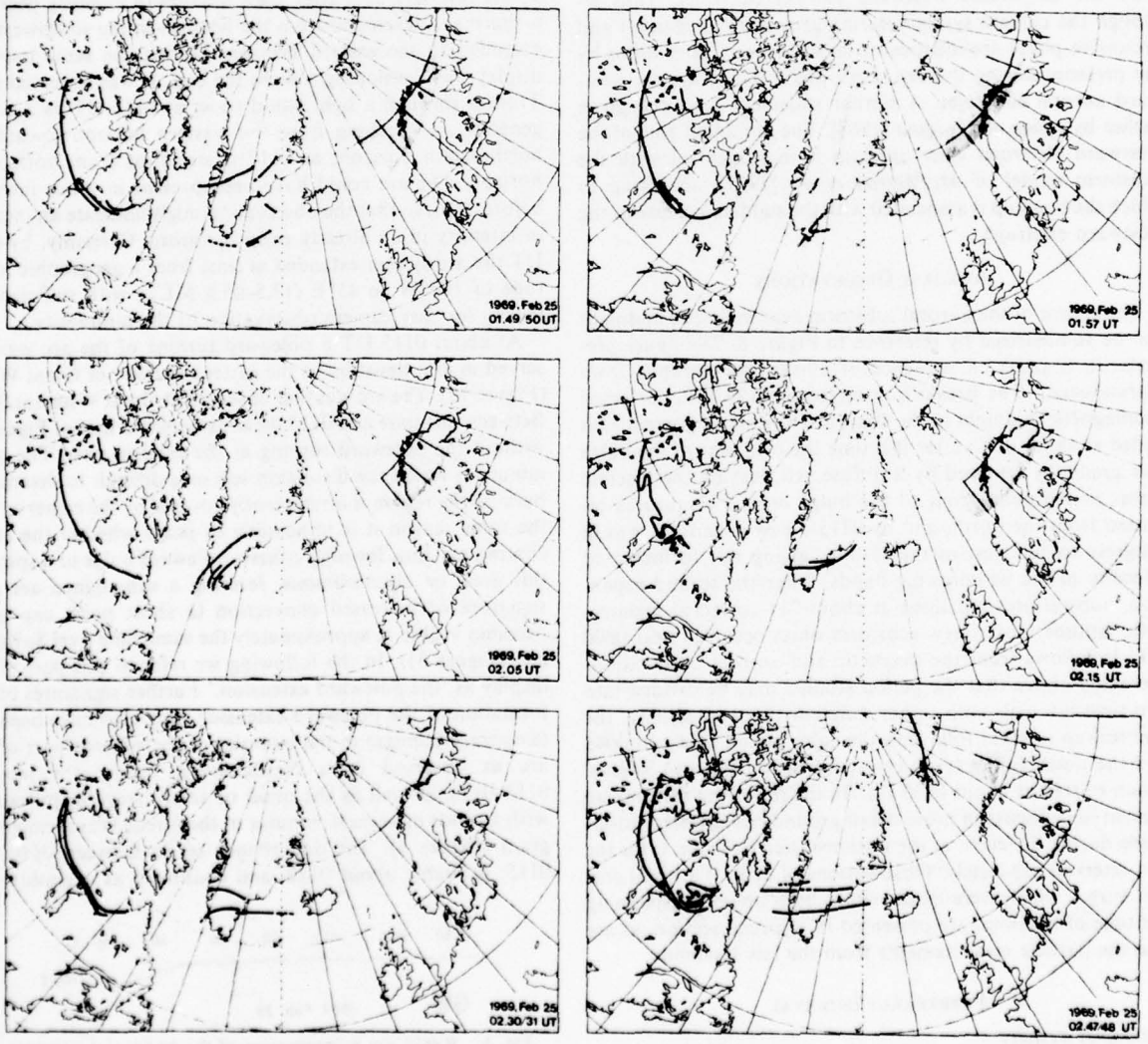

Fig. 4*b*. Development of auroral display, February 25, 1969. Recovery and second (minor) substorm.

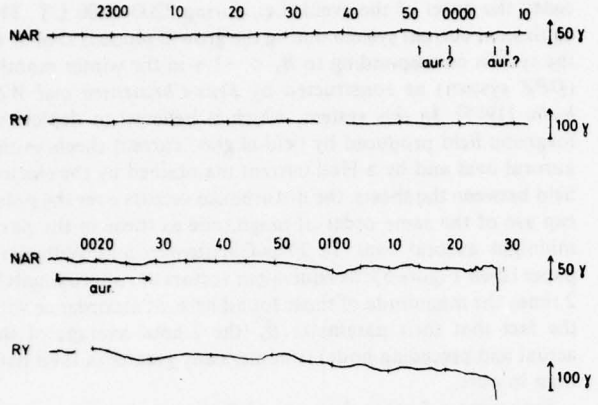

Fig. 5. Rapid run magnetograms showing the horizontal component at Narssarssuaq and Reykjavik, February 24–25, 1969. The gradual depression prior to abrupt onset of the magnetic substorm is clearly displayed.

0150 UT an intense westward auroral electrojet. Thus although the current systems during growth (B_z negative) and expansive phase are identical in most respects, they differ by the presence during the expansive phase of the intense westward auroral electrojet. A similar statement has been given earlier by *Iijima and Nagata* [1968]. The dominant role of the westward electrojet after breakup is in agreement with the substorm model of *McPherron et al.* [1973], according to which the breakup is associated with the sudden increase of the westward electrojet.

Auroral Observations

The course of the auroral substorm near magnetic midnight can be summarized by reference to Figure 8. The figure presents, in negative, a sequence of all-sky photographs from Narssarssuaq. The breakup occurred at 0128 UT, corrected geomagnetic midnight at the station. The poleward expansion ended at about 0137; after this time the oval part of the bulge was gradually replaced by a diffuse veil, leaving the discrete forms in the polar front of the bulge only. The auroras returned from the north, and by 0213 a new expansion was in progress to the west of the station, giving rise to increased intensity in the withdrawing bands. After the second expansion, auroral arcs remained at about 71° corrected geomagnetic latitude until a new substorm onset occurred near 0600 UT. It follows from the magnetic and auroral observations presented above that the period studied may be divided into two time intervals with rather different types of activity, the prebreakup interval following the calm period at about 0045 and the postbreakup (expansion and early recovery) interval which started at about 0130 UT. In the following sections we present and discuss in more detail ground-based observations made during the event at the stations listed in Table 1, for the two intervals separately. Observations of drift of auroral arcs and surges which were made within both intervals, spanning the time of breakup, are presented in a special section, as are also the particle measurements from the Isis 1 satellite.

Prebreakup Interval

Buildup of Activity

The first observation of auroral light before the breakup was made near the midnight meridian at Narssarssuaq station. Although it is difficult to be certain because of the presence of moonlight and a few clouds, a faint arc stretching from the northeastern horizon up to about 10° elevation is possibly seen in the frames taken at 2353, 2358, and later at 0006–0008 UT. From the time of 0013–0014 an auroral band was definitely present and extended from the northeast horizon to the zenith. The band persisted as a single homogeneous arc until at 0050 the intensity increased gradually, beginning at the eastern horizon. Folds shaped like a narrow westward traveling surge moved from the horizon toward the zenith and combined with the original arc at 0100 to form a row of multiple arcs of moderate intensity. A few minutes later a new 'surge' was seen low in the northeast for about 5 min. The intensity increases and the westward movement of folds were accompanied by a negative bay in H with an amplitude of 20 γ in Narssarssuaq and Reykjavik (Figure 5).

Apparently as a continuation of the formation of parallel arcs over Narssarssuaq, the arc developed to the west, becoming first detectable within the Great Whale field of view at 0100 UT, at the eastern horizon of Fort Churchill at 0106, and crossing the sky to the northwestern horizon at 0109 (Figure 3). At Narssarssuaq, after a few minutes of intensity decrease, a sharp arc developed from the horizon in the southwest and extended to the eastern horizon. During the same time the display was developing toward the east. It was observed from Tromsø through a light cloud cover at 0116 UT as a homogeneous arc reaching from the western horizon toward the northeastern horizon; at 0117 it stretched from horizon to horizon. The arc could have been present in lower intensity before 0116, so that the observation might indicate an increase in intensity in an already existing aurora. Certainly, by 0125 UT the arc system extended at least from a geographic longitude of 100°W to 45°E (17.5–05.5 MLT) with sufficient intensity for easy camera observation of the luminosity.

At about 0115 UT a poleward turning of the arc was observed in low elevation at the eastern horizon of Great Whale (Figure 18). The arc was first observed at Great Whale at 0100. Between this time and 0115 the arc resembled that of Figure 18 without the poleward turning at the extreme east. The exact minute at which the distortion sets in is difficult to determine, because the region is insufficiently covered by the cameras. For the same reason it is impossible to judge whether the arc is continuous, thus forming either a poleward bulge or a spiral in this area, or discontinuous, forming a sun-aligned arc as a signature of increased convection (a short polar cap band becomes visible at approximately the same time over Spitsbergen (Figure 3)). In the following we refer to this part of the display as 'the poleward extension.' Further signatures of the formation of the poleward extension may also have been the temporary increase in the intensity of the western part of the arc as observed from Narssarssuaq during the interval 0113–0116, as well as the onset of small irregular pulsations with periods of several minutes in the Great Whale magnetogram (Figure 6). The disturbance set in between 0110 and 0115, probably about 0112, and continued as a gradual de-

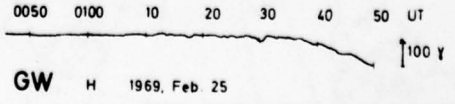

Fig. 6. Rapid run magnetogram of the horizontal component at Great Whale River, February 25, 1969. Note the small-scale perturbations during formation and approach of westward traveling surge.

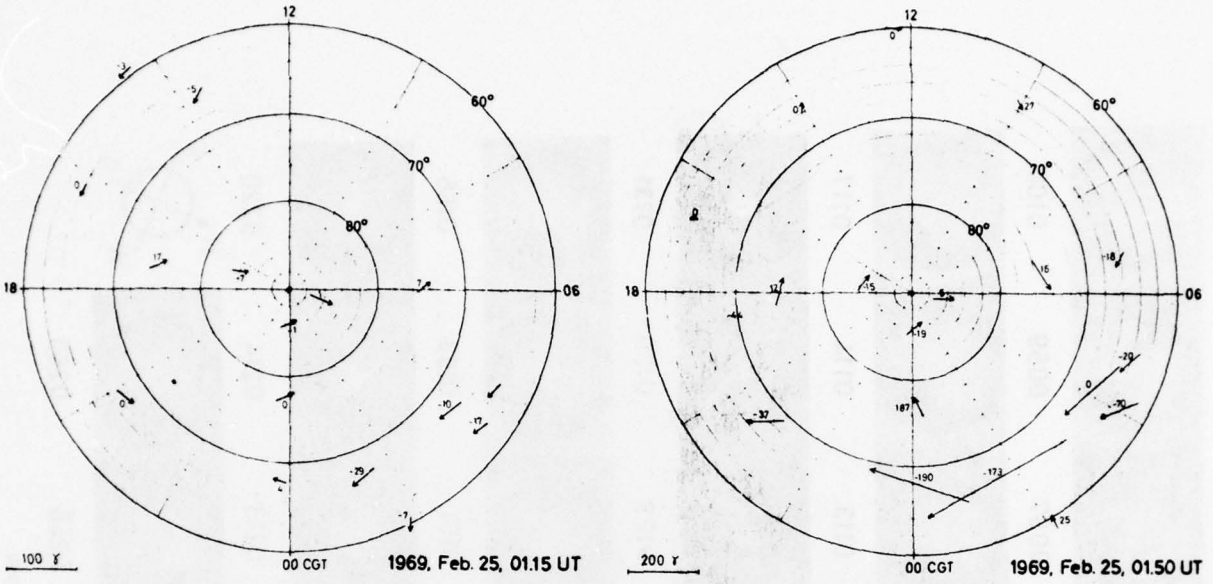

Fig. 7. Equivalent current vectors during prebreakup (growth) phase (0115 UT, left) and maximum of expansive phase (0150, right) of substorm on February 25, 1969. Numbers beside arrows indicate vertical magnetic perturbation in gammas. Note the different scale in the two diagrams.

crease of 100 γ as the westward traveling surge reached the station at about 0139.

Following the formation of the poleward extension the intensity again increased from the east in the southern arc (which at this time was the only one visible) over Narssarssuaq, the lower border became irregular, and the intensity increased from the west along the arc to meet the easterly increase near the meridian. Here the arc formed a sharp kink at 0125, and lateral movements were observed between 0125 and 0127. The intensity increase from the region of the poleward extension to the west of the station was accompanied by an obvious though small decrease in H (Figure 5). The actual breakup began at 0128–0129 very near Narssarssuaq as parallel arcs were formed along the northern border of the original arc. The abrupt onset of the magnetic perturbation in H occurred at 0128 in the Reykjavik magnetograms and less than ½ min later at Narssarssuaq (Figure 5).

Interpretation of Observations

The magnetic and auroral observations may be summarized as follows. Within minutes to tens of minutes after the shift of sign in B_z, precipitation of auroral particles is observed in the auroral oval close to magnetic midnight. The latitude of the oval is 68°. A gradual deviation of the magnetic elements at auroral zone stations is initiated at the same time, indicating the presence of a *DPZ* (convection) current system, and signatures of increased cross-tail or ring currents are seen in the records of H at low-latitude stations. The observations indicate an increasing convection set up by the negative value of B_z. A minor disturbance (double bay) at about 0020 is visible in stations from the polar cap to low latitude. This is probably a *DP*2 disturbance [*Nishida*, 1968], which may indicate irregularities in the convection rate. The increase in auroral intensity at 0050 followed by a narrow westward traveling surge and a development toward morning and evening of the quiet arc is consistent with the description of a confined substorm given by *Lui et al.* [1975]. In their example the magnetic effect of the substorm was about 20 γ. The decrease of H in our 0050–0110 event is approximately 20 γ and shows the signatures of a confined substorm. This disturbance is immediately followed by changes in the auroral pattern which could be associated with the convection pattern, i.e., a poleward turn of the arc before midnight and a polar cap aurora in the morning. The observations from the last 10 min before breakup give the impression of increasing convection and precipitation accompanied by increasing instability of the arcs, which finally result in the breakup and expansion.

EXPANSION AND EARLY RECOVERY

The rapid poleward expansion, initiated by the breakup, was completed by 0137 as the breakup arcs covered the entire area from a few degrees south of Narssarssuaq to Søndre Strømfjord (Figures 8 and 9). Simultaneously with this expansion the southernmost arcs moved equatorward with decreasing intensity; at the end of the poleward expansion, all discrete forms except those at the highest latitudes dissolved, and an equatorward broadening of a diffuse veil took place, which soon covered most of the sky. At the same time the discrete forms at the poleward edge of the display began a slow equatorward retreat.

The westward border of the region of poleward extension between Canada and Greenland appears to have remained relatively stationary during the expansive phase. However, as the expansion proceeded, a narrow zonal 'fiord' did develop in the low-latitude part of this westward extension. The formation of this fiord is evident in Figure 4*a* in the 0130 UT frame between 60° and 70° west longitude. The Great Whale photographs show that it developed into a small loop which became more and more elongated toward the west, eventually opening, thus forming two bands a few degrees north of the original band. These bands, shown in the 0139–0157 UT frames of Figures 4*a* and 4*b*, reached the Great Whale meridian at about 0141 but did not continue into the Fort Churchill field of view. The development of the western loop was accompanied by a

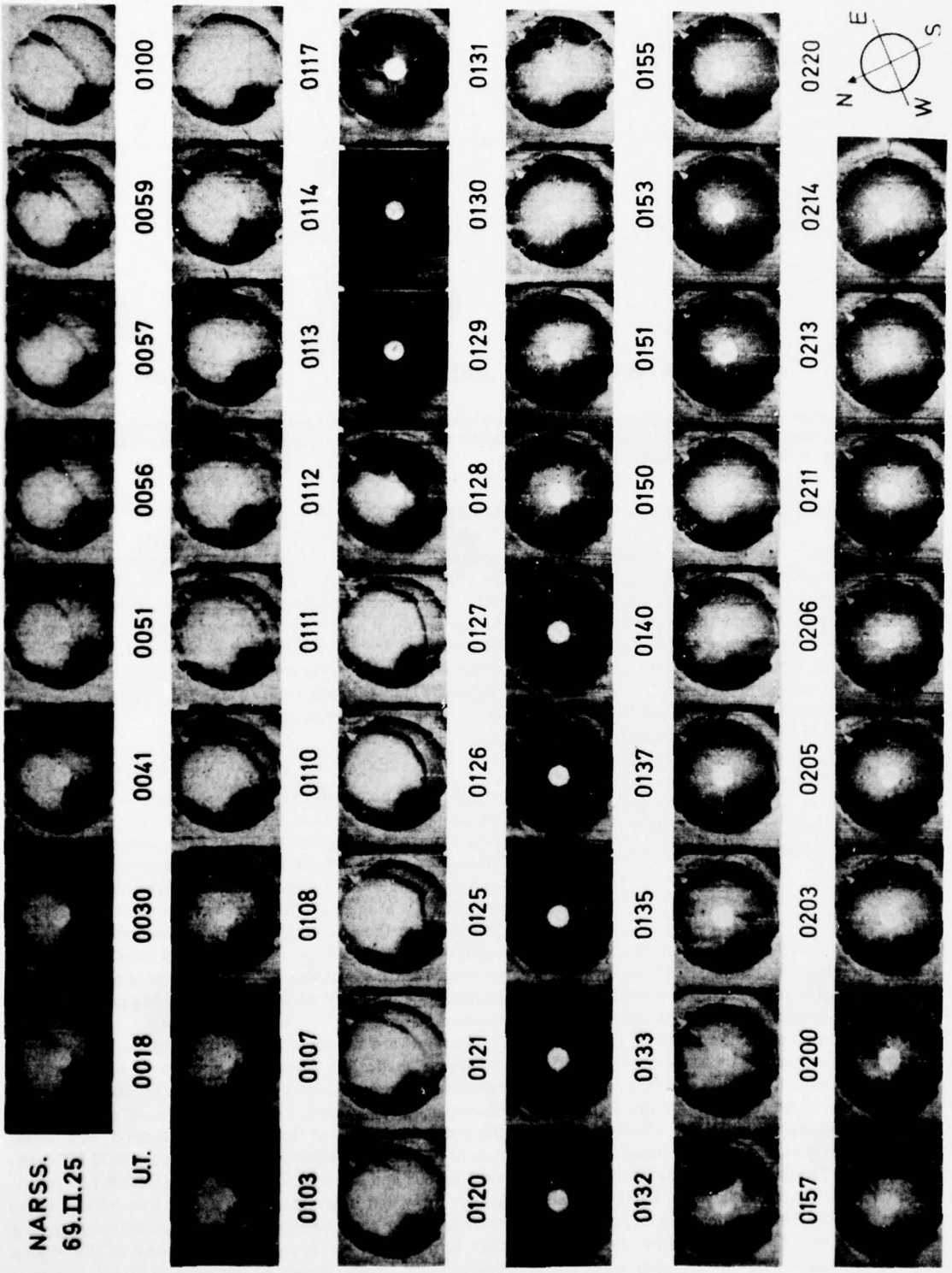

Fig. 8. All-sky camera photographs from Narssarssuaq, February 25, 1969.

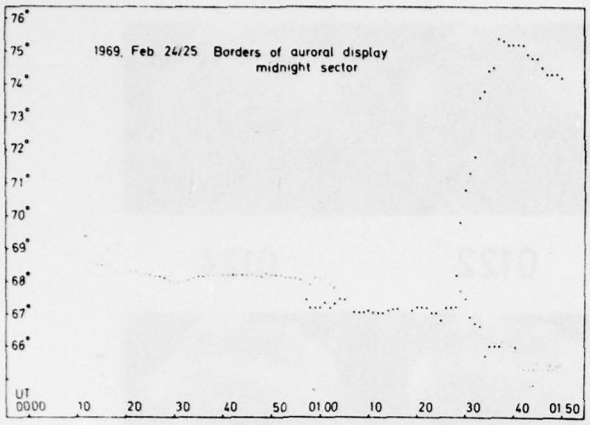

Fig. 9. Position in corrected geomagnetic latitude of the auroral arcs at Narssarssuaq. During the growth phase the position is indicated by the open dots. The positions of the northernmost and southernmost arcs during expansion are shown by the solid dots. The hatched area is more or less filled by discrete and diffuse auroras. The dense hatching indicates the equatorward border of the diffuse veil.

gradual decrease in H at Great Whale (Figure 6). Thus the loop behaved like the westward traveling surge as described by *Akasofu* [1968] with the exception that the westward border of the poleward expanding bulge did not move toward the west together with the surge but remained stationary on the evening side of the poleward extension of the arcs. In a single snapshot of the auroral display taken in the interval 0139–0157 UT the loop would have been interpreted as multiple discrete auroral arcs linked with the western limit of the poleward expanding bulge. A DMSP satellite photograph showing just this situation on November 24, 1971, has been published by *Pike and Whalen* [1974]. Our study, based on all-sky camera data, demonstrates how such multiple arcs may develop from a loop on the western border of the poleward expanding bulge.

The propagation toward the morning sector of the disturbance associated with the breakup and expansion phase may be observed from Tromsø, which was situated 4 hours after geomagnetic midnight. A sequence of all-sky photographs illustrating the development of the display at this station is presented in Figure 10. The intensity of the arc immediately to the north of Tromsø began to increase at 0130. Two minutes later a parallel arc of lower intensity became visible on the equatorward edge of the original one and slowly increased in intensity. At about 0137 the two arcs were dislocated equatorward, and after 0139, diffuse auroras with bandlike structure appeared on the equatorward side of the arcs. The movement of the original arc, which seemed to constitute the poleward edge of the display, as well as the movement of the boundaries of the diffuse aurora, has been plotted in Figure 11. This figure also shows the distribution of auroral light along the meridian as recorded by the spectral camera C-180-S at Loparskaya in the Murmansk area. Auroral data are not available before 0130 because of snow, but after this hour, spectrograms of 10-min exposure time were recorded. A comparison of the two plots in Figure 11 shows good agreement between the stations with regard to the latitudinal shift, but a time lag of 10 ± 5 min is observed between the equatorward shifts. Apparently, the low-latitude diffuse area propagated eastward with an approximate velocity of 1°/min (or 50 km/min). On the assumption that the diffuse cloudlike aurora was produced by electrons which had become trapped on near-earth field lines during the breakup and expansion process in the magnetosphere, their energy may be estimated by using a formula deduced by *Sletten et al.* [1971] from a paper by *Hamlin et al.* [1961]. The formula, which gives an expression for the drift period of nonrelativistic electrons mirroring close to the atmosphere, may be written $T(\mathrm{s}) = 4 \times 10^{6}(LE)^{-1}$, where T is the azimuthal drift period in seconds, E is the energy in keV of the trapped electrons, and L is the McIlwain shell parameter. L is approximately 6, and the stations are separated by 12°. The observed time lag of 10 ± 5 min gives an estimated particle energy of $E = 37 \pm 10$ keV (≃40 keV). If we assume that the electrons became trapped on near-earth field lines ($L \simeq 6$) no earlier than at the breakup, then they would have drifted along this shell for no more than 10 min before arriving at Tromsø. This places the eastern limit of the trapping region only about 10° to the west of Tromsø, i.e., between Iceland and Scandinavia.

The observations from Narssarssuaq (Figure 9) indicate that the first possible incidence of auroral particles at $L = 6$ takes place at 0133–0134, about 4 min before the effect at Tromsø. Thus it seems probable that the diffuse low-latitude aurora is formed practically without time delay all along the auroral oval from midnight to shortly before 0400 geomagnetic time, with a delay at later local times which may be explained by the assumption of energetic electrons drifting in the geomagnetic field.

The diffuse cloudy auroras over northern Scandinavia began to withdraw gradually toward the auroral zone at about 0200 UT. During the withdrawal the luminosity concentrated into a few diffuse bands. At 0215–0220 the southern border was near Tromsø, and at 0230 the display was no longer detectable in the all-sky photographs. Thus the poleward retreat of the equatorward boundary matches well the recovery of the horizontal field at Tromsø (Figure 1).

OBSERVATION OF AURORAL DRIFT

Equatorward Shift of the Oval in the Evening Sector

From the first occurrence of auroral light a gradual equatorward drift of the arc was observed in the evening sector. The position of the arc observed in the early evening at Fort Churchill (19 geomagnetic time) and at Great Whale (21 geomagnetic time) is shown in Figure 12. The figure shows the drifts to be similar at the two stations with a steadier drift occurring at Fort Churchill. The irregularities at Great Whale centered at 0122 and 0130 depict the passage of two large wavelike structures, the first of which was a forerunner to the small surge that is easily detectable in the photographs of 0121–0123 (Figure 13).

The equatorward shift of the arc was measured to be 3°/hour and therefore cannot be attributed solely to the natural shift of the position of the auroral oval in the course of the evening. The change in the latitude of the Feldstein oval (Q = 3) at 20 MLT is approximately 1°/hour equatorward, from which we can infer an equatorward drift in the position of the arc relative to the oval of 2°/hour or about 4 km/min. This observation agrees with results reported by *Starkov and Feldstein* [1971] that auroral forms generally drift equatorward during an hour or so prior to the expansive phase of a substorm, but it should be noted that in our observations the equatorward drift was found only in the evening part of the oval. Neither at midnight nor in the morning sector could a similar drift be found.

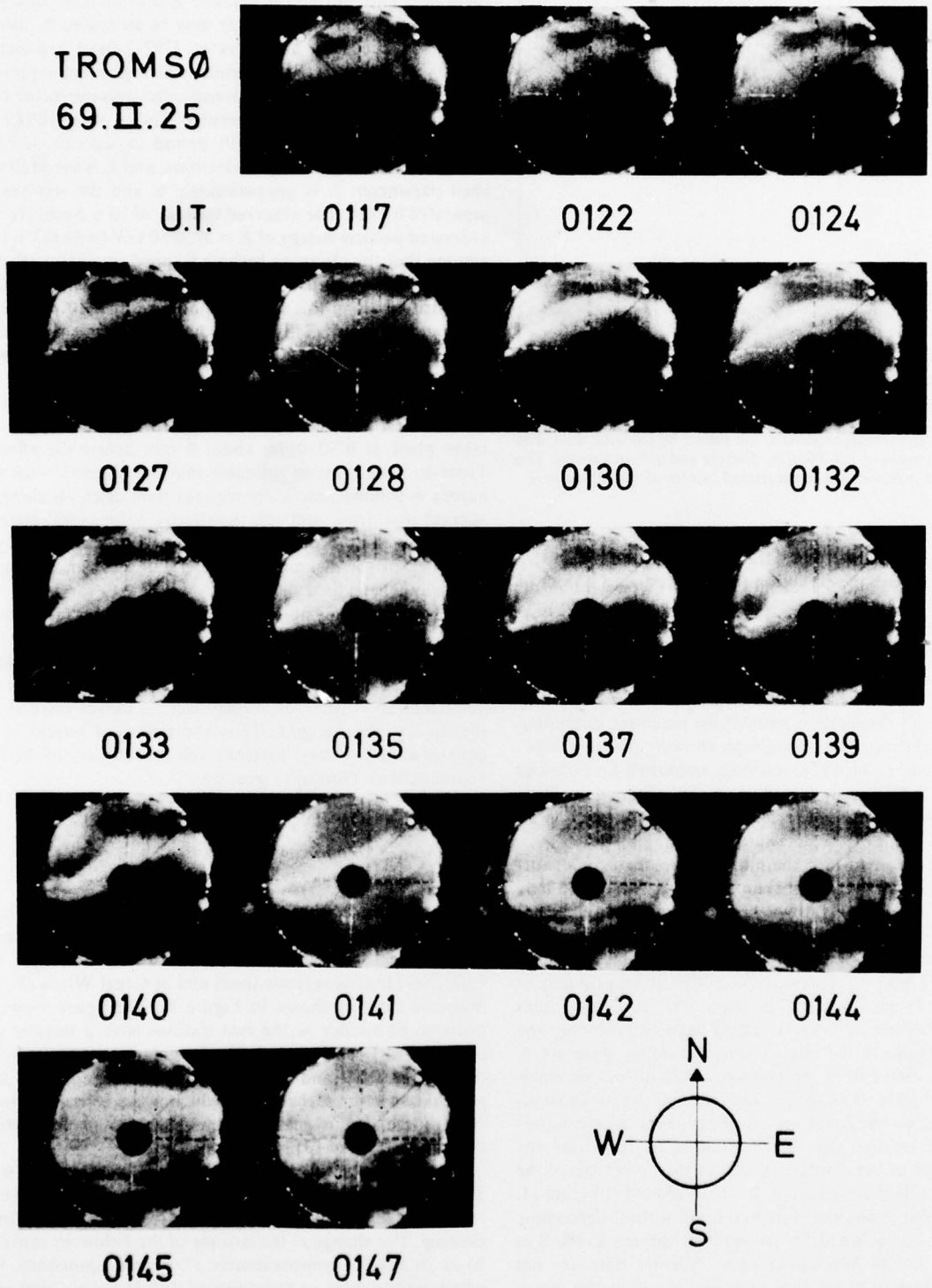

Fig. 10. All-sky camera photos from Tromsø, February 25, 1969.

It is of particular interest to note that the equatorward drift continued through the growth and expansion phases but stopped at the two evening stations a few minutes before the poleward expansion ended. This was also a few minutes before the narrow westward traveling surge arrived at Great Whale. If we make the tentative assumption that the equatorward drift of the arc results from a westward ionospheric field (see, for example, *Kelley et al.* [1971]; *Mozer* [1971]), the magnitude of this field, given by $\mathbf{v} = (\mathbf{E} \times \mathbf{B})/B^2$, is 4 mV/m westward. Our observations show that this field was present during the growth phase and most of the expansion phase and then suddenly disappeared.

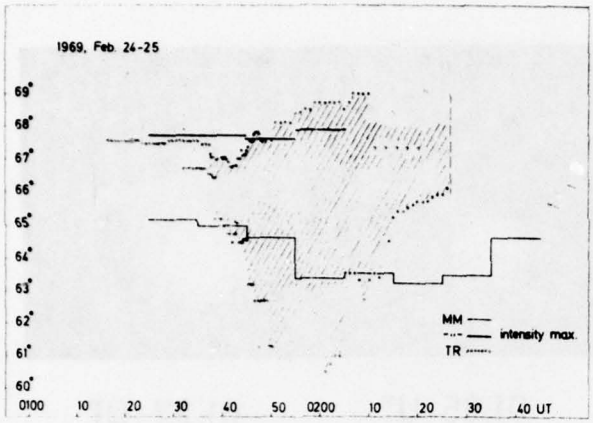

Fig. 11. Broadening of auroral display at Tromsø (dots) and Murmansk (line segments), based on all-sky camera (TR) and spectrograph (MM). The intensity maximum in the spectrographic record is indicated by a narrow double line. In the spectrogram the poleward boundary could not be determined with sufficient accuracy. After 0225, observations were not possible at Tromsø because of cloudiness.

Symmetrically Traveling Disturbances

In the morning sector the equatorward broadening was initiated by the passage of an eastward traveling, small but distinct bulge in the main arcs. The movement of the bulge can be followed in Figure 10. A closer inspection of the figure shows that the arc was dislocated slightly equatorward on both sides of the bulge. The combined effect of this dislocation and the bulge produces the depression of the northern arc at 0135–0145 shown in Figure 11. The projection on the ground of the arc system which clearly shows the bulge is presented in Figure 14. More detailed measurements of the eastward shift of the position of the bulge are given in Figure 15. Note that the ordinate in the figure gives the distance of the maximum deviation in the bulge along the arc from an arbitrary zero meridian, measured in degrees of geomagnetic longitude.

At Great Whale a disturbance similar in shape to but of smaller dimension than a westward traveling surge was seen to move from the vicinity of the great poleward bulge between Canada and Greenland toward the west. As is shown in the photographic sequence of Figure 13, the surge was first detected at 0120; at 0125 it appears to have reached the Great Whale meridian, but at this time it was difficult to distinguish because of the presence of a great number of small-scale folds along the arc. At 0131–0132 the band was again more regular, with a single bulge in the western end, quite similar to the disturbance present near Tromsø at the same time. The westward movement of this bulge and that of the bulge originally approaching Great Whale from the east (presumably the same form) are plotted in Figure 15 and labeled GW. As it approached the western horizon at Great Whale, it became observable in low elevation from Fort Churchill, and the motion measurements taken from the Fort Churchill photographs are plotted in the same figure (labeled FC). A few minutes later the Fort Churchill camera stopped operation for 4 min, enough time for the bulge to become rather poorly defined. But the few observations made at Fort Churchill before the break follow the trend in the Great Whale plot. The displacement in longitude results from the uncertainty in selecting the same point on the aurora from the two stations. At any rate, the observations from these two stations show that a small bulge moved westward across the Great Whale field of view and into the Fort Churchill field of view during the time interval 0120–0139. Between 0134 and 0142 the eastward drift of a similar bulge near Tromsø was measured. The two surges appeared to have about the same drift speed; in the time interval 0135–0138, when the Tromsø measurements were most accurate, the eastward drift speed was 2.2° ± 0.3° geomagnetic longitude per minute, while the westward drift speed of the bulge near Great Whale was measured to be 2.0° ± 0.5° geomagnetic longitude per minute. The bulge at Tromsø drifted close to the 107° geomagnetic longitude meridian, and the one at Great Whale drifted near the 357° meridian. Thus during this short interval the two bulges were of similar shape and were observed to drift symmetrically in relation to the geomagnetic midnight meridian (≃50° geomagnetic longitude).

The western irregularity became visible in the Great Whale field of view a few minutes after the formation of the poleward extension between Canada and Greenland. The drift velocity of this and accompanying irregularities along the arc was relatively constant or slightly decreasing until 0134–0135, when an increase in the velocity occurred. Unfortunately, data are not available to show whether the drift stopped at 0139–0140, as is the case with the eastern irregularity, although the shape of the drift curve of Figure 15 does indicate this possibility. At Tromsø the drift stopped completely for about 2 min at 0139–0140, after which it continued with the same velocity as before. If the symmetric drift of the two irregularities is more than a coincidence, it can perhaps be thought of as an effect associated with changes in the convection and thus in the polar cap electric field during the expansion.

SATELLITE PARTICLE OBSERVATIONS

At 0115 UT the Isis 1 satellite passed over the arc at a position 10.3° east of Great Whale. The electron spectrogram of the southbound pass is presented in Figure 16, where the electrons associated with the visual arc appear distinctly at an invariant latitude of about 68° and a magnetic local time of 20.8 hours. Immediately poleward of this precipitation is a restricted region containing electrons of energies in the 100- to 250-eV range. Equatorward of the auroral precipitation the spectrogram shows photoelectrons of energy between ≃10 eV and ≃60 eV, coming down the field lines from sunlit magnetically conjugate points.

The electron differential number spectrum measured near

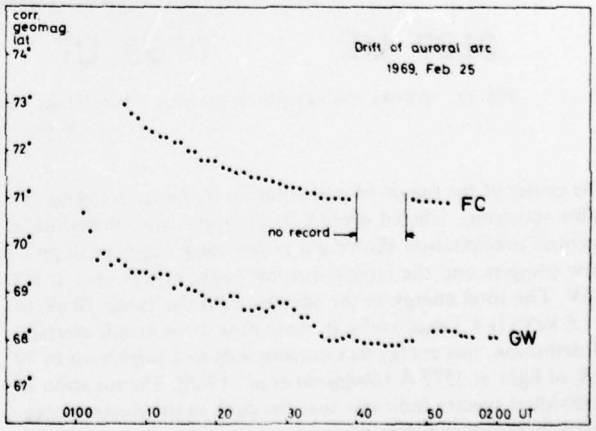

Fig. 12. Equatorward drift of auroral arc in the evening sector. (Top curve) Fort Churchill (19 MLT). (Bottom curve) Great Whale River (21 MLT).

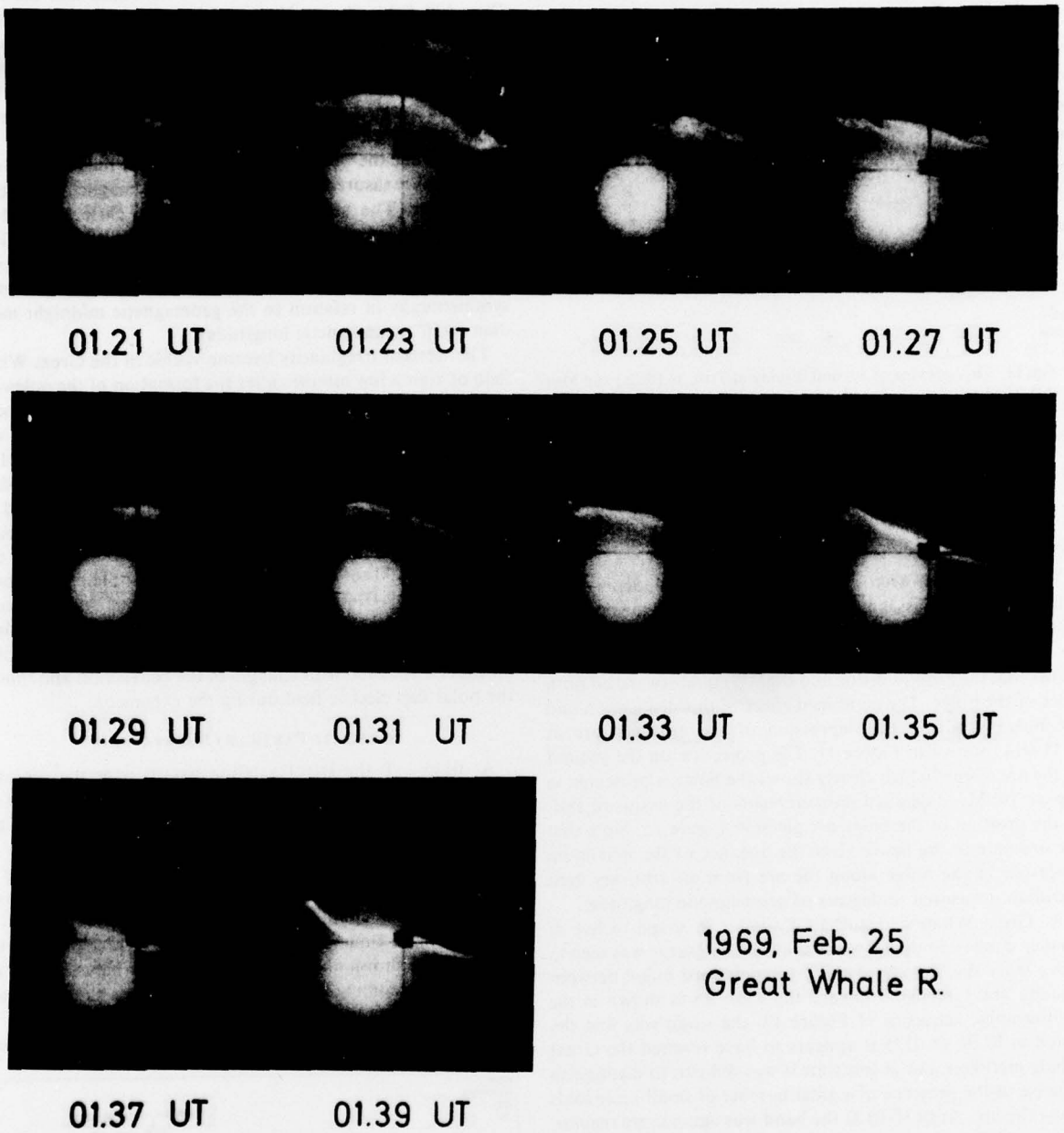

Fig. 13. All-sky photographs from Great Whale River, February 25, 1969, showing westward movement of irregularities in the auroral arc.

the center of the region of precipitation is shown in Figure 17. This spectrum, labeled dN/dE, is characteristic of nightside auroral precipitation showing a rather steep negative slope at low energies and the typical auroral peak, in this case at 1.3 keV. The total energy in the spectrum (in the range 10 eV to 11.6 keV) is 4.3 ergs/cm² s sr. Assuming an isotropic electron distribution, this energy flux corresponds to a brightness of 20 kR of light at 5577 Å [*Dalgarno et al.*, 1965]. Examination of individual spectra indicates that the peak in the electron spectrum increases and then decreases as the arc is crossed. Such a latitudinal morphology has been referred to as an 'inverted V' structure by *Frank and Ackerson* [1971] and is a common feature associated with many auroral arcs.

The enlarged photograph of Figure 18 shows the arc as it was observed from the Great Whale River Observatory at 0115 UT. The small white circle near the right edge of the photograph marks the point at which the geomagnetic field line, through which the satellite passed at the time the maximum energy flux was detected (0114:56), intersects the height of maximum auroral luminosity. As is shown by the 'energy flux' curve of Figure 17, most of the energy was carried at $\simeq 3$ keV, which places the height of maximum luminosity at about 120 km [*Rees*, 1969].

The soft particle spectrometer also provided a measurement of protons in the range of energies 10 eV to 11.6 keV. Within this energy range, protons were observed to precipitate over a

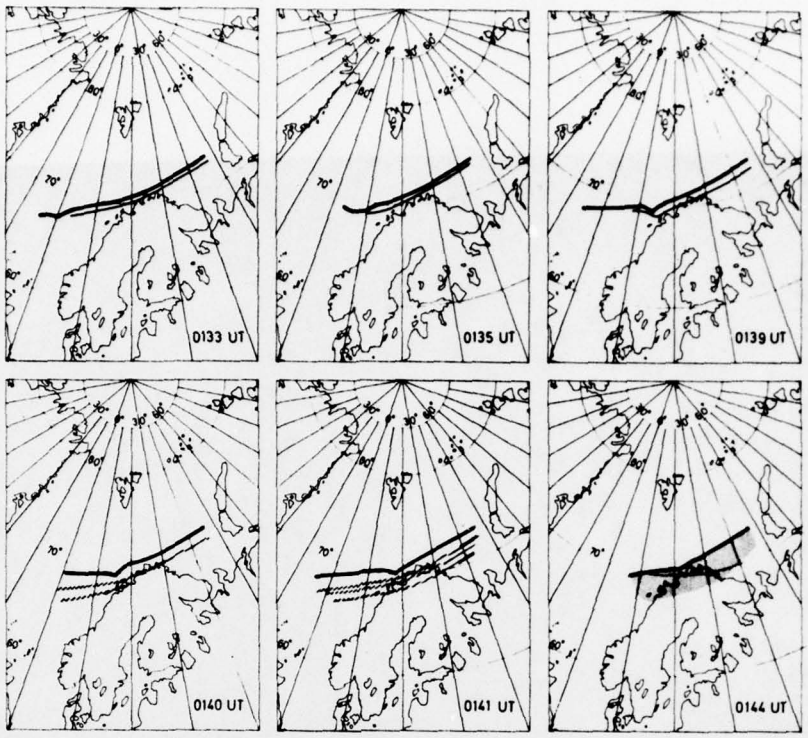

Fig. 14. Maps showing eastward movement of surge in the morning sector, as observed from Tromsø.

region extending from an invariant latitude of 67.4°–66.6°. The proton energy flux profile is plotted in Figure 19, which clearly demonstrates that the proton precipitation occurred equatorward of the electron precipitation associated with the visual arc. The energy associated with the protons over this range of invariant latitude averaged 3.0×10^{-2} erg/cm² s sr. Because of low count rates it was not possible to measure a proton spectrum, but the average proton energy appeared to be near 4 keV.

Since the satellite crossed the region of particle precipitation before the time of maximum disturbance, it is possible to estimate energy input into the auroral ionosphere before the onset of the expansive phase. Figure 19 shows the electron energy flux profile measured as the satellite passed over the arc. A directional intensity of 0.2 erg/cm² s sr corresponds to 1 kR of light at 5577 Å, which is near the visibility threshold above the background light of the night sky. As the figure indicates, an electron flux in excess of this value was detected for four consecutive spectral sweeps or for 8 s. The satellite horizontal speed was 7 km/s, so that at the satellite altitude of 620 km the 'arc width' was 56 km. Integrating across the arc, the rate of energy input per unit length of the arc was 5×10^7 ergs/s cm. The prebreakup arc was observed by cameras from west of Fort Churchill to east of Tromsø and most likely

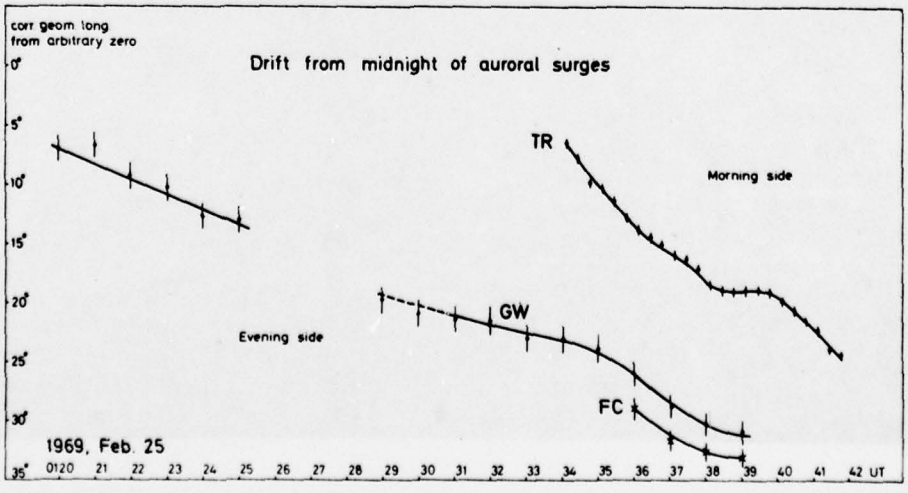

Fig. 15. Drift from midnight of auroral surges. The drift seen at Great Whale and Fort Churchill is westward; that at Tromsø is eastward.

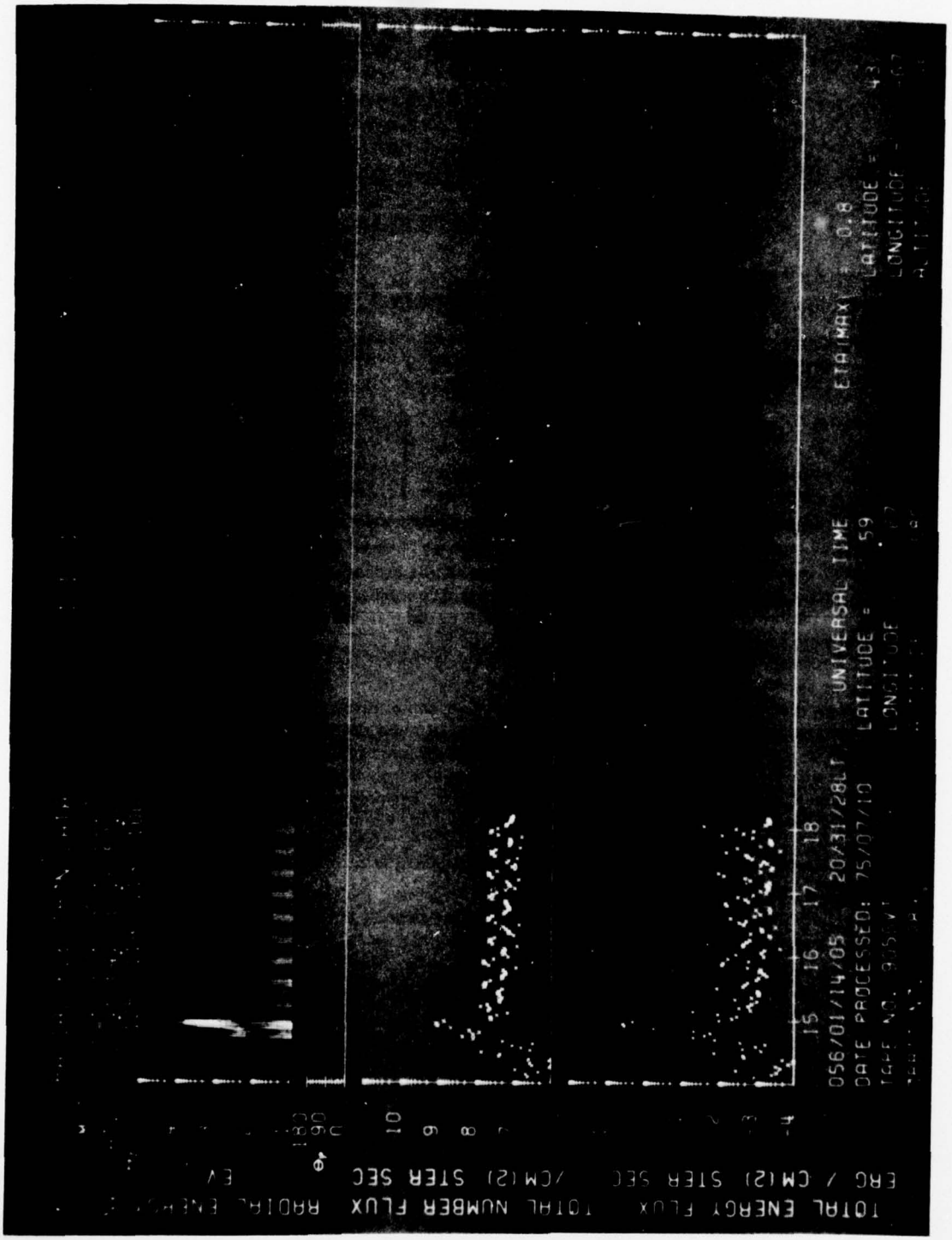

Fig. 16. Electron spectrogram for the southbound pass of February 25, 1969, beginning at 0114:05 UT.

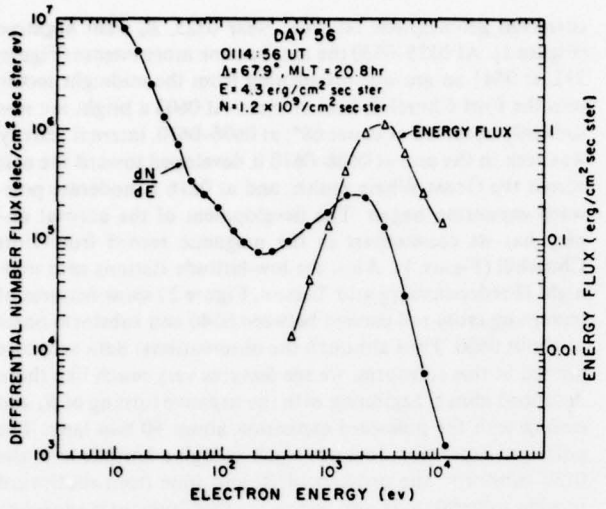

Fig. 17. Electron differential number spectrum (dN/dE) and energy flux measured by the Isis 1 soft particle spectrometer at 0114:56 UT on February 25, 1969.

extended much further in both directions. A length of 7×10^3 km approximates this distance, and with this assumption the total energy input rate was 3.5×10^{16} ergs/s. The arc was visible for at least ½ hour before breakup; therefore an energy of 7×10^{19} ergs was deposited into the auroral atmosphere by the electrons before breakup. The protons in the region equatorward of the arc carried considerably less energy than the electrons, a feature not unusual in auroral events. The ratio of the energy of the protons equatorward of the arc to that of electrons within the arc was 1.6×10^{-2}.

The question of whether or not auroral arcs always occur on closed magnetic field lines continues to be a matter for determination. We have attempted such a determination for the arc observed on February 25 by making use of the S-50 detector of the Isis 1 energetic particle experiment (compliments of J. R. Burrows, National Research Council, Ottawa, Canada). This detector responds to electrons of energy >40 keV and offers the advantage of a large geometric factor of 4×10^{-2} cm² sr. Figure 20 shows the S-50 flux plotted against universal time and invariant latitude, where the counts have been averaged over pitch angle in order to compare the trapped particle flux outside the 63° loss cone with the downcoming ($\alpha < 63°$) and upcoming ($\alpha > 117°$) fluxes. At latitudes below about 68° the trapped flux exceeds the precipitated flux, indicating a closed field line configuration. From the figure it is not possible to tell exactly where the angular distribution changed, but it must have been between 67.9° and 68.4°. *Fritz* [1970] would identify this location as $\Lambda_{1.0}$, a boundary defined to be the lowest latitude at which isotropy occurs for electrons of $E > 35$ keV. We note that on the nightside this boundary always occurs at a latitude lower than the Λ_b of *McDiarmid and Burrows* [1968], which is the lowest latitude at which counts fall to cosmic ray background and which is interpreted by them as the high-latitude limit of closed field lines. In the present case, λ_b was above latitude 71.2°, the highest latitude tracked on this pass. Thus we can state that the electron arc is associated with or lies below the boundary between open and closed field lines and that the proton arc clearly lies on closed magnetic field lines.

Discussion

Growth Phase

It has been shown that the substorm under study here, which followed a period of magnetic calm, appears to have been preceded by an interval before breakup with activity corresponding to the growth phase defined by *McPherron* [1970]. The gradual development of the activity starts shortly after the southward turning of the interplanetary magnetic field; the magnetic deflections at auroral latitudes as well as at middle and low latitudes, the auroral activity, the westward magnetospheric electric field deduced from the auroral drift, and the precipitation of auroral particles measured by the satellite all support McPherron's suggestion that the start of the substorm growth phase indicates either a commencement or a gradual enhancement of magnetospheric convection. The observation of symmetrically drifting auroral surges during growth and expansion phases as well as of auroral patterns similar to part of the convection pattern may give further support to this idea. In the present case we are apparently concerned with a situation in which increased convection initiated by a negative B_z is terminated by several substorms: first a very small confined substorm and then two greater substorms with clear breakup and poleward expansions which are not separated from each other but which seem to belong to the same disturbance event.

The very small substorm occurred at about 0100 UT approximately ½ hour before the expansion phase of the major substorm. It was characterized by a small westward traveling surge and a small magnetic bay of $\simeq 20\ \gamma$ and therefore fits the description of a weak substorm along a contracted oval as concluded from ground-based observations [*Montbriand*, 1971] and DMSP 2 imaging [*Akasofu*, 1974*b*]. The southward turning of the IMF preceded even this event by more than an hour, and the first departure from magnetic quiet was observed at auroral zone as well as low-latitude stations about 1

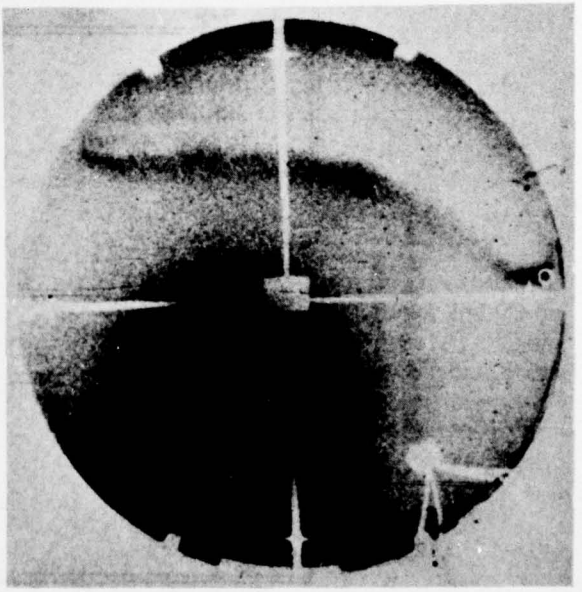

Fig. 18. All-sky photograph taken at Great Whale River Observatory at 0115 UT on February 25, 1969. The small white circle designates the field line intersection point at 120 km.

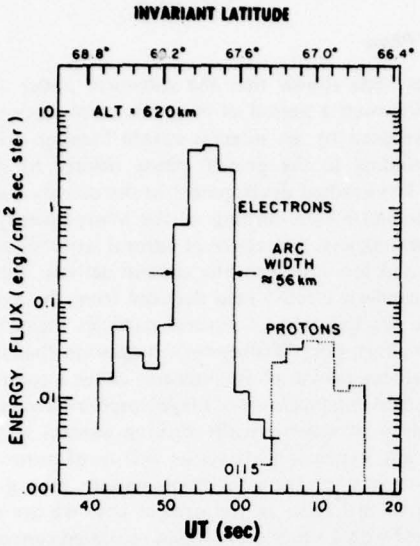

Fig. 19. Electron and proton energy flux latitudinal profiles. The proton precipitation lies distinctly equatorward of the electron precipitation associated with the visual arc. Minute 15 of hour 01 is labeled as 0115 and begins at the 00 mark on the abscissa.

hour before the appearance of the small substorm. Accordingly, we take the view that this substorm may also have resulted from the southward turning of the IMF and represented a small release of energy before the much greater release at 0130.

As in the main event under study, the 0600 substorm which appears at Fort Churchill and Great Whale River was preceded by a short interval of activity, which is similar to the growth phase of the 0130 substorm: following the recovery of substorm activity at 0400, quiet arcs were situated near 71° corrected geomagnetic latitude. Near 0525, B_z went negative (Figure 1). At 0525–0530 the arcs became more intense (Figure 21); at 0541 an arc was broadening from the midnight sector into the Fort Churchill field of view. At 0603 a bright arc was suddenly observed at about 68°; at 0606–0610, internal activity was seen in the arc; at 0608–0610 it developed toward the east across the Great Whale zenith; and at 0616 a moderate poleward expansion began. The development of the auroral display has its counterpart in the magnetic record from Fort Churchill (Figure 1). Also, the low-latitude stations near midnight (Fredericksburg and Tucson, Figure 2) show features of increasing cross-tail current between 0540 and substorm onset at about 0600. Thus although the observational data are more limited at this substorm, we see features very much like those described above, beginning with the negative turning of B_z and ending with the poleward expansion about 50 min later. The poleward expansion does not reach as high a latitude as in the 0130 substorm; the product of B_z and time from southward turning to breakup is also less in the 0600 substorm [*Arnoldy*, 1971].

Our observations do not determine whether the expansive phase trigger mechanism is internal or external. We can only point to our observations that the southward turning of the IMF was followed by clear signatures of increased magnetospheric convection: *DPZ* equivalent current systems of gradually (though not monotonically) increasing intensity, signatures of an increasing cross-tail and/or ring current, precipitation of auroral particles in an increasing longitudinal sector of the midnight auroral oval, and finally a poleward curvature of arcs in the premidnight area that resembles the drift pattern in the polar cap. Minor signatures of instability or activity are followed by the sharp breakup.

It is apparent from the observations presented here as well as from observations of *Subbarao and Rostoker* [1973], *Hones et al.* [1973], *Akasofu et al.* [1973], *Rossberg* [1974], and *Aka-*

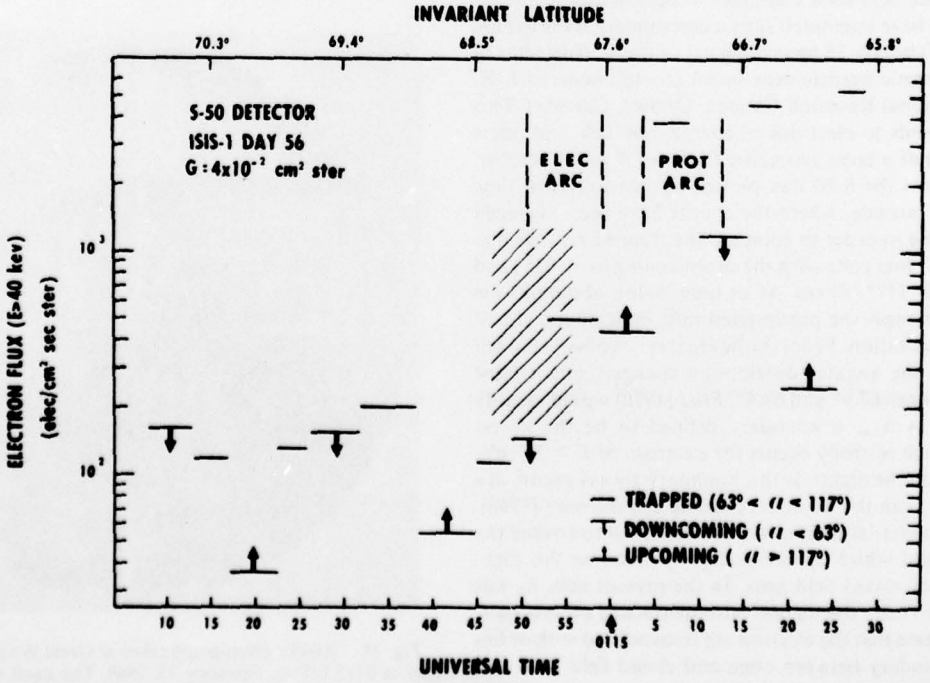

Fig. 20. High-energy electron fluxes averaged over pitch angle. The low-latitude limit of the position of the boundary between open and closed field lines lies between invariant latitudes 67.9° and 68.4°, indicated by hatching. The arrow on the abscissa labeled 0115 indicates the beginning of minute 15 of hour 01 (UT).

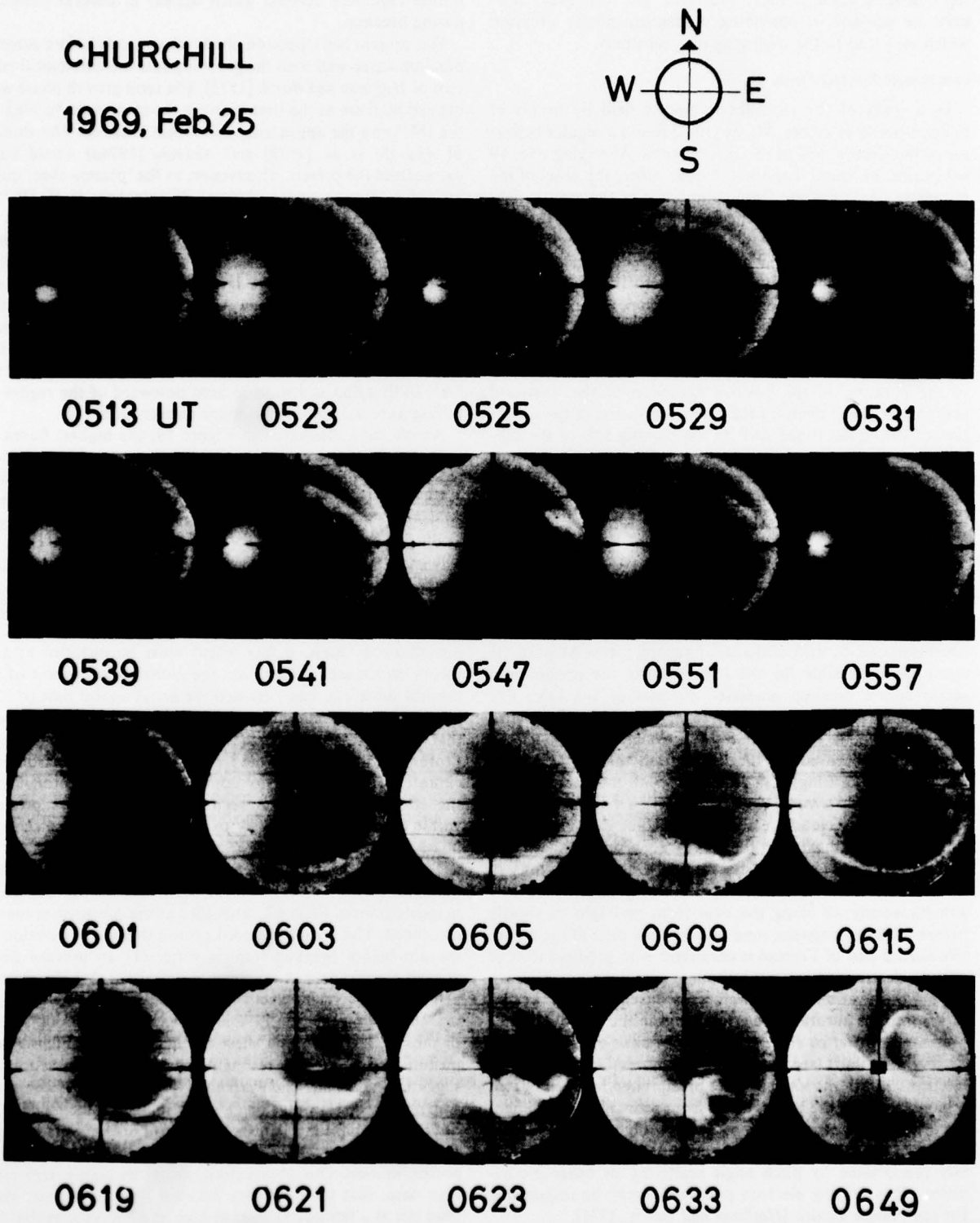

Fig. 21. All-sky photographs from Fort Churchill, February 25, 1969, showing auroral activity during the prebreakup (growth) phase and beginning of expansion phase of the later substorm.

sofu [1975] that some substorms have a gradual and easily defined growth or development phase, while others do not. Obviously, there is no clear one-to-one relation between the growth phenomenon and the substorm. It is in agreement with current substorm theories that a B_z-negative-caused magnetospheric convection, if it is continued for a sufficiently long period, may result in substorm activity, as in the case studied here. However, the evidence discussed above seems to argue against the use of the term growth phase when it is applied with the same weight as the term 'expansive phase' in describ-

ing a definite phase of every substorm. The term may, however, be suitable in describing a magnetospheric situation which may lead to the triggering of a substorm.

Ionospheric Electric Fields

In a study of the ionospheric electric field by means of balloon-borne detectors, *Mozer* [1971] found a regular behavior of the electric field in the auroral zone. Averaging over 19 substorms, he found that about 1 hour before the onset of the expansive phase the westward component of the electric field increased from zero and reached a maximum value at the time of breakup. The field remained at this level throughout the expansion phase and then began a return toward zero. The southward component remained at a zero level until it suddenly increased at the onset of the expansion. Our observation that the equatorward drift of the auroral arc appears during the growth phase, continues through the expansive phase, and then suddenly stops is in agreement with Mozer's observation of the duration of the positive excursion of the westward component of the electric field. Our observation of the limitation of the equatorward drift to the evening side of the substorm center appears, however, to be new. It is not obvious from Mozer's balloon measurements. His conclusions are based on average values without information about the location of the balloons in relation to the substorm.

Particle Precipitation and Relationship to the Magnetosphere

The particle precipitation associated with this auroral display has been studied both by direct measurement and by observation of the drift of cloudlike auroral forms. Most of the electrons responsible for the luminosity in the premidnight sector before breakup possessed energies of 1–5 keV. The cloudlike form observed drifting from Tromsø to Murmansk was produced by electrons of ≃40-keV energy. This energy determination, based on the assumption that the electrons were gradient drifting, is in agreement with the photographic observations of *Stormer* [1955], which give a mean height of 94 km for ordinary cloudlike auroras over Norway. The ionization production maximum for 40-keV electrons has been calculated by *Rees* [1963] to be 92 km. Our observations of diffuse aurora indicate that such electrons appeared nearly simultaneously all along the oval from midnight to shortly before 0400 geomagnetic time and that the drift of the cloudlike aurora east of Tromsø is consistent with gradient drift of 40-keV electrons at auroral latitudes.

This observation agrees well with the model for precipitation into the auroral zone of electrons in the >30-keV range presented by *Sletten et al.* [1971] on the basis of observations by several authors (see their list of references). In their model, electrons within the loss cone are precipitated in an elongated region following the auroral oval from geomagnetic midnight toward dawn. Electrons with other pitch angles drift eastward, following the L shells from this source region, and are gradually precipitated by pitch angle scattering or other mechanisms. This drifting electron population may be responsible for the mantle aurora [*Hoffman and Burch*, 1973].

Thus our observations support a mechanism which would inject 40-keV electrons into the auroral oval during the expansive phase of the substorm. The observation by the Vela satellites [*Hones et al.*, 1973] of an enhancement in the $E > 45$-keV electron flux at the time of rapid thinning of the plasma sheet at the satellite suggests that these electrons may be of the same population as that responsible for the production of the diffuse cloudlike auroras which appear at auroral latitudes during breakup.

Our present Isis 1 electron observations made before auroral breakup agree well with the growth phase morphological pattern of *Hoffman and Burch* [1973]. The term growth phase was defined by them as the time between the southward turning of the IMF and the appearance of auroral breakup. The studies of *Akasofu et al.* [1973] and *Akasofu* [1974*a*] would have categorized the present observation as the 'plasma sheet quiet arc' of a 'growth phase pattern.' *Winningham et al.* [1975], using Isis 1 and 2 particle data, have amplified the patterns of *Hoffman and Burch* [1973] but do not include a pattern representing a preexpansive phase, IMF south condition (since this condition does not always initiate a complete substorm sequence). They do state, however, that an observation of the kind we report would be categorized as representing their 'boundary plasma sheet' (BPS) region during a period for which the IMF is directed southward (see their Figure 19). This BPS region is always located poleward of the region of diffuse aurora and often contains discrete arcs.

As we have illustrated in Figure 19, the highest fluxes of protons of about 4-keV energy were measured within a region equatorward of the electron arc. A similar latitudinal profile, characteristic of the premidnight hours, has been obtained statistically with airborne [*Eather and Mende*, 1971] and ground-based [*Fukunishi*, 1975] Hβ observations. The study of *Fukunishi* [1975] clearly places the belt of proton precipitation equatorward of discrete auroral arcs during times which he defines as the 'quiet' phase and the 'prebreakup' phase. Our particle observations show that the separation can occur on an instantaneous basis, a fact which must be included in any theory which seeks to explain the global development of an auroral substorm. Isis 1 crossed the arc at a local time of 20.5 hours and a magnetic local time of 20.8 hours. We also note that apparent separation between the region of maximum proton precipitation and the region of maximum electron precipitation (the arc) does not completely exclude protons from the electron precipitation region; it only excludes protons within the energy range 10 eV to 11.6 keV and above an energy flux level of $\simeq 10^{-3}$ erg/cm^2 s sr.

The observed protons were most likely associated with the quiet time ring current, which, according to the San Juan magnetogram of Figure 2, intensified as the substorm sequence continued. The greatly reduced proton flux at the position of the arc before breakup implies either (1) an upward field-aligned electric field at the auroral arc or (2) that the mechanism which energizes electrons and protons does not precipitate the protons efficiently. Only when the proton population of the near-earth plasma sheet reaches a critical intensity are protons precipitated by resonant wave-particle interactions as suggested by *Kennel and Petschek* [1966]. Adiabatic compression operates on protons on closed field lines in the tail region, but the dominant mechanism is betatron or transverse energization which operates on the transverse component of the proton motion. Our observation, using the high-energy electron data, that the boundary between open and closed field lines lies at a latitude at least as high as 67.9° insures that the protons we observed were on closed magnetic lines.

SUMMARY AND CONCLUSIONS

A comprehensive study of the major substorm of February 25, 1969, at 0130 UT and several weak substorms before and after this event has resulted in the following observations.

1. The preexpansive phase auroral arc extended approxi-

mately along the auroral oval from 17.5 to 05.5 MLT and was responsible for an energy input rate of $\simeq 3 \times 10^{16}$ ergs/s before the breakup.

2. In the evening sector, from the earliest observation of auroral light, an equatorward drift of 6 km/min was observed; this drift was present only in the evening sector and ceased after the onset of the expansive phase at the time of maximum poleward displacement of the breakup arcs.

3. In the evening–midnight sector the increase in the intensity of the preexpansive phase arc accompanied the increase in the deviation of the horizontal magnetogram component.

4. The equivalent currents obtained from the observed magnetic deflections were of the *DPZ* type (twin vortex mode) before the onset of the expansive phase. After the onset the *DPZ* currents were more intense by a factor of 2, but the dominating current during this period was an intense westward auroral electrojet.

5. During the expansive phase, symmetrically traveling disturbances were observed propagating eastward and westward away from the midnight sector. The propagation stopped for 1–2 min at the time of maximum poleward expansion and then continued (at least in the morning side) with the original velocity.

6. Electrons in the 1- to 5-keV range were measured by satellite over the preexpansion phase arc. They were observed near and probably within the low-latitude limit of the boundary between open and closed field lines.

7. Protons of $\simeq$4-keV energy were measured equatorward of the electron arc; their intensity was 1.6×10^{-2} that of the electrons within the arc, and they were definitely on closed field lines.

8. An injection of $\simeq$40-keV electrons as determined from the observations of diffuse cloudlike aurora occurred during the expansive phase. At times later than 04 MLT the cloudlike aurora associated with the 40-keV electron population was observed to drift eastward toward later morning hours.

The major substorm at 0130 UT and a smaller substorm at 0600 UT show growth phase features in their visual and magnetic signatures. However, other investigations show that many substorms have occurred for which there is no classic growth pattern and also that some growth phase patterns do not always result in a complete substorm sequence [*Kokubun et al.*, 1977]. Accordingly, we emphasize the usefulness of the growth phase concept in describing a magnetospheric condition which is initiated by a southward turning of the IMF but stress that in general it should not be expected to bear a one-to-one correspondence with the substorm expansive phase.

Acknowledgments. We are indebted to H. Derblom, Ionosfaerobservatoriet, Uppsala; S. I. Isaev, Polar Institute, Apatity, Murmansk; M. J. Neale, National Research Council (NRC), Canada; J. Sommer, World Data Center CI, Copenhagen; and O. Holt, Nordlysobservatoriet, Tromsø, for placing copies of records at our disposal. We also wish to thank J. R. Burrows and M. Wilson, NRC, Canada, for providing the energetic particle data from Isis 1; P. Hedgecock, Imperial College, London, for magnetometer data from Heos 1; and J. Frazier of the University of Texas at Dallas (UTD) and L. Kaufman of the Florida Institute of Technology for technical assistance. The UTD portion of the work was supported by NASA contract NGR 44-004-150 and by Air Force contracts AFCRL F 19628-75-C-0032 and AFCRL F 19628-76-R-0009. We also gratefully acknowledge research funds provided by the Danish Meteorological Institute and by the Florida Institute of Technology.

REFERENCES

Akasofu, S.-I., The development of the auroral substorm, *Planet. Space Sci., 12*, 273, 1964.

Akasofu, S.-I., Auroral substorm and associated magnetic disturbances, in *Polar and Magnetospheric Substorms*, D. Reidel, Hingham, Mass., 1968.

Akasofu, S.-I., The aurora and magnetosphere, The Chapman memorial lecture, *Planet. Space Sci., 22*, 895, 1974*a*.

Akasofu, S.-I., A study of auroral displays as photographed from the DMSP-2 satellite and from the Alaska meridian chain of stations, *Space Sci. Rev., 16*, 617, 1974*b*.

Akasofu, S.-I., The roles of the north-south component of the interplanetary magnetic field on large-scale auroral dynamics observed by the DMSP satellite, *Planet. Space Sci., 23*, 1349, 1975.

Akasofu, S.-I., P. D. Perreault, and F. Yasuhara, Auroral substorms and the interplanetary magnetic field, *J. Geophys. Res., 78*, 7490, 1973.

Arnoldy, R. L., Signature in the interplanetary medium for substorms, *J. Geophys. Res., 76*, 5189, 1971.

Dalgarno, A., I. D. Latimer, and J. W. McConkey, Corpuscular bombardment and N_2^+ radiation, *Planet. Space Sci., 13*, 1008, 1965.

Eather, R. H., and S. B. Mende, Airborne observations of auroral precipitation patterns, *J. Geophys. Res., 76*, 1746, 1971.

Feldstein, Y. I., Auroras and associated phenomena, in *Solar-Terrestrial Physics*, edited by E. R. Dyer, p. 152, D. Reidel, Hingham, Mass., 1972.

Frank, L. A., and K. L. Ackerson, Observations of charged particle precipitation into the auroral zone, *J. Geophys. Res., 76*, 3612, 1971.

Friis-Christensen, E., and J. Wilhjelm, Polar cap currents for different directions of the interplanetary magnetic field in the *y-z* plane, *J. Geophys. Res., 80*, 1248, 1975.

Fritz, T. A., Study of the high-latitude, outer-zone boundary region for $\geq$40-keV electrons with satellite Injun 3, *J. Geophys. Res., 75*, 5387, 1970.

Fukunishi, H., Dynamic relationship between proton and electron auroral substorms, *J. Geophys. Res., 80*, 553, 1975.

Hamlin, D. A., R. Karplus, R. C. Vik, and K. M. Watson, Mirror and azimuthal drift frequencies for geomagnetically trapped particles, *J. Geophys. Res., 66*, 1, 1961.

Hoffman, R. A., and J. L. Burch, Electron precipitation patterns of substorm morphology, *J. Geophys. Res., 78*, 2867, 1973.

Hones, E. W., Jr., J. R. Asbridge, S. J. Bame, and S. Singer, Substorm variations of the magnetotail plasma sheet from $X_{SM} \simeq -6\ R_E$ to $X_{SM} \simeq -60\ R_E$, *J. Geophys. Res., 78*, 109, 1973.

Iijima, T., and T. Nagata, Constitution of polar magnetic disturbances, *Rep. Ionos. Space Res. Jap., 22*, 1, 1968.

Iijima, T., and T. Nagata, Signatures for substorm development of the growth phase and expansion phase, *Planet. Space Sci., 20*, 1095, 1972.

Kelley, M. C., J. A. Starr, and F. S. Mozer, Relationship between magnetospheric electric fields and the motion of auroral forms, *J. Geophys. Res., 76*, 5269, 1971.

Kennel, C. F., and H. E. Petschek, Limit on stably trapped particle fluxes, *J. Geophys. Res., 71*, 1, 1966.

King, J. H., Interplanetary magnetic field data book, report, NASA, April 1975.

Kokubun, S., and T. Iijima, Time-sequence of polar magnetic substorms, *Planet. Space Sci., 23*, 1483, 1975.

Kokubun, S., R. L. McPherron, and C. T. Russell, Triggering of substorm by solar wind discontinuities, *J. Geophys. Res., 82*, 74, 1977.

Lui, A. T. Y., C. D. Anger, and S.-I. Akasofu, The equatorward boundary of the diffuse aurora and auroral substorms as seen by the Isis 2 auroral scanning photometer, *J. Geophys. Res., 80*, 3603, 1975.

McDiarmid, I. B., and J. R. Burrows, Local time asymmetries in the high-latitude boundary of the outer radiation zone for different electron energies, *Can. J. Phys., 46*, 49, 1968.

McPherron, R. L., Growth phase of magnetospheric substorms, *J. Geophys. Res., 75*, 5592, 1970.

McPherron, R. L., C. T. Russell, and M. P. Aubry, Satellite studies of magnetospheric substorms on August 15, 1968, 9, Phenomenological model for substorms, *J. Geophys. Res., 78*, 3131, 1973.

Montbriand, L. E., Proton aurora and auroral substorm, in *The Radiating Atmosphere*, edited by B. M. McCormac, p. 366, D. Reidel, Hingham, Mass., 1971.

Mozer, F. S., Origin and effects of electric fields during isolated magnetospheric substorms, *J. Geophys. Res., 76*, 7595, 1971.

Nishida, A., Geomagnetic *DP*2 fluctuations and associated magnetospheric phenomena, *J. Geophys. Res., 73*, 1795, 1968.

Pike, C. P., and J. A. Whalen, Satellite observations of auroral sub-

storms, *J. Geophys. Res.*, *79*, 985, 1974.
Rees, M. H., Auroral ionization and excitation by incident energetic electrons, *Planet. Space Sci.*, *11*, 1209, 1963.
Rees, M. H., Auroral electrons, *Space Sci. Rev.*, *10*, 413, 1969.
Rossberg, L., Remarks on the growth phase of substorms, in *Magnetospheric Physics*, edited by B. M. McCormac, p. 367, D. Reidel, Hingham, Mass., 1974.
Rostoker, G., Polar magnetic substorms, *Rev. Geophys. Space Phys.*, *10*, 157, 1972.
Sletten, A., J. Stadsnes, and H. Trefall, Auroral-zone x-ray events and their relation to polar magnetic substorms, *J. Atmos. Terr. Phys.*, *33*, 589, 1971.
Starkov, G. V., and Ya. I. Feldstein, Substorms in auroras, *Geomagn. Aeron.*, *11*, 478, 1971.
Stormer, C., *The Polar Aurora*, p. 108, Oxford University Press, New York, 1955.
Subbarao, S., and G. Rostoker, Relationship of southward drifting auroral arcs to the magnetospheric electric field and substorm activity, *J. Geophys. Res.*, *78*, 1100, 1973.
Winningham, J. D., F. Hasuhara, S.-I. Akasofu, and W. J. Heikkila, The latitudinal morphology of 10-eV to 10-keV electron fluxes during magnetically quiet and disturbed times in the 2100–0300 MLT sector, *J. Geophys. Res.*, *80*, 3148, 1975.

(Received February 18, 1976;
accepted July 18, 1977.)